

REVIEW

[View Article Online](#)
[View Journal](#) | [View Issue](#)

Click chemistry for 3D bioprinting

Lei Nie,^a Yanfang Sun,^c Oseweuba Valentine Okoro,^b Yaling Deng,^{*d}
Guohua Jiang^{ef} and Amin Shavandi^gCite this: *Mater. Horiz.*, 2023,
10, 2727

Bioinks are employed in the fabrication of 3D scaffolds containing cells and macromolecules that can be applied in regenerative medicine. The use of such bioinks facilitates the controlled introduction and localization of macromolecules, bioactives and cells for the biofabrication of living tissues. To enable the successful preparation of the bioinks, strategies involving the use of so-called cross linkers, which may be ionic, chemical, photo-etc. based, are employed. Some of these strategies such as the use of glutaraldehyde as a crosslinker or harsh crosslinking conditions may however compromise the cytocompatibility of the bioink. To circumvent this challenge, the employment of click chemistry technology has been proposed. This is because, click chemistry can enable the preparation of well-tuned bioinks in the absence of problematic cross-linkers, while ensuring that favorable gelation rate, degradation rate, and cell viability properties of the bioinks are not compromised. Indeed, the bio-orthogonal nature of click chemistry has been suggested to enhance the maintenance of high cell viability in scaffolds. In this regard, the current study explored the potential of using different click chemistries in specific bioprinting techniques. Major bioinks produced using click chemistry were also identified, with existing challenges and future trends discussed. It is anticipated that this review will be invaluable to the tissue engineering field by providing an important resource for bioengineers and a basis of future decisions regarding the selection of the preferred click chemistry for specific bioink functionalities.

Received 5th April 2023,
Accepted 27th April 2023

DOI: 10.1039/d3mh00516j

rsc.li/materials-horizons

Wider impact

The use of bioinks in 3D bioprinting has significantly advanced the development of regenerative medicine, allowing for the fabrication of living tissues with controlled introduction and localization of cells and macromolecules. However, some cross-linking strategies employed in bioink preparation, such as the use of glutaraldehyde or harsh crosslinking conditions, can compromise the cytocompatibility of the bioinks. To address this challenge, the use of click chemistry technology has been proposed. Click chemistry enables the preparation of well-tuned bioinks in the absence of problematic cross-linkers, while ensuring favorable gelation rate, degradation rate, and cell viability properties are not compromised. The bio-orthogonal nature of click chemistry has been suggested to enhance the maintenance of high cell viability in scaffolds.

The wider impact of this research is multifaceted. Firstly, it provides a solution to a critical challenge faced in the field of tissue engineering, by offering a method to improve the cytocompatibility of bioinks without compromising their desired properties. Secondly, the study highlights the versatility and flexibility of click chemistry in the design and preparation of bioinks. This information could pave the way for the development of new bioinks that have improved properties for specific applications. Additionally, the review article serves as a valuable resource for bioengineers, providing them with the knowledge to make informed decisions regarding the selection of click chemistry for specific bioink functionalities. Finally, the potential of click chemistry in 3D bioprinting technology and bioinks could lead to the development of novel strategies for the regeneration of damaged tissues and organs. The successful application of this technology could significantly impact the field of regenerative medicine, improving patient outcomes and overall quality of life.

^a College of Life Sciences, Xinyang Normal University (XYNU), Xinyang 464000, P. R. China. E-mail: nieleifu@yahoo.com, nielei@xynu.edu.cn; Tel: +86-13600621068^b Université libre de Bruxelles (ULB), École polytechnique de Bruxelles – 3BIO-BioMatter unit, Avenue F.D. Roosevelt, 50 - CP 165/61, 1050 Brussels, Belgium.
E-mail: amin.shavandi@ulb.be^c College of Life Sciences and Medicine, Zhejiang Sci-Tech University, Hangzhou, Zhejiang, P. R. China^d College of Intelligent Science and Control Engineering, Jinling Institute of Technology, Nanjing 211169, P. R. China. E-mail: dengyaling1119@163.com^e School of Materials Science and Engineering, Zhejiang Sci-Tech University, Hangzhou, P. R. China^f International Scientific and Technological Cooperation Base of Intelligent Biomaterials and Functional Fibers, Zhejiang Sci-Tech University, Hangzhou, P. R. China^g These authors contributed equally to this work and should be considered co-first authors.

1. Introduction

In recent years, tissue engineering and regenerative medicine have become important strategies to treat human organ damage and loss of function caused by injury, disease, or surgery.¹ With the rapid development and application of 3D bioprinting technologies, including extrusion, stereolithography, inkjet printing, and laser-assisted printing, it is becoming possible to realize and improve tissue structure, printed both *in vitro* and *in situ*.² The combination of cells, biomaterials, and growth factors during 3D bioprinting, could enable the accurate fabrication of desired constructs.^{3,4} The desirable properties of the bioinks employed in the fabrication of the constructs include good biocompatibility, appropriate mechanical properties and chemical signals to promote tissue regeneration.^{3–5}

Bioink is an important part of bioprinting, and could be composed of cell-loaded biomaterials, bioactive factors, or biomaterial mixtures and employed in the fabrication of biologically active and functional 3D tissue structures.¹ Cell activity, viability and stability of growth factors are key properties to ensure the effective combination of cells and scaffolds in the 3D constructs. In this regard, bioinks should have suitable viscosity, cross-linking performance, printability, biodegradability, and biocompatibility, and they can provide growth environments similar to the extracellular matrix (ECM) for cells in the printing process.^{6–8} During the printing process, the bioink solution is cross-linked to form a gel with a 3D structure, which physically binds and protects the suspended cells from damage and hostile external conditions. Crucially, however, the use of crosslinker may affect the mechanical properties, physicochemical properties, and cell behavior of loaded cells.⁹ The harsh crosslinking conditions have negative effects on cytocompatibility. For example, the extended UV, high polymer concentration (15–20 wt%), restricted temperature range (15–20 °C) significantly decrease the rate of cell migration.^{10–12} Additionally, the use of some synthetic cross-linking agents such as carbodiimide, poly-carboxylic acids *etc.*, have been reported to have limitations such as low biodegradability and low biocompatibility.¹³ An approach that limits or avoids the use of such crosslinkers is therefore required, with the application of click chemistry widely proposed in this regard.

Click chemistry is a bio-orthogonal reaction that can be performed without crosslinking reactions of functional groups. Bioinks can spontaneously form a hydrogel based on click chemistry without the need for templates and linkers. Click chemistry can also improve the flexibility and versatility of bioinks and aid the design of hydrogels with controllable gel formation times, mechanical properties, and degradation.^{14,15}

Herein, we begin by exploring the types of click chemistry and application of click chemical reactions for 3D bioprinting technology and bio inks. The specific bioprinting techniques and the bioink prepared using click chemistry were then extensively discussed with the limitations of the click reactions employed in the preparation of the bio inks, highlighted. Finally, this paper discusses the future application and potential of click chemistry in bioink preparation with special

emphasis on the progress, challenges, and opportunities in using click chemistry reactions for 3D bioprinting.

2. Click chemistry

Inspired by the synthesis of biological molecules in nature, click chemistry focuses on the efficiency, spontaneity, selectivity, and modularity of chemical reactions. It can synthesize various molecules *via* splicing or dynamic combination of small units in a short time. Under the strict control of technical requirements, click chemical reaction refers to a chemical technology that utilizes active reactants to 'link' molecular substances or components based on C–X–C bond, under mild reaction conditions.^{16,17} It has several advantages, such as the availability of raw materials, insensitivity to water or oxygen, fast reaction rate, easy separation of products, and high yield. In this section, common click chemistry reactions in the field of 3D bioprinting are therefore introduced in Fig. 1 and discussed in the subsequent section.

2.1 Azide–alkyne cycloaddition reaction

Azide–alkyne cycloaddition reaction, known as CuAAC reaction, occurs between the azide and alkyne groups catalyzed by copper. This reaction was firstly reported by Arthur in 1983 and was established as an important class of reactions by Huisgen *et al.*¹⁸ Here, the alkyne group acts as a dipole, and the azide acts as 1,3-dipole. The alkyne group retains its stability under most conditions and can be deprotonated to form highly electrophilic Cu(I) acetylide in CuAAC reactions,¹⁹ while the Azide group is easily activated when combined with the Cu(I) alkyne complex.¹⁹ Unlike other click reactions, the CuAAC reaction mechanism involves the transient formation of super reactive coordination complexes catalyzed by clusters of Cu(I) atoms.²⁰ These Cu(I) clusters rapidly react to form aggregates to achieve gelation.²¹ However, copper ions can be toxic to cells since they can promote oxidation leading to cDNA degradation, polysaccharide denaturation, and protein denaturation.^{22,23} For example, neuronal oxidant damage produced by copper may trigger neurodegenerative diseases, Parkinson's disease, and Alzheimer's disease.²⁴ Long-term exposure to high levels of copper(II) can accumulate and cause damage to the liver and kidney, along with an imbalance in cellular processes.²⁵

The cross-linking density can be adjusted by variation of azide:alkyne molar ratio in pre-functionalized biopolymers.²⁶ For instance, hydrogels synthesized by alkyne-modified chitosan and azide-modified dextran, at varying azide:alkyne molar ratios from 1:0.5, 1:1, 1:1.5, to 1:2, showed a positive correlation between the increasing crosslinking densities and increasing molar ratios of azide to alkyne group.

The gelation time can also be tuned by varying the molar ratio of azide:alkyne and catalyst concentration. In the presence of copper(I) catalyst, the gelation time of cellulose derivatives bearing azide and alkyne moieties was between 55 s and 1594 s. Moreover, the gelation time depends on the degree

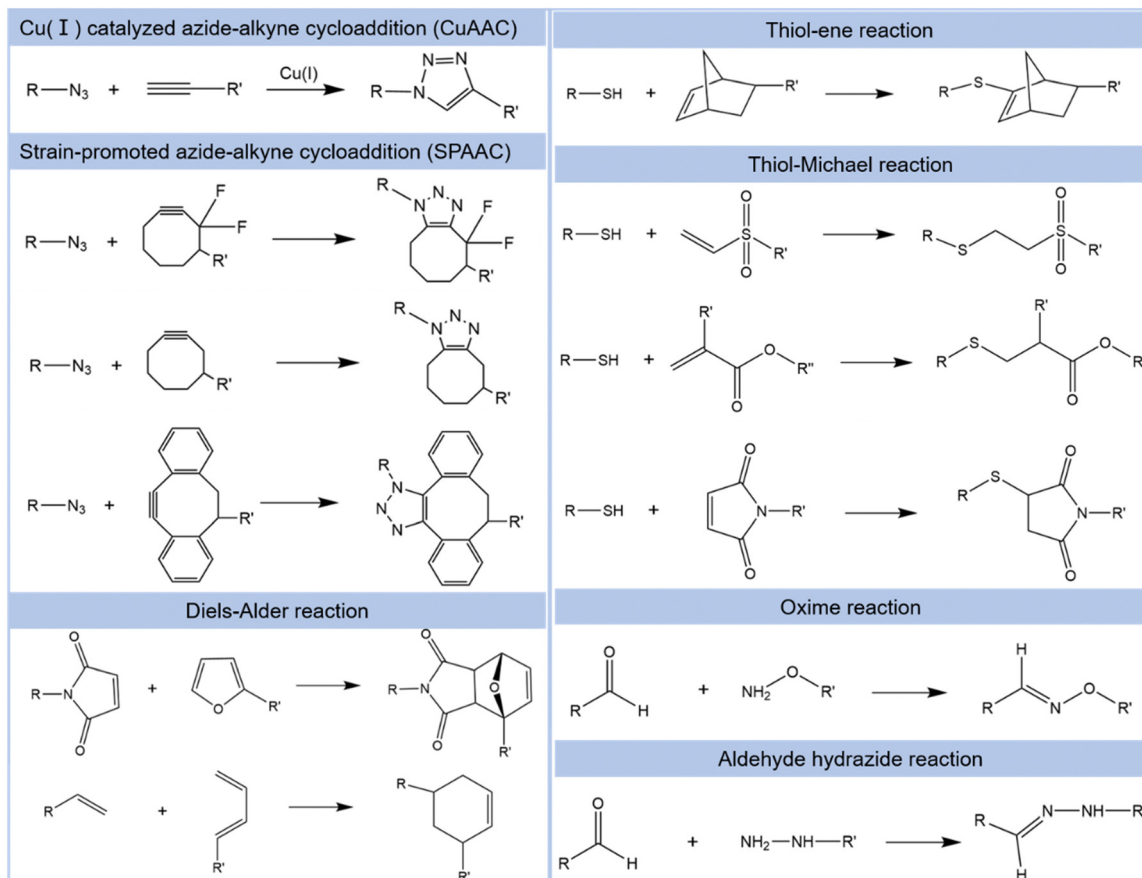


Fig. 1 Summary of click chemistry employed in 3D bioprinting.

of functionalization and the concentration of copper(i) catalyst. For instance, it was reported that the increase of copper concentration, from 5 to 10 mmol L⁻¹, increases the gelation rate of the mixture by a factor of 20.²⁷ The gel point and complete gelation of alkyne-functionalized PEG were detected after 13.5 min and 17.5 min, respectively. Without the reaction of Cu(I), the gelation kinetics was slow, and the gelation point was about 26.5 min.²⁸ The reason for the kinetics difference is the nucleophilic activation of the alkynes, which is produced from the Cu-ligand (L) complex.²¹

The cross-linking function of CuAAC is stable, and the degradation performance of the cross-linking scaffold depends on the intrinsic degradation characteristics of polymers. For example, hydrolytic stability of hydrogels synthesized with alkyne functionalized gelatin and PEG-diazide crosslinkers have been reported to retain stability for > 7 weeks at 37 °C.²⁹ Another study reported that PEG with spiropyran groups hydrogels, synthesized *via* CuAAC, remained stable for 2 weeks, after being implanted.³⁰ PEG-PTMC (poly(trimethylene carbonate)) hydrogels formed with CuAAC prolonged the degradation time of PEG hydrogels under the same conditions, from 1 to 8 days.³¹ CuAAC chemistry reaction can be utilized in 3D bioprinting, such as extrusion printing for immobilization of bioactive molecules,³² and inkjet printing for modification in mesoporous silica particles to tune microdot arrays.³³

2.2 Strain-promoted azide-alkyne cycloaddition

Strain-promoted azide-alkyne cycloaddition (SPAAC) was initially reported by Bertozzi *et al.*, in 2004.³⁴ This biological orthogonal reaction is driven by the high tension of active cyclo-alkynes, which can produce a chemical region-selective click reaction without a copper catalyst. As a catalyst-free biorthogonal chemical reaction, SPAAC has good biocompatibility, proceeds effectively in a mild reaction environment, and effectively forms a crosslinked triazole.^{34,35} Although the reaction rate constant of SPAAC (0.01–1 M⁻¹ s⁻¹) is lower than CuAAC (10–200 M⁻¹ s⁻¹),^{36,37} it can still achieve rapid gelation for 3D bioprinting applications by combining other cross-linking strategies. For example, the synthesis of hydrogel with cyclooctyne-functionalized PEG and azide-functionalized PEG, was reported to have a short gelation time of 5 min.³⁸ By mixing the azide- and monofluoro-substituted cyclooctyne (MFCO)-PEGs to fabricate PEG-based hydrogels, the gelation time was determined to range from 8–120 min. Moreover, the gel time varied with changes in the different polymer concentrations.³⁹ It was also reported that when SPAAC and non-covalent ionic bonds of Ca²⁺ and bisphosphonate groups, where combined, the PEG-based macromers gelled rapidly (*i.e.* < 60 s).⁴⁰ This rapid gelation rate facilitates the application of injectable hydrogel formulations to repair tissue defects.

Since there is no copper catalyst involved in the reaction, SPAAC effectively avoids cytotoxicity and is suitable for cell encapsulation in the hydrogel. According to the literature, PEG precursors (PEG-AZ and PEG-MFCO) and unmodified PEG have similar properties, such as little toxicity and cell viability of > 85%.³⁹ However, the cell viability of hydrogels formed by PEG-AZ and PEG-MFCO through SPAAC is higher and maintained at 95%, even after a 16 h incubation.³⁹ Thus, bone marrow stromal cells encapsulated in poly(ethylene glycol)-*co*-polycarbonate hydrogels, prepared with SPAAC click chemistry (about 10^6 cells mL⁻¹), were reported to present higher cellular viabilities than those encapsulated in photo-cross-linked hydrogels.⁴¹ Lee *et al.*⁴² determined that keratinocytes diffused and formed a confluent layer on the surface of SPAAC cross-linked collagen gels, whereas this phenomenon was absent on non-cross-linked gels.⁴² In addition, keratinocytes coverage areas on the SPAAC crosslinked gel surface (> 95%) were higher than non-cross-linked gels (< 50%).

SPAAC reaction can be used to prepare UNiVersal Orthogonal Network (UNION) bioinks since the SPAAC reaction can graft bioorthogonal groups onto the polymer backbone and modify the cross-linker molecules. The crosslinking agent molecules diffuse into the bioinks, and SPAAC crosslinking reaction occurs to enable the crosslinking of the hydrogel, without loss of biocompatibility.⁴³ The UNION bioink was reported to enable the maintenance of good viability and functional expression when employed in the encapsulation of human corneal mesenchymal stromal cells (c-MSCs) and human-induced-pluripotent stem cell-derived neural progenitor cells (hiPSC-NPCs).⁴³

2.3 Diels–Alder reaction

Diels–Alder is a cycloaddition reaction between a conjugated diene and alkene/alkyne, in which the cycloaddition products are fabricated by the overlap of two molecular orbitals.⁴⁴ They are the highest occupied molecular orbitals of the diene 4π electrons and lowest occupied molecular orbitals of the dienophile 2π electrons, respectively.⁹ The formation of σ bonds drives the reaction because it has better energy stability than π bonds. The [4+2] cycloaddition reactions between electron-rich dienes (cyclopentadiene and furan derivatives, *etc.*) and electron-deficient dienes (maleimide derivatives, *etc.*) form a stable cyclohexene compound.⁴⁵ Diels–Alder chemistry reaction usually proceeds at moderate reaction conditions without a metal catalyst. The reaction is thermal reversible between a diene and a dienophile, and the synthesized polymer is decomposed into the original monomer when heated.⁴⁶ The Diels–Alder reaction has high reaction efficiency, especially in water, since the reaction rate was reported to be up to 10^4 times compared to the rate in organic solvents.^{47,48} The bioink formed by the Diels–Alder reaction exhibits good shear thinning, excellent printable performance, and long-term stable shape fidelity.⁴⁹ For instance, the PEG crosslinking bioink modified by Diels–Alder reaction maintains the mechanical properties of the printed constructs and effectively improves cell viability (90–95%).⁵⁰ For the hydrogels formed

with Diels–Alder adducts and hydrazone bonds, the adjustment of viscoelasticity is accomplished by changing the ratio of two types of crosslinks. Hydrazone crosslinks displayed dynamic properties and a short lifetime (in the order of ~ 800 s). This makes the resulting hydrogels easy to process during the first stage of gelation. The Diels–Alder cross-linking also enhances the mechanical strength and structural stability of the hydrogel network. Hence, these hydrogels are suitable for extrusion-based 3D printing.⁵¹

2.4 Thiol–ene reaction

Thiol–ene chemistry is carried out by a stepwise growth polymerization mechanism, containing three steps.⁵² Firstly, the thiyl radical is added to the carbon of ene group. Secondly, the hydrogel of the thiol group is extracted by the carbon radical and then transferred to thiyl radical. Lastly, the reaction is terminated by radical coupling.

Thiol–ene click reaction enables the formation of the covalent bond between thiolated (–SH/thiol) molecules and alkene (C=C double bond) groups with the “ene” groups containing vinyl, allyl, and norbornene.⁵³ This reaction products have low volumetric shrinkage, less sensitivity to oxygen,⁵⁴ and fast reaction kinetics.⁵⁵ If there are some compounds with different groups, a heterogeneous polymer network will be formed.⁵⁶ Thiol–ene can be carried out in a mild environment to obtain highly biocompatible hydrogels. Some natural and synthetic polymers can be functionalized with thiol or ene groups, such as hyaluronic acid (HA), gelatin, alginate, and polyethylene glycol.

Photoinitiated thiol–ene chemistry is a well-suited technique for handling compounds that require a low/oxygen-free environment for efficient cross-linking. It is an efficient, orthogonal chemical reaction with good oxygen resistance and relatively fast kinetics, and can form a homogeneous hydrogel network.^{57,58} These properties make the thiol–ene reaction suitable for bioprinting. Since the thiol–ene click reaction follows the base catalysis mechanism, the reaction process is characterized by fast gelation speed and controllable gelation time. The gelation time varies from 18 s to 2 min depending on the pH, molar ratio, and polymer concentration conditions.⁵⁹ The homogeneous network hydrogel *via* thiol–ene photocrosslinking provides a suitable environment for cell encapsulation. For instance, the keratinocytes loaded onto a thiol–ene produced hydrogel enabled the formation of a compact, dense, skin-like epidermal layer.⁶⁰ Additionally, hMSCs encapsulated in thiol–ene cross-linked hydrogels achieved proliferation and diffusion within one day.⁶¹ This is because reason thiols can adjust the stress relaxation of the crosslinked network structure such that excess free thiols react with thioesters in the linker through transesterification reaction to generate new thioesters and release thiolate. This pathway for the generation of new thioesters and release of thiolate accelerates the stress relaxation rate of the cross-linked structure and adjusts the viscoelasticity. This relaxation ability also allows the cells to spread through the gel.

2.5 Thiol-Michael reaction

In the 1960s, Allen, Fournier, and Humphlett first reported the thiol-Michael addition reaction.⁶² This reaction involves heteroatomic donors of thiol and electron-deficient enes. During the reaction process, a thioester bond is formed by the addition of the thiol group to the double bond of vinyl sulfone, acrylate, or maleimide.⁶³ The formation of a side reaction disulfide bond promotes the use of protective groups. As a high-efficiency and modular click reaction, the thiol-Michael addition reaction is performed in mild, solvent-free conditions,⁶⁴ with the reaction rate of Michael addition related to the electron deficiency of the acceptor.^{65–67} Increasing the concentration of the thiolate anion and pH enhances the gelation and storage modulus.^{68,69} Different groups can be utilized to modulate gelation in thiol-Michael addition click reaction. The gelation time of poly(*N*-isopropylacrylamide) (PNIPAAm) hydrogels fabricated by thiol-vinyl, poly(ferrocenylsilane)-PEG based hydrogel prepared with thiol-acrylate, and dextran-PEG hydrogel crosslinked with thiol-acrylate is 25–40 s, 60 s, and 22–50 s respectively.^{70–72} Thiol Michael addition reaction has been applied in cross-linked hydrogel synthesis for cell encapsulation. For instance, PEG crosslinking bioinks formed by thiol-vinyl sulfone were reported to have a larger printable range than that of PEGX-ACR, with the viability of encapsulated cells ranging from 90–95%.⁵⁰ Furthermore, the storage modulus of bioinks formed *via* the thiol-Michael reaction, in the weak phase, is ~ 350 Pa, which is larger than the storage modulus of PEGX-gelatin bioinks.⁷³ Hyaluronic acid (HA) modified with thiol groups (HA-SH), and poly(ethylene glycol) (PEG) functionalized with vinylsulfone (PEG-VS) were crosslinked to form 3D network hydrogels within 14 min, *via* thiol-Michael addition reaction.⁷⁴ The chondrocytes were homogeneously dispersed into the hydrogels and showed increased adhesion and proliferation of human fibroblasts cells. These features enable Michael addition chemical reactions to be used in tissue engineering for novel bioink applications.

2.6 Oxime click reaction

The oxime click reaction, containing similar orthogonal functionalities, occurs between an aldehyde or ketone group and aminoxy or hydrazide group. The formation of oxime bonds does not require catalyst, UV, or a high temperature, and has been reported to have a high reaction rate and chemoselectivity, with water constituting the only byproduct.^{75,76} This allows the oxime reaction to synthesize environmentally friendly and highly functional polymers. Moreover, the dynamic characteristics of the reaction give the oxime group material reversible covalent properties.⁷⁷ Compared to semicarbazone and hydrazone gels, oxime gel presents frequency dependence with good viscoelasticity.⁷⁸ These bioinks have good printability and form a stable grid structure. The oxime bond formed by aminoxy under water conditions increases the stability of the hydrogel.⁷⁹ After the functionalization of RGD adhesion peptide with a ketone, MSCs were encapsulated in hydrogels cross-linked with oxime to determine cell viability.

The results showed that cells survived in the crosslinking process and proliferated. The disadvantage of oxime chemical reactions for bioconjugation is the necessity of neutral pH conditions to reduce the possibility of the oxime exchange reactions.¹⁶

2.7 Aldehyde hydrazide reaction

Aldehyde hydrazide reaction as a dehydration reaction that involves the bonding of aldehyde molecules with hydrazide polymers without light irradiation, to form a hydrazone bond. This reaction is simple, versatile, and without toxic end products with high reversibility. Compared to the oxime reaction, the crosslinking network structure fabricated by hydrazone is more stable.

Aldehyde hydrazide click chemistry reaction is suitable for 3D bioprinting. The crosslinked hydrogel prepared with aldehyde hydrazide reaction exhibits rapid gelation. The gelation time of hydrazone crosslinked alginate-hyaluronic hydrogel is from 30 s to 5 min, and is determined by polymer concentration and components.⁸⁰ These hydrogels can support human pluripotent stem cell-derived neuronal cell growth, and lowering polymer concentration is beneficial for neuronal growth. Aldehyde-modified HA and carbonylhydrazide-functionalized gelatin enable the formation of the hydrogel in seconds. The pore size of these hydrogels ranges from 15 μm to 55 μm , making it suitable for the migration of endothelial cells.⁸¹ These injectable hydrogels showed prolonged degradation ranging from 1 day to 3 weeks in PBS at 37 $^{\circ}\text{C}$, which is beneficial for inducing angiogenesis.⁸¹ In addition, the hydrolytic degradability capacity can be adjusted at neutral pH values, and the time range is from weeks to months.⁸² Thus, the clearance rate of the printed scaffold can be controlled.

Having explored the different click reactions, several limitations that may affect their utility in the preparation of bioinks become apparent. For instance, the application of CuAAC chemistry in practical 3D bioprinting can be limited by copper toxicity with structural heterogeneity due to poor diffusion of copper in the bioink.⁸³ The application of the CuAAC may also be limited by poor spatial and temporal control during fabrication. Toxicity concerns may also limit the applicability of thiol-ene chemistry since there is a risk that the radicals employed to initiate the reaction are toxic to cells that are encapsulated.⁸³ The challenge of long gelation time may also limit the applicability of Diels-Alder and CuAAC click reactions for cell encapsulation. For the photo initiated click chemistry (*i.e.*, thiol-ene) there may be a reduction in the reduced biocompatibility of the bioink when a UV-sensitive initiator is used.⁸³

3. 3D bioprinting techniques

Three-dimensional (3D) bioprinting, deriving from additive manufacturing, has been developed significantly over the past decade. These strategies provide the application foundation for tissue engineering and regenerative medicine. It involves 3D printing technology, cell biology, material science, and other

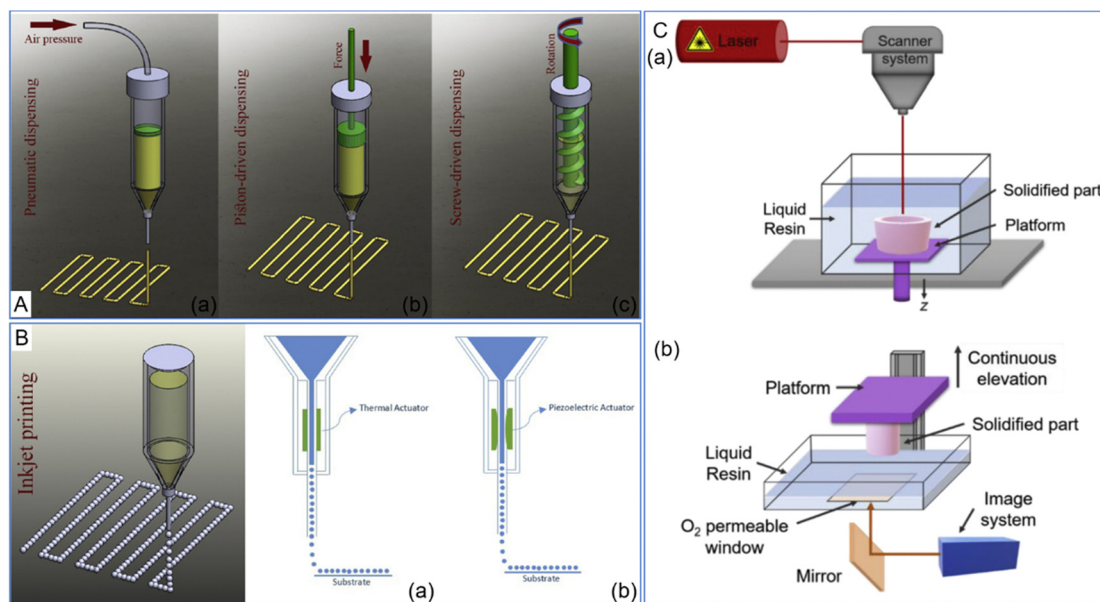


Fig. 2 Schematic illustrations of bioprinting techniques. (A) Extrusion bioprinting. (a) Pneumatic, (b) piston-driven, and (c) screw-driven dispensing method. The three driving forces are air pressure, mechanical displacement, and rotation to drive the continuous flow of biomaterials through the nozzle⁸⁷ (Copyright 2018 Elsevier B.V.). (B) Inkjet printing method. (a) The thermal printing head uses a heating element to increase the local temperature and generate bubbles to drive the droplets through the nozzle. (b) When a piezoelectric head is used with a material, the shape of the material changes and is pushed out under the voltage⁸⁷ (Copyright 2018 Elsevier B.V.). (C) Stereolithography bioprinting. (a) Conventional stereolithography, (b) continuous liquid interface production⁸⁸ (Copyright 2020 Elsevier B.V.).

disciplines. Generally, biomaterials used for 3D bioprinting have the ability to load biomolecules and living cells.⁸⁴ During bioprinting, units with micrometer accuracy can fabricate target products through depositing bioinks onto the platform. Owing to printing and deposition of living cells, 3D bioprinting has some advantages compared with traditional printing, such as precise control of the cell distribution and cell deposition with high resolution.⁸⁵ In general, 3D bioprinting process is divided into three steps: (1) acquire the information of the desired area and structure from the medical images, including magnetic resonance imaging (MRI) or computed tomography (CT),⁸⁶ and then design the 3D model using CAD software; (2) choose the appropriate bioprinting process for different bioinks, such as cells, growth factors; (3) post processing. Form connections between dispersed cells, and then obtain certain functions of tissue or organ with some methods.⁸⁴ In this

section, the 3D bioprinting strategies related to click chemistry are discussed (Fig. 2 and Table 1).

3.1 Extrusion bioprinting

The extrusion bioprinting technique has a wide range of selectivity for cells and materials with the ability to disperse highly viscous bio-inks with high cell density. The extrusion bioprinting system forms 3D structure of layer-by-layer fabrication *via* continuously squeezing bio-inks through nozzles.⁸⁹ The typical extrusion bioprinting system has four components. (1) Dispensing head. It consists of a syringe or cartridge carrying bioinks and can control temperature. (2) Positioning system. It moves the dispensing head along the *X*, *Y*, and *Z* directions, and controls the accuracy of arriving at the target position. (3) Printing platform. This platform controls the position and temperature. (4) Computer. The computer can

Table 1 Comparison of 3D bioprinting techniques

Bioprinting methodology	Extrusion bioprinting	Stereolithography bioprinting	Inkjet bioprinting	Ref.
Printing mode	Line-by-line	Layer-by-layer	Drop-by-drop	168
Processing speed	Slow ($10\text{--}50\ \mu\text{m s}^{-1}$)	Fast ($<1\ \text{h}$)	Fast ($1\text{--}10\,000\ \text{droplet s}^{-1}$)	93,169,170
Viscosities of bioinks	$30\ \text{mPa s}^{-6} \times 10^7\ \text{mPa s}$	No limitation	$<10\ \text{mPa s}$	85,93
Cell viability	80–90%	$>90\%$	80–95%	120,121,149,171
Cell density	High density ($>10^8\ \text{cells mL}^{-1}$)	Medium cell density ($<10^8\ \text{cells mL}^{-1}$)	Low cell density ($<16 \times 10^6\ \text{cells mL}^{-1}$)	84
Resolution	100 μm	100 μm	50 μm	120,121,172
Quality of printed construct	Good	Good	Poor	173
Printer cost	Moderate	Low	Low	118,172
Click reaction	Thiol-ene, CuAAC, Diels-Alder, aldehyde-hydrazide,	Thiol-ene	CuAAC, thiol-ene,	14,33,101,110,113,132, 138,155,160,164,167,174

adjust the relevant parameters, involving the position and temperature. At the beginning of printing process, the bioinks are loaded into syringe or cartridge. Then, the bioinks are extruded through the nozzle under the drive of pneumatic or mechanical to form continuous filaments. That is arranged on the platform following the predetermined trajectory. Finally, the desired model is obtained through layer-by-layer construction.⁹⁰

Generally, there are three driving modes for extrusion bioprinting, which are pneumatic driven, piston driven, and screw driven respectively. The principle of pneumatic driven is to use compressed sterilized air as a driving force to dispense liquid. And the viscosity of the bioinks plays a vital role in the printing process. Due to its shear thinning property, hydrogels can remain filament state after extrusion. This shows that hydrogels with a wider range of viscosity can work sufficiently with a pneumatic drive system. The disadvantage is that the deposited mass is difficult to accurately control. In piston driven system, the guide screw connects the piston and motor. During the operation, the rotating motion of the guide screw drives the piston to achieve linear movement, so as to extrude the bioinks from the nozzle to form a filament. This system is suitable for high viscosity biomaterials due to mechanical force driving. Screw driving is also a mechanically driven system. It is similar to the piston-driven system in that the screw is used to connect the motor and extrude bioinks without compressed air. This system provides higher pressures than piston driven system and is suitable for biomaterials with higher viscosities. Extrusion 3D bioprinting has several advantages, such as good flexibility, versatility, high printing speed, and easy operation. Nevertheless, cell deformation and even apoptosis induced by shear stress during extrusion are the main disadvantages.⁹¹

Extrusion bioprinting fabricates the persistent filaments under continuous extrusion pressure to provide well-defined structural integrity. Therefore, this technology is used to form some viscous biomaterials and cells with different densities.⁹² Bioinks with viscosity ranging from 30 mPa s to 6×10^7 mPa s and high cell densities ($>10^8$ cells mL⁻¹) are suitable for extrusion bioprinting, which follow non-Newtonian fluids.^{93,94} Bioinks with high viscosity provide structural support for printed tissues/organs, however the higher shear stress is harmful to encapsulated cells.⁹⁵ In contrast, low viscosity bioinks provide cellular bioactivity for the target product and minimize nozzle-clogging, but cannot retain shape following extrusion leading to poor feature definition.^{96,97} Its viscosity will decrease when subjected to deforming forces during the extrusion process. The relationship between steady-state viscosity (η) and shear rate ($\dot{\gamma}$) of bioinks is characterized by fitting the power law equation ($\eta = K\dot{\gamma}^{(n-1)}$) and derived values of consistency index (K , defined as the viscosity when the shear rate is 1 s⁻¹) and shear-thinning index (n , also referred to flow behavior index).⁹⁸ The printability of bio-ink depends almost entirely on its shear thinning coefficient. For hydrogels of alginate, chitosan, xanthan gum (XG), kappa-carrageenan (κ CA), gelatin, and gelatin methacrylate (GelMA), they shear-thinned with $n < 1$.⁹⁹ After adding nanoparticles, the

shear-thinning behaviors is changed, and the n decreases from ≈ 1 to ≈ 0.5 , leading to retain the desired shape after printing.¹⁰⁰

Extrusion printing requires the filament to be able to maintain the stability of the pre-designed micro/structure during the whole printing process. The microbalance between the bioink viscosity and the filament rigidity is necessary for keeping the cell active and functional. It prevents cell membrane damage. According to research findings, the thiol-ene chemistry between thiol-modified peptide and norbornene-modified pectin offers precise regulation of hydrogel stiffness and micro-structure (Fig. 3).¹⁰¹ Matrix stiffness plays a major role in the cellular response of proteinase-degradable 3D hydrogels and controls biochemical and mechanical properties. During the reaction process, norbornene moieties supply rapid chain transfer power and relative polymerization rate due to their high electron density.^{65,102,103} Meanwhile, the addition of thiyl radical to the double bond leads to the significant relief of ring strain and the higher hydrogen-abstraction rate of thiol hydrogen by the carbon center radical.¹⁰² Since norbornene-modified pectin provides crosslinking and functionalization of post printing hydrogel, bioinks have a rapid curing rate. In consequence, the microbalance can also be tuned during the gelation process. The stable filament shape and printing resolution could keep the microstructure fidelity and avoid collapse, thus promoting printing accuracy and structural integrity as demonstrated in the study by Daniel *et al.*¹⁰⁴ In the study, gelatin modification was mixed with norbornene moieties (GelNB) and lithium phenyl-2,4,6 trimethyl-benzoylphosphinate (LAP) photoinitiation into bioinks, and then the influence of thiol-ene chemistry and LAP on extrusion bioprinting accuracy, was assessed.¹⁰⁴ It was determined that for two sizes of nozzles, 18 gauge (838 μ m i.d.) and 20 gauge (6–3 μ m i.d.), GelNB-based bioinks could be extruded smoothly through two sizes of nozzles to form a regular filament. On the other hand, GelMA based bioinks could be only extruded through the 18 gauge nozzle to provide regular filament. During deposition, GelNB was crosslinked *via* thiol-ene click chemistry. The storage modulus evolution was increased due to the addition of LAP and GelNB, which improve photocuring kinetics and construct fidelity. During the printing process, some parameters will affect the final structure, including temperature, extrusion pressure, speed, nozzle diameter, movement speed, *etc.*^{105–107} Changing the temperature condition can also be used to adjust the rheological properties of bioinks to maintain the shape of the filament for microextrusion printing. For instance, a 3.5% w/v GelNB-PEGdiSH showed gelation changes with temperature variations. The sol-gel transition takes place at 15 °C with the transformation of gelatin molecules from the coil to helix, and the gel-sol transition occurs at 37 °C, and the gel becomes liquid.^{108,109} For GelNB-PEGdiSH precursor, the storage modulus increases as the holding time increase due to the formation of helical structures. When the temperature was 37 °C, the gelation time of 3.5% w/v GelNB-PEGdiSH precursor was about 420 s, and G' stabilized within 40 min with a steady state value of 130 Pa. Similarly, when the precursor solution

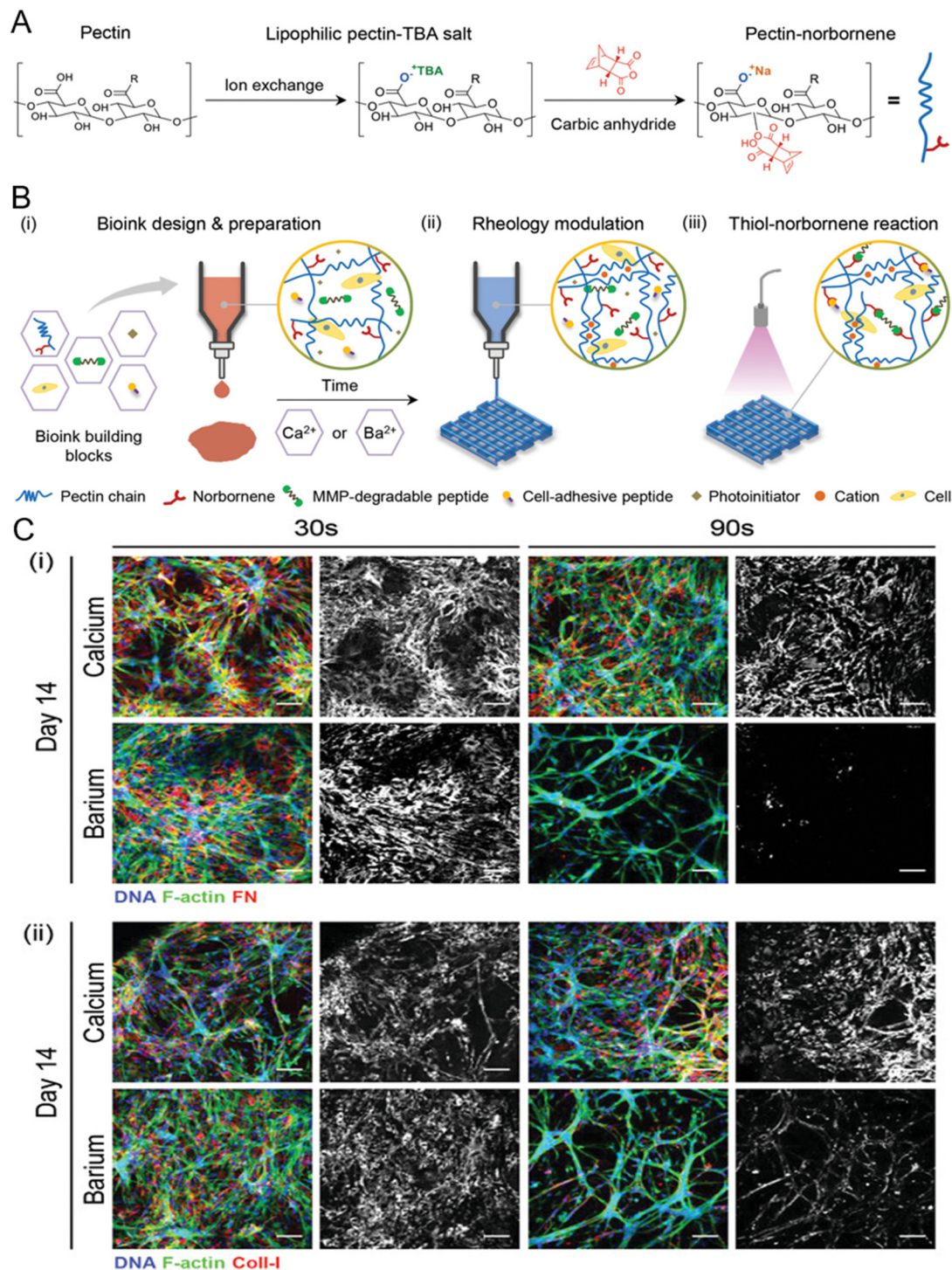


Fig. 3 The design and microstructure embedded by cells of photoclickable pectin bioinks. (A) The diagram of the synthesis of norbornene-modified pectin. (B) Bioprinting process contains bioink preparation, the adjustment of rheological properties of bioinks, and the photoinitiated thiol–norbornene reaction. This post-processing process occurs between the norbornene group and the cross-linker of the cysteine matrix metalloproteinase (MMP) sensitive peptide and the mono-cysteine cell–adhesive peptide. (C) Confocal images of cell morphology and ECM deposition in hydrogels, including fibronectin (red, Ci) and collagen type-I (red, Cii). The green and blue areas represent the F-actin and nuclei.¹⁰¹ (Copyright 2021 IOP Publishing).

was cooled to 4 °C and subsequently kept at 15 °C, G' stabilized at 150 Pa.¹¹⁰ These results suggest that, although the temperature-induced gelation process is time-dependent, the steady-state G' of the precursor at equilibrium depends mainly on temperature. The

printability of this system depends on rheological properties and printing temperature. By adjusting rheological properties with the change of temperatures, such as viscosity, yield stress, and shear modulus, it can become a universal system for bioprinting.

Click bioconjugation method has been popularly utilized to bind biomolecules to modify printed hydrogel. Combined with click conjugation, the heterogeneous hydrogel can be printed to provide defined products. Alkyne and azide groups facilitate complete bioorthogonal reactions for molecule binding.^{111,112} Ru(II)-Catalyzed click reaction has been utilized to conjugate alkyne-terminated poly(ϵ -caprolactone) (PCL) and azide-terminated peptide.¹¹³ These PCL-peptide conjugates have good thermal stability (85–95 °C, 2 h), such that M_n and PDI have no significant change. Thermal stability is an important factor in determining 3D printing of materials. Therefore, PCL-peptide conjugates are suitable for biofabrication through melt extrusion printing. This strategy successfully fabricated the heterogeneous scaffold with user defined spatial patterning of peptides by characterizing multi-material segmented printing. Some valuable growth factors or bioactive molecules are important for scaffolds.^{114–116} In the click reaction, alkyne-azide cycloaddition, *via* tethering these biomolecules to the scaffold, can be undertaken to achieve post 3D printing surface modification. The process is as follows: functional molecules of bioinks, 3D printing, and functional scaffold with active biomolecules *via* click reaction after printing. Matthew L. Becker *et al.*³² covalently fixed osteogenic growth peptide (OGP) or bone morphogenic protein-2 (BMP-2) peptides on poly(ester urea) (PEU) scaffolds through CuAAC post printing.³² Before printing, the tyrosine monomers were modified by propargyl, and azide-peptides were synthesized, which were then used to attach peptides to PEU for post-3D printing. During filament production and extrusion printing, the structure of propargyl was retained. The results showed that PEU scaffolds functionalized with OGP and BMP-2 peptides improved *hMSCs* osteogenic differentiation.

3.2 Stereolithography bioprinting

Stereolithography (SLA) bioprinting is a nozzle-free 3D printing technology that achieves layered curing by photoinitiation. Based on the principle of polymerization of ultraviolet photosensitive materials, the liquid photosensitive polymers are selectively solidified layer by layer, to build the 3D models from the bottom up.¹¹⁷ A complete SLA system includes fluid container filled with photosensitive materials, light source (usually choose UV, visible light, or laser), control system for controlling the movement of light beams in a horizontal movement, and platform that can move in a vertical direction.¹¹⁸ The liquid photosensitive materials contain monomers, photoinitiators, and additives.

The process of stereolithography bioprinting is as follows. Before printing, the appropriate amount of liquid photosensitive materials were added to the fluid container. The platform is below the liquid level, just one layer. According to the slicing layer of the software, the polymer solution is rapidly solidified at the specific areas *via* a patterned UV/laser beam scanning the surface of the liquid to form 2D patterns as the first layer. Then the platform moves by a defined layer height in the vertical plane, and the liquid flows to this level, subsequently solidifying the second layer on the top of the first layer.^{118,119} This

process is repeated using layer-by layer, and the platform moves stepwise until the whole model is printed to obtain a 3D construct. In the printing process, all the complete patterns are projected onto the printing plane. Therefore, the printing process takes the same time, even if the pattern is complex in one layer. This reduces the printing time of the whole process, about less than 1 h.^{120,121} SLA has the characteristics of high spatial resolution ($<100\ \mu\text{m}$ ^{120,121}), excellent quality, rapidly printing speed (draw rate $\sim 500\ \text{mm h}^{-1}$ ¹²²), and the potential to mimic and print the complex structures of tissues/organs. Curing kinetics can be adjusted by controlling print parameters, such as light intensity and exposure time. UV spectrum with wavelength of 100–400 nm is usually utilized to achieve fast photocrosslinking.^{123,124} The accompanying problem is that it is difficult to fully crosslink the cell loading hydrogel within 30 seconds, and it usually takes several minutes. Prolonged exposure to UV light can trigger DNA damage^{125,126} or cell cancerization.^{127,128} Given these considerations, the light sources with wavelength of 405 nm were introduced to implement fast crosslinking. The ultrafast crosslinking process was achieved within 10 seconds, and obtained the hydrogel with 8 mm diameter exhibited higher cell viability (over 90%).¹²⁹ The drawbacks of stereolithography are cytotoxicity induced by photosensitizers and the risk of cell damage, which limits its use.

Stereolithography approach assisted with thiol-ene click reaction can be utilized to develop a prepolymer. This constitutes an effective pathway to keep the geometry with high resolution for 3D printing. It is suitable for various polymer precursor systems, which are synthesized by polymer or ceramics with appropriate treatment.¹³⁰ Photoresins produced by thiol-ene reaction is appropriate to stereolithography, which forms a highly crosslinked gel and provides the opportunity to functionalize the surface. For example, for poly(ethylene glycol) divinyl ether and pentaerythritol tetrakis(3-mercaptopropionate), polymer initiated by the wavelength of 266 nm UV light has good biocompatibility.¹³¹ The solutions containing more than 2:1 thiol group result in the functionalization of thiol groups on the surface, such as utilizing copper-catalyzed azide-alkyne cycloaddition chemistry. The initiator-free stereolithographic method combined with thiol-ene reaction has the potential to fabricate scaffold-like structures *via* 3D bioprinting. During the prepolymerization process, there is no gelation phenomenon, which reduces the polymer inner stress and compensates for the volume shrinkage. The cross-linking points are uniformly distributed in the gel, resulting in a homogeneous network without defects. A. Hoffmann *et al.* developed three-component thiol-ene material systems for stereolithography, that are two monomers (5-vinyl-2-norbornene and 1,10-decanedithiol) and one crosslinkers (1,3,5-triallyl-1,3,5-triazine-2,4,6(1*H*,3*H*,5*H*)-trione or glyoxal bis(diallyl acetal)).¹³² The results showed that prepolymer photo resin of two monomers improves the mechanical properties. The elongation and elastic modulus of the prepolymer with two monomers and crosslinker of 1,3,5-triallyl-1,3,5-triazine-2,4,6(1*H*,3*H*,5*H*)-trione are 32.4% and 30.1 kPa respectively, which is higher than

un-prepolymer. The polymer with a crosslinker of glyoxal bis(diallyl acetal) has the same phenomenon. The prepolymer has a higher elongation (19.1%) and elastic modulus (40.8 kPa) than the un-prepolymer. In addition, prepolymerization is also suitable for the preceramic polymer. The infusible thermosets are printed using preceramic polymer solution *via* photocuring. The Si-based preceramic polymers with C=C bonds contain polysiloxane, polycarbosilane, and polycarbosilazane with side vinyl groups.¹³³ In the process of photocuring and printing, the free radicals produced by the cracking of the photoinitiator initiate the reaction between the thiol group and alkene groups. Finally, rigid infusible thermosets products with defined geometries are obtained. This method can be applied to polymer derived ceramics, producing a ceramic structure with a smooth surface and fully dense for the various fields.

Stereolithography printing enables crosslinking *via* free radical chain growth under photo irradiation. The crosslinking of polymer molecules allows the liquid to solidify rapidly under the irradiation of UV. For example, terpenes are an excellent choice for the manufacture of photocrosslinked resin due to their double-bond characteristics. For five terpenes, limonene, terpinene, geraniol, nerol and linalool, that have a thiol-ene reaction with pentaerythritol tetrakis(3-mercaptopropionate) (PETMP) respectively.¹³⁴ After irradiation of UV, these photocrosslinked polymers displayed elastomeric behavior. The strain at break of limonene with the treatment of irradiation is 180%, linalool, nerol, and geraniol have similar fracture strain, from 92% to 110%.¹³⁴ These strain properties are significantly better than current materials with the strain of 50% or less.^{135–137} The materials treated with this method have extremely low shrinkage (less than 1%), which can be successfully used for microstereolithography 3D printing.

However, the uncontrolled polymer chain growth in free radical polymerization results in networks with characteristic robust, brittle, highly shrinkage, and residual stress issues.¹³⁸ The stereolithography materials also have low viscosity and elastic deformation,¹³⁹ which limits application. thiol-ene photochemistry enables the creation of a crosslink network with little shrinkage under a small dose of light.⁵⁴ The molar volume change per reacted double bonds of thiol-ene reaction is 12–15 mL mol^{−1}, which is much lower than the molar volume change of the acrylate double bonds, 22–23 mL mol^{−1}.^{140,141} The chain growth polymerization of free radical between alkene and thiol control the network density and mechanical properties.¹⁴² The combination of stereolithography and thiol-ene chemistry can solve the incompatibility of oxygen-inhibited for delamination. R. F. Shepherd *et al.*, developed a rapid gel speed of thiol-ene, about $\sim 3 \text{ cm h}^{-1}$, under the little photodosages, $H_e \sim 10 \text{ mJ cm}^{-2}$.¹³⁸ The prepared materials with this strategy have a wide range of mechanical properties, including elastic moduli ($6 < E < 287 \text{ kPa}$), ultimate elongation ($48\% < \gamma_{\text{ult}} < 427\%$), ultimate stresses ($13 < \sigma_{\text{ult}} < 129 \text{ kPa}$), toughness ($16\text{--}37 \text{ J m}^{-3}$), great fatigue resistance, and rapid autonomic self-healing (Fig. 4). Hoyland *et al.*,¹⁴³ introduced four-armed thiol pentaerythritol tetrakis (3-mercaptopropionate) to allyl modified poly(carbonate) to form cured resin. The

mechanical properties, such as Young's modulus ($13.1 \pm 0.5 \text{ MPa}$), ultimate tensile strength ($3.0 \pm 0.1 \text{ MPa}$), and elongation at break ($22.6 \pm 1.0\%$), are applicable to cartilaginous tissues. After the cell culture 5 days, intervertebral disc cells have 100% survival rate on the crosslinked network. A. Linnenberger *et al.*, decorated polyethylene glycol dimethacrylate (PEGDMA) with RGD, thiol-ene, and thiol-ene modified with RGD.¹⁴⁴ The cells patterned in thiol-ene with RGD have the great viability and fuses in 4 days after encapsulation, which results in the initial stages of multi-nucleated cells. Therefore, these hydrogels have good biocompatibility.

Kagome tower constructs under the compressive load of 5% 6000 materials at $F = 0 \text{ N}$ (c), (d) 5% 186 at $F = 1 \text{ N}$, (e) 5% 6000 at $F = 1 \text{ N}$, (f) 2.5% 6000 at $F = 1 \text{ N}$.¹³⁸ (Copyright 2017 The Royal Society of Chemistry).

In stereolithography printing, the poor solubility and poor reactivity of some photosensitive polymers, limit the *in situ* formation of biomaterials.¹⁴⁵ To circumvent this issue, two-photo approaches combined with [2+2] cycloaddition can be used. The principle is to absorb two photons simultaneously at the same point on a liquid photosensitive polymer, as one photon with two wavelengths. Moving the focus solidifies the 3D structure without using liquid photosensitive polymers to build a platform inside. The principle of maleimide reactivity in two-photo mode is that the reactivity is determined by excitation of low absorbance transition, breaking up the formation of donor-acceptor polymer.¹⁴⁶ This showed the formally forbidden pathway of the [2+2] cycloaddition chemistry. This technique achieves a resolution of up to 100 nm, which is the highest resolution among all 3D printing technologies.¹⁴⁷

3.3 Inkjet bioprinting

Inkjet 3D printing, as a non-contact printing form, is also the most commonly used method in biological 3D printing. The operating principle is that ultrasound or heat drives bioink droplets to be sprayed onto the defined position on the platform, and eventually build up a complete pattern *via* layer by layer. The basic characteristic of this technology is microdroplet, high flux, non-contact, and on-demand drop.

Generally, inkjet printing can be classified into two categories, drop-on-demand inkjet system and continuous inkjet system. These two technologies can precisely deliver varieties of different materials and cells to specific locations to build the complex and heterogeneous biomimetic structures without contamination and ink waste. The diameter of inkjet head, about 50 μm , is similar to a single nonadherent cell (10–30 μm). The tiny droplets sprayed by the print head are the basic forming unit of inkjet printing.¹⁴⁸ The volume of droplets generated by inkjet printing is 1–100 pL, and the spread radius is 10–50 μm after dropping onto the platform,¹⁴⁹ which is suitable for high-precision localization of microscopic biological elements in digital patterns. The biomaterials used in inkjet bioprinting require low viscosity¹⁵⁰ to avoid nozzle clogging. Higher standards are also required because fluid density and surface tension of biomaterials hinder their flow and droplet formation. The recommended parameters for biomaterials for

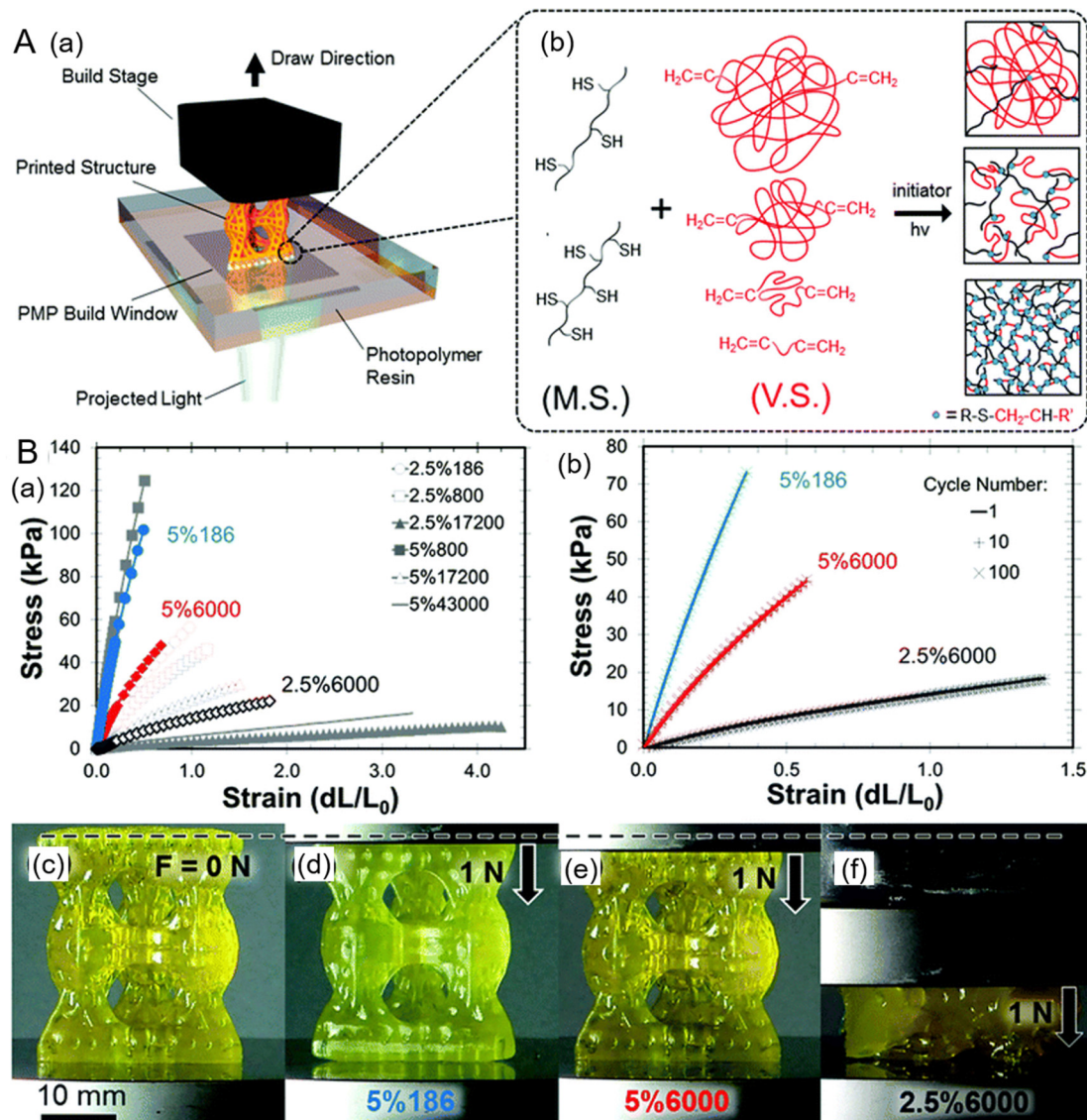


Fig. 4 Stereolithography based on thiol-ene photochemistry and its mechanical behavior. (A) Stereolithography printer and thiol-ene reaction. (a) 3D construct is printed under patterned light. (b) Schematic diagram of the photopolymerization reaction. (B) Mechanical properties of printed objects. (a) Data of tensile tests to failure. (b) Cyclic tensile test with the ultimate elongation of 75%.

inkjet printing are as follows: viscosity of 3–30 mPa s, the surface tension of 20–70 mJ m⁻², and density of ~1000 kg m⁻³.¹⁴⁹ An important problem of inkjet bioprinting is that suspended particles larger than the diameter of the nozzle orifice (~50 µm) can cause nozzle clogging,¹⁵¹ low viscosity prevents build-up, and low strength. Bioinks loaded with cells must not exceed a specific cell density, $\rho \leq 1 \times 10^6$ cells mL⁻¹.¹⁵² Because it has been shown that high cell concentration is directly proportional to viscosity. The settling effect of biological cells will also lead to nozzle obstruction, resulting in the heterogeneity of the printing structure.^{153,154}

The molecules of bioinks are decorated to modulate the viscosity properties, resulting in a stable image on the surface of the platform. Increasing the solubility enables the control of the concentration of materials and, thus, the properties of the

printed material. For some supermolecular polymers, such as polyimide, the chain-folding limits the solubility and prevents the adjustment of the concentration of printable material. Click cycloaddition chemistry has previously been adopted to develop poly(ethylene glycol) with the chain-folding diimide residue.¹⁵⁵ Two chain folding motifs are introduced into polyimides to improve the solubility. These orderly chain-folding polyimides are highly soluble in chloroform and THF compared with random polymers,¹⁵⁶ with the absence of the diol viscosity modifier considered as the main reason for the low viscosity. The π -electron rich polymer 15 and π -electron deficient polyimide 14 are successfully deposited *via* piezoelectric drop on demand inkjet printer.¹⁵⁵

During inkjet printing process, the shear force generated in the process of bioink extrusion can deform the biomolecules

and cells of bioinks, thus limiting the application of inkjet bioprinting technology.^{157,158} The post functional *via* click reactions can protect the biomolecules and brings better printed products, such as mesoporous silica microdots arrays. Inkjet printing, evaporation-induced self-assembly (EISA), and click chemistry are combined. Before printing, azide group modified microdots were prepared with (3-azidopropyl) triethoxysilane (AzPTES)³³ and then the condensation reaction of AzPTES and TEOS occurred during the EISA process.¹⁵⁹ When one layer is completed, the second layer is deposited and subsequently cured. A biobased elastomer, consisting of an unsaturated diacrylate monomer and partially oxidized silicon-based copolymer, is constructed by adopting this strategy.¹⁶⁰ Due to the shear thinning, these inks have low viscosity and shear rate ($\dot{\gamma}$) of above 10^1 s^{-1} . For inkjet printing, the shear rate ($\dot{\gamma}$) of ink is usually more than 10^4 s^{-1} .^{161,162} Therefore, the yield stress has sufficient ability to keep the structure after printing. During the inkjet printing, UV triggered thiol-ene reaction of bis(2-(acryloyloxy)ethyl)octadec-9-ene-dioat (AEOD) and [4-6% (mercaptopropyl)-methylsiloxane]-dimethylsiloxane (MMDS) disulfide oligomer, that formed crosslinked elastomer.¹⁶⁰ The printed elastomer has well reprocessed by compression molding, and the average tensile strength was recovered to 100% (Fig. 5).

For inkjet printing, the bioinks should have good stability. Agglomerations of some particles used in bioinks limit their application in inkjet printing. Thiol-ene click reaction effectively avoids the agglomeration and self-polymerization of monomers, improving stability and degree of cross-linking.¹⁶³ For example, carbon black modified with γ -methacryloxypropyltrimethoxysilane (MEMO) and sodium 3-mercapto-1-propanesulfonate (MPS) *via* thiol-ene reaction shows better self-dispersing properties, which is verified by zeta potential with the stable value.¹⁶⁴ The properties of microsized particles as drug delivery systems, such as dispersion, size dimensions, morphology, and release kinetics, can be modulated *via* inkjet printing and thiol-ene click chemistry. Bioinks, consisting of allyl-modified polycarbonates, semi-branched poly(glycidol allylglycidyl ether)s, and dithiol-PEG cross-linkers, are deposited on the platform *via* piezoelectric inkjet printing, subsequently the microsized particles with crosslinking network formed *via* thiol-ene reaction by UV irradiation.¹⁶⁵ The results confirmed that these microparticles had a uniformly spherical shape. And the particle size can be low as 2–14 μm *via* adjusting the polymer composition ratio of inks, that is suitable for distributing of microparticles into tissues. The particles with about 14 μm is considered ideal for bronchi, trachea, and

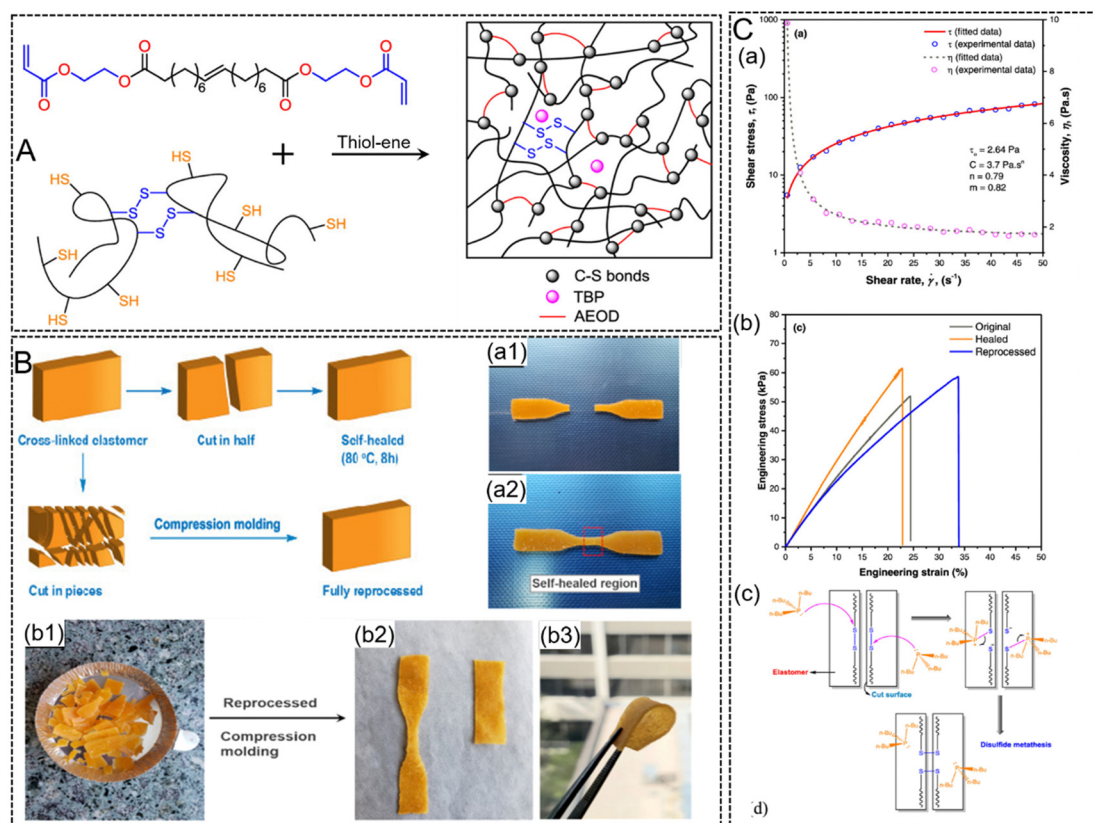


Fig. 5 Inkjet 3D printable biobased elastomer utilizing photoinitiated thiol-ene click chemistry. (A) Thiol-ene reaction between AEOD and MMDS-disulfide oligomer. (B) Inkjet 3D printing crosslinked elastomer with self-healed (a) and reprocessed (b) properties. (C) Rheological and mechanical properties of the ink and the self-healing mechanism. (a) Shear stress and viscosity of the ink as a function of the strain rate. (b) Typical engineering stress-strain curves of the original, self-healed, and reprocessed samples. (c) Schematic of the disulfide metathesis reaction during self-healing of the elastomer.¹⁶⁰ (Copyright 2020 American Chemical Society).

alveoli, owing to their even distribution.¹⁶⁶ The data from the cross-section of these bioinks show that fluorescent molecules have good integration. In other words, the loaded drug will be uniformly distributed in the micro-sized particles. The modified particles have excellent self-dispersibility and stability properties, that is suitable for preparing inks for inkjet printing.

The properties of inkjet printed materials could be evaluated using click chemistry, such as self-healing and stress properties. Micro-sized capsules are prepared through extrusion printing and inkjet printing. The polymer grid structures are manufactured *via* extrusion printing, and then the voids are filled with liquid polymer with the way of drop-on-demand.¹⁶⁷ Finally, the top layer of the capsule is enclosed through the extrusion process. When subjected to compressive stress, the liquid encapsulated in the microcapsule is released. Subsequently, the click reaction occurs. According to the change in fluorescence intensity of the dye, the self-healing properties are determined. This method can be applied to damage detection and reaction control and keep the active ingredients unaffected by the printing process.

Having explored the different click chemistry reactions and the common 3D bioprinting techniques it can be stated that different click chemistry reactions may favor different bioprinting techniques. For instance, the ability of some click reactions to be initiated *via* external coupling agents or functional groups (*i.e.* AAC and Diels–Alder) highlights that the resulting bioink may be employed in the fabrication of 3D structure using bioprinting techniques such as extrusion.⁸³ Similarly, cross linking *via* click chemistry (*i.e.* thiol–ene chemistry) that is based on exposure to photo initiators may so permit spatial control of the fabrication process by SLA printing.⁸³

4. Bioinks

Bioink refers to the solution of biomaterials or a mixture of various biomaterials and cells, in the form of hydrogel. The desired bioinks should meet three basic requirements, printability, good structural integrity and stability after printing and suitable cytocompatibility. The suitable bioink determines the quality of the defined target product and even the effectiveness of the future clinical application. Bioink can be used as filaments for extrusion bioprinting or as aqueous solutions for inkjet bioprinting. The choice of bioink depends on the specific application, such as the target tissue, cell type, and printing strategy. The composition and cell-loaded formulation of bioinks is the most crucial step for the success of bioprinting. A variety of natural and synthetic macromolecules or biomaterials have been taken as bioinks. Currently, macromolecules used as bioinks include hyaluronic acid, chitosan, alginate, cellulose, polyethylene glycol, pluronic, and polyvinylpyrrolidone, *etc.* In most 3D printing processes, the bioink is squeezed out and then quickly reaches a stable state. Due to the suitable viscosity or some external stimulus, the liquid bioinks are turned into solids, which is beneficial to maintain the printed structure.¹⁷⁵ Despite the development of bioinks,

viscous bioinks are subjected to shear forces during printing that reduces the viability of cells. Therefore, modification and design of bioinks are important to obtain a fine structure. In this section, we will focus on typical bioinks for bioprinting. The modification and application of click chemical reactions in bioinks are also introduced (Tables 2 and 3).

4.1 Hyaluronic acid bioink

Hyaluronic acid (HA) is a natural acidic glycosaminoglycan with good biocompatibility and favorable hydrophilic properties.¹⁷⁶ It can regulate the viscoelasticity of biological fluids through non-covalent bond interaction with water molecules, and plays a substantial role in cell migration, proliferation, differentiation and vascular regeneration.^{177–180} However, pure HA does not form mature bioinks satisfying multiple conditions due to its viscous-liquid behavior and lack of gelation ability to maintain a three-dimensional structure.^{181,182} The deficiency of HA can be effectively compensated by modifying HA with thiol or ene groups. This can solve issues in cell encapsulation, bioprintability, microcytotoxicity, and so on.

4.1.1 Norbornene-modified HA. Norbornene-modified HA (NorHA) macromer, used as representative bioinks, is cross-linked into hydrogel and improves printability, cellular compatibility and bioactivity.¹⁸³ Visible light irradiation occurs before bioink deposition to achieve *in situ* crosslinking *via* the thiol–ene reaction.¹⁸⁴ Stable hydrogel filaments were obtained and easily extruded. During the printing process, the shear force exerted on the cell reduced, thus, high cell viability (>85%) after 7 days of printing was maintained.¹⁸⁵ Mesenchymal stromal cells were evenly distributed into a 3D structure. After culturing in chondrogenic media, the compressive moduli of the printed disc increased from 5.2 ± 1.5 kPa to 42.0 ± 13.9 kPa. Biochemical content, including DNA, sulfated GAG, and collagen, also increased. Norbornene-modified HA combined with hydrazides-modified HA and aldehyde-modified HA to fabricate hydrogel with shear-thinning and self-healing properties for 3D bioprinting.¹⁴ The post-crosslinking of norbornene-modified HA improved the mechanical properties and stability of construct. After encapsulating 3T3 fibroblasts cells in these hydrogels, 80–90% viability was obtained. Photocrosslink interpenetrating network introducing into this hydrogel with thiol–ene reaction increased modulus, by ~300% with the hydrogel displaying good shape fidelity, stability, and cytocompatibility for fibroblasts. The viscosity of bioinks was improved as the concentration of NorHA increased, which is detrimental to inkjet bioprinting.¹⁸⁶ However, the addition of thiol-modified polymers to react with NorHA increases the crosslinking degree and has little effect on viscosity. This does not adversely affect the droplet formation ability of the bioinks. In addition, the increase in drug loading and concentration has no effect on the mechanical properties of printed gel.^{186,187}

HA bioinks decorated with norbornenes and methacrylates are capable of double crosslinking, with the use of thiol–ene crosslinking, facilitating the production of hydrogels with good printability and high cell viability. Indeed, high cell viabilities

Table 2 Detailed characteristics of typical bioinks for 3D printing

Type	Characteristic	Click reaction	Network precursor	Gelation process	Printer type	Cell type	Cellular concentration	Cell viability	Construct resolution	Construct shape and size	Applications	Ref.
Gelatin	Thermos-responsive, high cell viability and cell proliferation	Thiol-ene, thiol-vinyl, Diels-Alder	Gelatin-norbornene, thiol-modified gelatin, gelatin-vinyl, methacrylate, furan-gelatin, allylated-gelatin	Photo cross-linking	Extrusion, two-photon micro-fabrication, digital light processing (DLP)	HUVECs, MSCs, fibroblast cells, cardiomyocytes, human osteosarcoma cell line MG63, normal human dermal fibroblasts (NHDF)	5×10^6 cells mL^{-1}	>80% after 24 h	50 μm	500 μm	Vasculogenesis, vascular tissues, liver tissue	215–217, 232,234, 239
Hyaluronic acid	Cell carrier, promote cell proliferation, easily functionalization, hydrophilic, good viscosity	Thiol-acrylate Michael addition, SPAAC, thiol-ene, aldehyde-hydrazide	Thiol-modified HA, methacrylated HA, malic acid sodium HA, norbornene-HA	Photo cross-linking	Extrusion, inkjet printing	L929 cells, long-term neuroepithelial stem cells (ft-NES), human neuroblastoma cells, MSCs	2×10^6	>85% after 24 h	200 μm	Disk with 5 mm diameter, filaments with size of 200–700 μm	cartilage, cardiovascular tissue	14,186, 188,203, 208,211
Alginate	Short crosslinking time, modulated viscosity, good cell viability	Michael addition, thiol-ene, CuAAC	Norbornene-alginate, sulfhydryl-alginate, azide-alginate	Photo cross-linking	Extrusion	MSCs, L929 fibroblast cell line, human periosteum derived cells, HUVECs, hADSCs	10^6	>80%	200 μm	Ear scaffold with $35 \times 15 \times 15$ mm	Cartilage, micro-tissue, ear structure,	247, 249–251
Chitosan	Good mechanical properties, anti-bacterial activity	Michael addition, Diels-Alder	Maleic chitosan, furan-chitosan, algininate	Photo cross-linking	Extrusion	L929 cells, human U87 glioblastoma cells, human glioma U87-MG cells	7×10^5	>80%	200 μm	Grid line with approximately 600 μm wide, and the macro-pore of 1800 μm length	Bone tissue	174,281
Collagen	Minimal immune response, tissue regeneration ability, good cell carrier	Thiol-ene, CuAAC	Norbornene-collagen, thiol-collagen, methacrylamide-collagen	Photo cross-linking	Extrusion, SLA, two-photon microfabrication	Human dermal fibroblasts (HDFBs), HUVECs, L929 mouse fibroblasts	5×10^5	>90%	200 μm	Six layers with a height of 1.5 mm	Cartilage tissue	267,268
Cellulose	Renewable natural polymers, rich hydroxyl groups, good bioactivity, biodegradation	Thiol-ene, CuAAC	Norbornene-carboxymethyl cellulose, carboxy functionalized carboxymethyl cellulose, azido-hydroxyethyl cellulose, propargyl carboxymethyl cellulose, norbornene-methylcellulose	Photo cross-linking	Extrusion	hMSCs, NIH 3T3 fibroblasts, HUVECs, human immortalized skin fibroblasts cell line, mMSCs	2 M cells mL^{-1}	>90% after 24 h	20 μm	(Scaffolds with the of thick > 3 mm in height), lattice constructs with square-shaped pores	Spinal cord tissue	273,274, 276
Polyethylene glycol	Easily modification, good mechanical properties,	Thiol-ene, Michael addition reaction, aldehyde-hydrazide, SPAAC, Diels-Alder	Thiol-PEG, norbornene-PEG, azide-PEG, acrylated-PEG, vinyl sulfone-PEG, multivinyl-hyperbranched PEG (HB-PEG), hydrazide-PEG	Photo cross-linking	Extrusion, inkjet	mMSCs, L929 fibroblasts	5×10^6 cells per	>88% after 1 h, >80% after 24 h	200 μm	Lattice constructs with square-shaped pores, 3 mm diameter honeycomb, a hollow 2 cm tall \times outer diameter 10 mm and inner diameter 8 mm cylinder	Cartilaginous, ear, human nose, thyroid cartilage	43,50, 203,276, 281,283, 284,286, 288

Table 3 The functionalized bioink chemical structure for click reaction

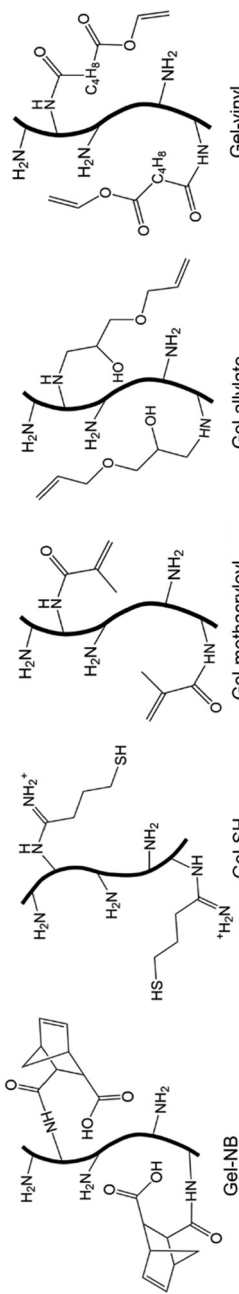
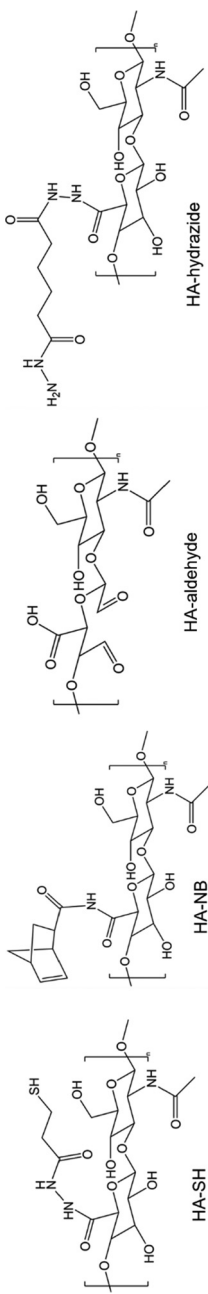
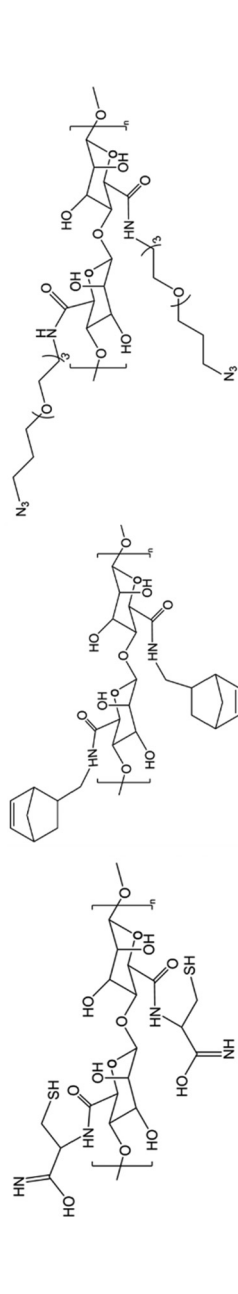
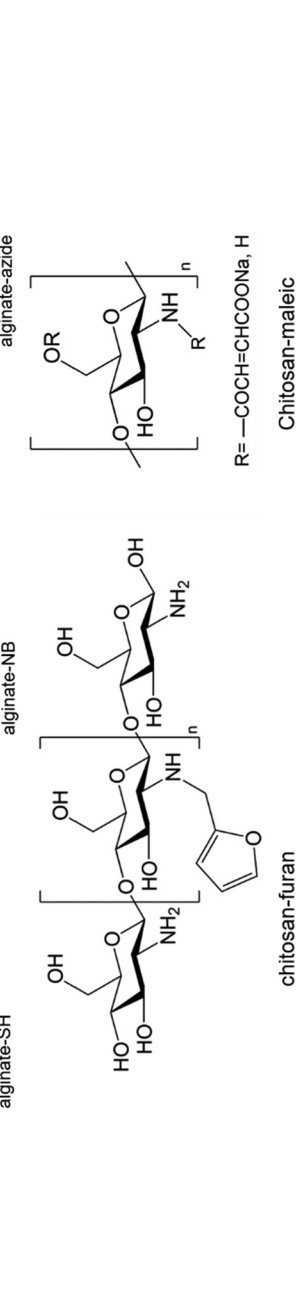
Type	Chemical structure
Gelatin	 <p>Gelatin</p>
Hyaluronic acid	 <p>Hyaluronic acid</p>
Alginate	 <p>Alginate</p>
Chitosan	 <p>Chitosan</p>

Table 3 (continued)

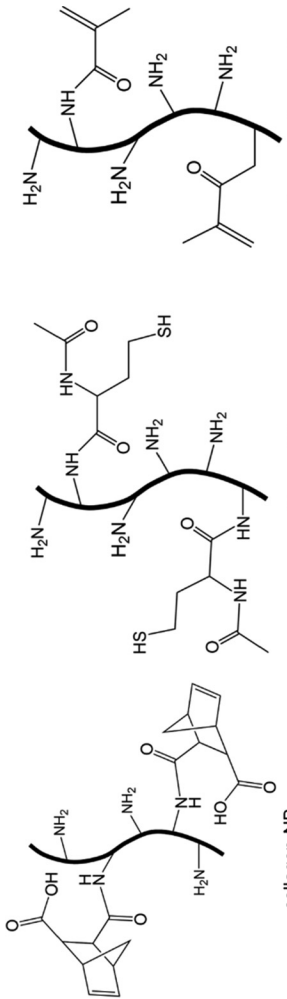
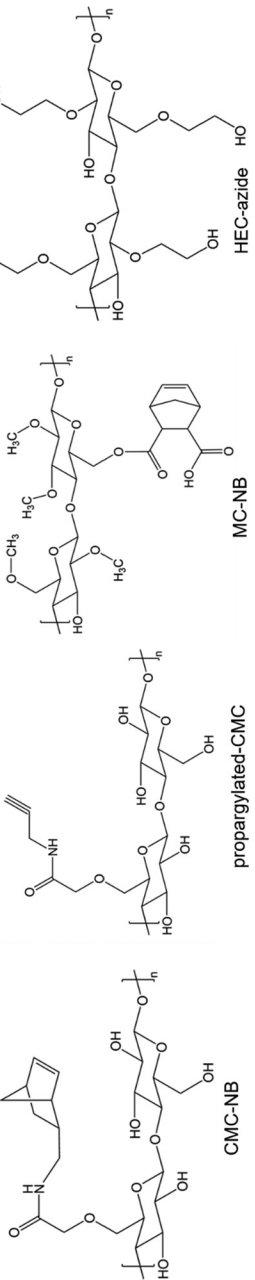
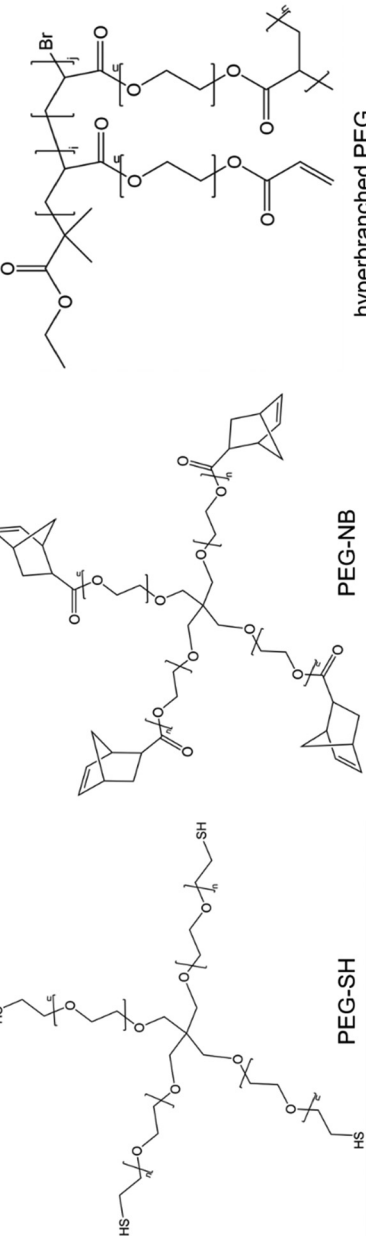
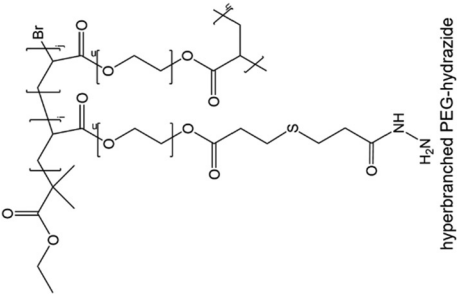
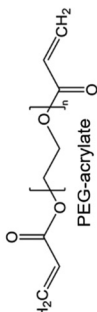
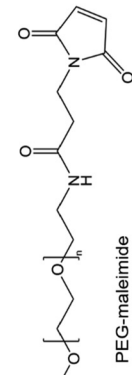
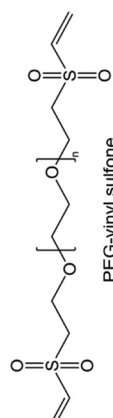
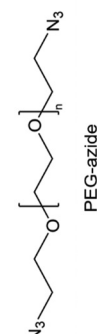
Type	Chemical structure
Collagen	 <p>collagen-NB</p> <p>collagen-SH</p> <p>collagen-methacryloyl</p>
Cellulose	 <p>CMC-NB</p> <p>propargylated-CMC</p> <p>MC-NB</p> <p>HEC-azide</p>
Polyethylene glycol	 <p>PEG-SH</p> <p>PEG-NB</p> <p>hyperbranched PEG</p>

Table 3 (continued)

Type	Chemical structure
	 <p>hyperbranched PEG-hydrazide</p>
	 <p>PEG-acrylate</p>
	 <p>PEG-maleimide</p>
	 <p>PEG-vinyl sulfone</p>
	 <p>PEG-azide</p>

of about 96% and 87% after day 0 and day 7 of printing were reported.¹⁸⁸ For the micro-scale printing process of the living cells, the hydrogel matrix provides a good substrate environment for cell attachment. Rapid solidification of hydrogels is critical in the printing process, since it prevents excessive dehydration of the printing droplets and can effectively maintain a stable structure. Hydrogel combined with thiolated hyaluronic acid and porcine gelatin (HyStem-C) crosslinked using PEG norbornene is suitable for 3D cell printing and culture.¹⁸⁹ For mammalian NIH-3T3 cells, they have been printed in HyStem-C hydrogel *via* quill lithography (QPL). At 18 h after printing, cells attach to the glass substrate, accompanied by diffusion and the growth of long pseudopodia. By 32 h, cells started to proliferate, and then by 100 h, cells began to escape the printed matrix and diffused into the glass surface. NIH-3T3 cells displayed efficient affinity, survival and proliferation.

For some biological tissues, such as knee meniscus, cartilage and myocardium, the anisotropy of ECM and cell arrangement play critical roles in some biological processes, including cell differentiation and proliferation. Currently, microfibers in the gel system are mostly randomly distributed without specific fiber direction, resulting in random cell proliferation or failure to support cell culture.¹⁹⁰ In order to introduce directional microfibers into the hydrogel, NorHA electrospun fibers were incorporated into bioinks. These cell-degradable bioinks were printed with extrusion bioprinting, and shear stress induced the alignment of microfibers and cell orientation.^{191,192} Bioinks with 3% GelMA showed the highest cell spreading and fiber alignment. The microfiber bioinks with 5% GelMA effectively supported the cell spreading and orientation alignment of MFC, MSC, and CF throughout the culture.¹⁹³

Norbornene-modified HA can be used to develop jammed microgel bioinks *via* thiol-ene crosslinked HA. Microgels, with a diameter of 100 μm , were previously prepared from NorHA, poly(ethylene glycol) diacrylate (PEGDA), and agarose, under light irradiation.¹⁹⁴ In jammed systems, microparticles are surrounded and fixed through physical interactions, resulting in macroscopic solid properties.¹⁹⁵ By removing the solution medium, microgels can be filtered to produce an extrudable ink. These ink of NorHA microgels exhibited shear-thinning and self-healing behavior. It has the properties of an elastic hydrogel under low strain, however, the inks yield under high strain.¹⁹⁴ These microgel ink could resist interaction force within the hydrogel to preserve the microstructure. After encapsulating cells in NorHA microgel, the high cell viability, about 70%, was obtained under jamming and printing. During the printing process, microgel bioinks effectively protect the cell and achieve heterogeneous structure.

4.1.2 Thiol-modified HA. Thiol-modified HA-based hydrogel is suitable for cell growth *via* providing good environment, for the production of bioactive and cell friendly bioinks.¹⁹⁶ Thiol functionalized HA (HA-SH), and allyl-modified poly(glycidol)s (P(AGE-co-G)) (as crosslinker) were crosslinked into hybrid hydrogels bioink *via* thiol-ene reaction

under light irradiation in the literature.¹⁹⁷ In the study by,¹⁹⁷ human and equine mesenchymal stem cells (hMSCs) were embedded into the printed cylindrical structure with cross-linking of 8 s, with the hMSCs shown to survive during the printing process and subsequently differentiating into chondrocytes after 21 days. That proved the high cell survival rate of the hydrogel. Besides, the addition of 1 wt% of unmodified high molecular weight HA to 3 wt% HA-SH/P(AGE-co-G) improved cell bioactivity and ensured uniform distribution of ECM, for the long-term stability of tissue culture (Fig. 6).¹⁹⁸ The main reason is that HA, as the main component of ECM, can bind mesenchymal stromal cells (MSCs) *via* cell surface receptors to regulate interaction, such as attachment and migration, thereby promoting chondrogenic differentiation.¹⁹⁹ Thiol-HA bioinks can also print neural tissue scaffolds that can mimic the native spinal cord. This printed construct provides a suitable microenvironment for neural stem cells (NSCs). The NSCs maintained high cell viability, $95.45 \pm 3.14\%$, and showed excellent proliferation behavior.²⁰⁰

Selecting acrylate-based crosslinker and alkyne-based crosslinker, the bioinks comprised of thiolated-modified HA and gelation provide the creation of a series of compatible chemistry to print tissue constructs.²⁰¹ The biofabricated *in vitro* liver constructs, incorporating hepatocyte-specific media, exhibited high cell viability and measurable levels of albumin and urea ($>100 \text{ ng mL}^{-1}$, $>10 \text{ ng mL}^{-1}$). This thiol-HA bioink system is a universal tool for bioprinting with the potential to fabricate native tissues with complex structures. However, thiolated

HA-based cell aggregates and cellularized synthetic extracellular matrix (sECM) hydrogels are not suitable for bioprinting due to their tendency to clog the nozzle and the potential of poor structural integrity after printing. To address this issue, methacrylate HA and gelatin ethanamide methacrylate (GE-MA) are combined to prepare photocrosslinkable sECM hydrogel.²⁰² The results show that it is easy to obtain defined tubular hydrogel *via* extrusion-based system of gelatinous liquid. The structure is more solid after the second irradiation. These bioinks exhibit cytocompatible *in vitro* and biocompatibility *in vivo*.

Dual-stage crosslinking technology based on thiolated HA (HA-SH) offers independent printability. HA-SA was crosslinked with two step reaction, pre-crosslinking of polyethylene glycol-diacrylate (PEG-diacryl) *via* Michael addition and post-crosslinking of polyethylene glycol-diallyl carbamate (PEG-diallyl) *via* thiol-ene reaction.²⁰³ Grid constructs were well-printed, utilizing HA-SA bioinks with different molecule weights of 51, 230, and 410 kDa *via* a 330 μm nozzle. The average thickness of printed sheets was 630–730 μm . The high shape fidelity was obtained during and after printing. HA-SA inks with high molecular weight ($>200 \text{ kDa}$) produce a cross-linked structure with higher diffusivity, leading to the homogeneous distribution of extracellular matrix (ECM), consisting of aggrecan and collagen II. However, some growth factors could not be encapsulated in bioinks, such as TGF- β 1. In order to solve this problem, researchers tethered growth factors to 3D printed bioinks. For example, the thiol-modified TGF- β 1 was

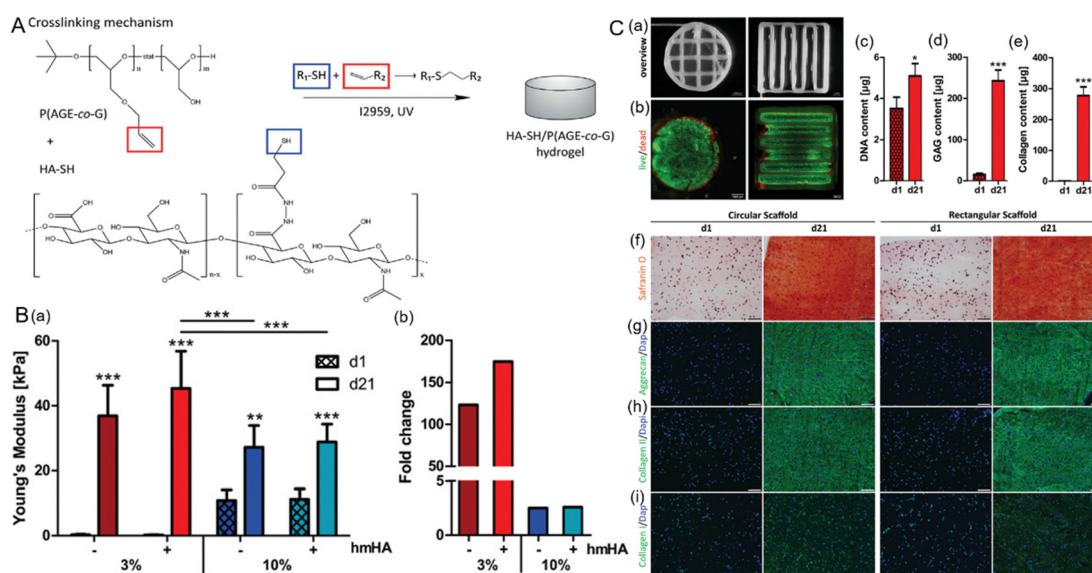


Fig. 6 (A) Chemical structure and crosslinking mechanism of HA-SH and P(AGE-co-G). Under the irradiation of UV, the covalent bond formed between the thiol group of HA-SH (blue) and the allyl group of P(AGE-co-G) (red). (B) Bioink composition affected construct stiffness after chondrogenic differentiation. (a) Young's modulus of constructs on day 1 and after 21 days of chondrogenic differentiation. (b) Fold-change in Young's modulus over time. (C) Homogeneous ECM distribution in 3D bioprinted PCL-supported constructs after chondrogenic differentiation of MSCs. (a) Overview and (b) live/dead staining of circular- and rectangular-shaped PCL scaffolds with embedded cell-laden 3 wt% HA-SH/P(AGE-co-G) + 1 wt% hmHA bioink. Living cells were labelled with calcein-AM and appeared in green, dead cells were stained red by EthD-III. Scale bars = 1000 μm . Quantitative analysis of DNA (c), glycosaminoglycan (GAG) (d) and collagen content (e) at day 1 and day 21 of chondrogenic differentiation. (f) Histological staining for deposition of GAG with safranin O after 21 days. (g) Immunohistochemical staining for aggrecan (green), (h) collagen type II, and (i) collagen type I (green) after 21 days.¹⁹⁸ (Copyright 2020 Wiley-VCH).

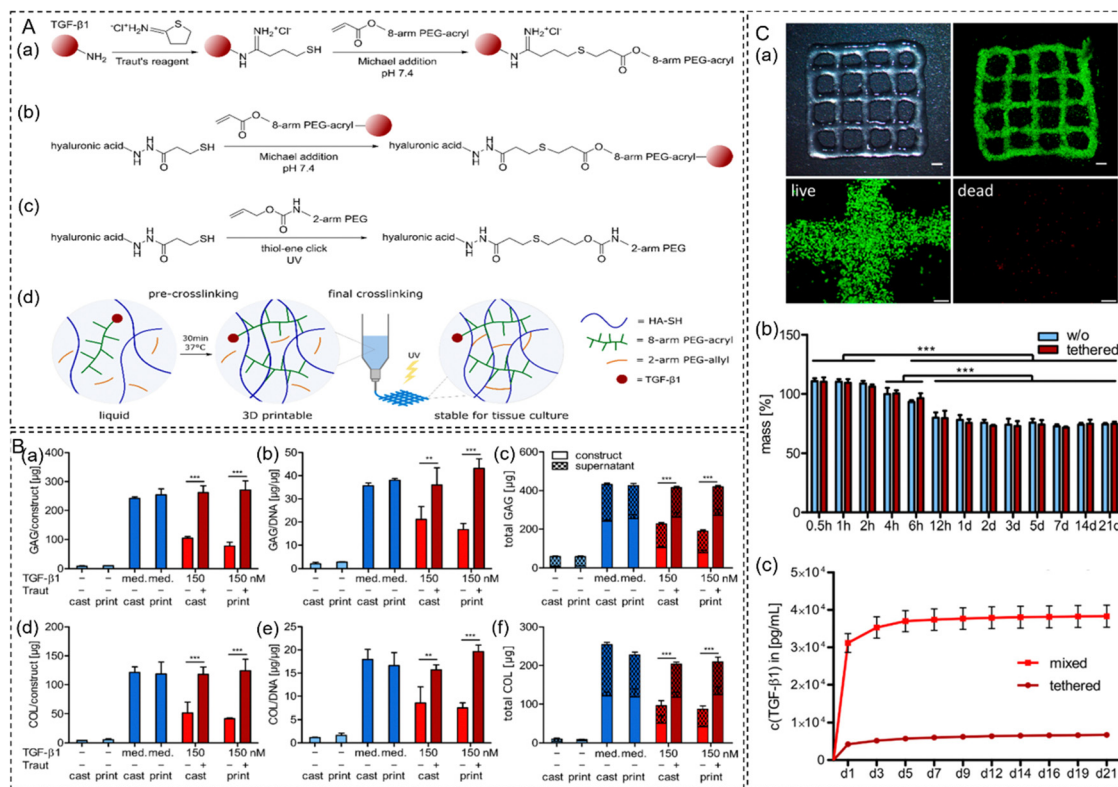


Fig. 7 Crosslinking mechanism and characterization of hyaluronic acid-based bioink tethered TGF-β1. (A) Ink crosslinking mechanism and functionalization with TGF-β1. (a) Thiol-functionalization of TGF-β1 and Michael addition with 8-arm PEG-acryl. (b) Michael addition of TGF-β1-modified PEG-acryl with HA-SH (pre-crosslinking). (c) UV-induced final crosslinking of residual HA-SH thiol groups with 2-arm PEG-allyl. (d) Dual-stage crosslinking mechanism and workflow of TGF-β1 tethered construct generation for chondrogenic tissue culture. (B) Quantification of MSC-derived ECM components in cast and printed constructs. Constructs with 150 nM mixed (–Traut) or tethered (+Traut) TGF-β1 were analyzed after 21 days. GAG content is shown for (a) the constructs and (b) normalized to DNA. (c) Total GAG production was quantified by adding the content of the constructs and the collective culture supernatant. Collagen content is shown for (d) the constructs and (e) normalized to DNA. (f) Adding the content of the constructs and the collective culture supernatant are used to quantify total collagen production. (C) 3D printing and ink characterization. (a) 3D printed grids and survival of MSCs after printing. Living cells are labelled with calcein-AM (green), and dead cells with EthD-III (red). Scale Bars = 2 mm. Scale bars of split channel images at higher magnification represent 200 μm. (b) Swelling analysis of constructs without or with 150 nM tethered TGF-β1 over three weeks. (c) TGF-β1 release from constructs with 150 nM tethered or mixed TGF-β1 over 3 weeks analyzed by ELISA ($n = 3$).²⁰⁴ (Open access 2022 MDPI).

tethered into HA-SH/PEG-acryl bioinks *via* Michael addition.²⁰⁴ Compared to non-covalently tethered TGF-β1, TGF-β1 covalently tethered into HA-based bioinks extended the availability of embedded MSCs and significantly improved chondrogenic differentiation. The results showed that covalently tethered TGF-β1 improved the expression of aggrecan and collagen II after 14 and 21 days of culture. Glycosaminoglycans and collagen contents in constructs were also higher than that of non-covalently tethered TGF-β1 (Fig. 7). These bioinks could produce high-quality cartilage tissue and did not require a continuous supply of exogenous growth factors. It has great application potential in cartilage regeneration.

Although bioinks composed of extracellular matrix materials have excellent printability and mechanical properties,²⁰⁵ they cannot support printed structures, and it usually requires sacrificed materials to support structures. So bioinks with self-supporting become particularly important. Thixotropic materials have been a good choice because of their shear-thinning properties. Researchers found that thixotropic bioinks consisting of thiolated hyaluronic acid, methacrylated

collagen I, and gelatin nanoparticles can be able to achieve good self-supporting function.²⁰⁶ In the printing process, intermolecular interactions begin to break down under the extrusion shear force, including hydrophobic and hydrophilic interaction, van der Waals force, and hydrogen bond. That allows the bioinks to change from a solid to a liquid. Finally, intersecting tubular structures with a diameter of 5 mm and wall thickness of 1 mm were printed without supporting materials. These bioinks also support HepG2 cell growth and proliferation. Dynamically hydrogel can solve the disadvantages of statically crosslinked sECMs in printing process, such as rupture of fully crosslinked gel, nozzle blockage due to the partially crosslinked of gel. Gold nanoparticles (AuNPs) can be developed to prepare dynamically crosslinkable thiolated HA-based hydrogel as a multivalent crosslinker.²⁰⁷ A network was formed by AuNPs crosslinker and thiol-modified HA and gelatin. 2% AuNP-sECM hydrogels curing for 24 h with G' (storage modulus) about 200 Pa are applied to bioprinting. AuNP-CMHA-S gels can be squeezed out through 18-gauge needle, keep their form, and prop up the three-dimensional structure.

After 24 h curing, bonds were formed through a portion of the thiols and AuNPs. After printing, dynamic crosslinking continuous to form. Rigidity and structural integrity are provided by intra-gel and inter-gel crosslinking, respectively. Finally, stacked cellular ring constructs were printed using cellularized and non-cellularized bioinks with AuNPs-thiol-modified HA and thiol-modified gelatin.

4.1.3 Methacrylated HA for thiol-ene. HA-based double crosslinked hydrogel was synthesized as bioink, combining HA-MA (methacrylated HA) and HA-SH (thiol-modified HA).²⁰⁹ When exposed to UV, these mixed solutions form a gel in seconds. The storage modulus of bioprinted samples exhibits linear change with the range of 0.1–90%. Hydrogel composed by HA-SH (1 w/v%) and HA-MA (1 w/v%), has the highest storage modulus, 120 Pa, and displays excellent pore structure. The cells were evenly distributed throughout the three-dimensional network structure, and the toxicity decreases with the increase of HA-SH contents. HA-MA/HA-SH double hydrogels had excellent swelling properties, such that the swelling rate reached $94.86 \pm 1.26\%$ within 6 h. Therefore, these double hydrogels can both absorb the exuding tissue fluid and obtain debridement effect in wound site.

Functionalized HA with acrylate or methacrylate is a hydrogel precursor and is widely applied in extrusion printing due to its excellent characteristics of biocompatibility and easy crosslinking.²¹⁰ The combination of maleated sodium hyaluronate (MHA) and thiolated sodium hyaluronate (SHHA) can be prepared stepwise *via* multiple crosslinking MHA/SHHA

hydrogels. Pre-crosslinking of thiol-acrylate Michael addition and, subsequently photopolymerization of thiol-acrylate and acrylate-acrylate occurs gradually.²⁰⁸ Hydrogels exhibited higher compressive strength of 2.18 ± 0.63 MPa and breaking strain of $71.93 \pm 0.23\%$ than pure MHA hydrogels. Meanwhile, good extruded consistency, structural integrity and stability were observed throughout the printing process (Fig. 8). The constructs have clearly visible and well-defined boundaries. MHA/SHHA hydrogels provide high resolution and shape fidelity and are suitable for 3D printing using the extrusion technique. Shape fidelity is the difference between the actual printed structure and the defined construct. This effectively address the issue of the poor mechanical properties of the pure MHA scaffold which results in poorly printed constructs. For instance, Jury *et al.*,²¹¹ fabricated 3D bioprinting-compatible modular HA-based hydrogel.²¹¹ In the study, full-size laminins (LNs) were successfully conjugated to HA-based hydrogel system *via* biorthogonal copper-free click reaction and retained for 7 days. The human neuroblastoma cells (SH-SY5Y cells) encapsulated in LN-functionalized HA-based hydrogel were well protected and were not affected by lethal shear forces. High cell viability was maintained, 24 h after bioprinting.

4.2 Gelatin bioink

Gelatin is a natural polymer of partial hydrolysis of collagen, obtaining from the connective tissue of animals, such as skin cartilage, and bone.²¹² As a collagen derivative, gelatin is more soluble in water and still has excellent biodegradability,

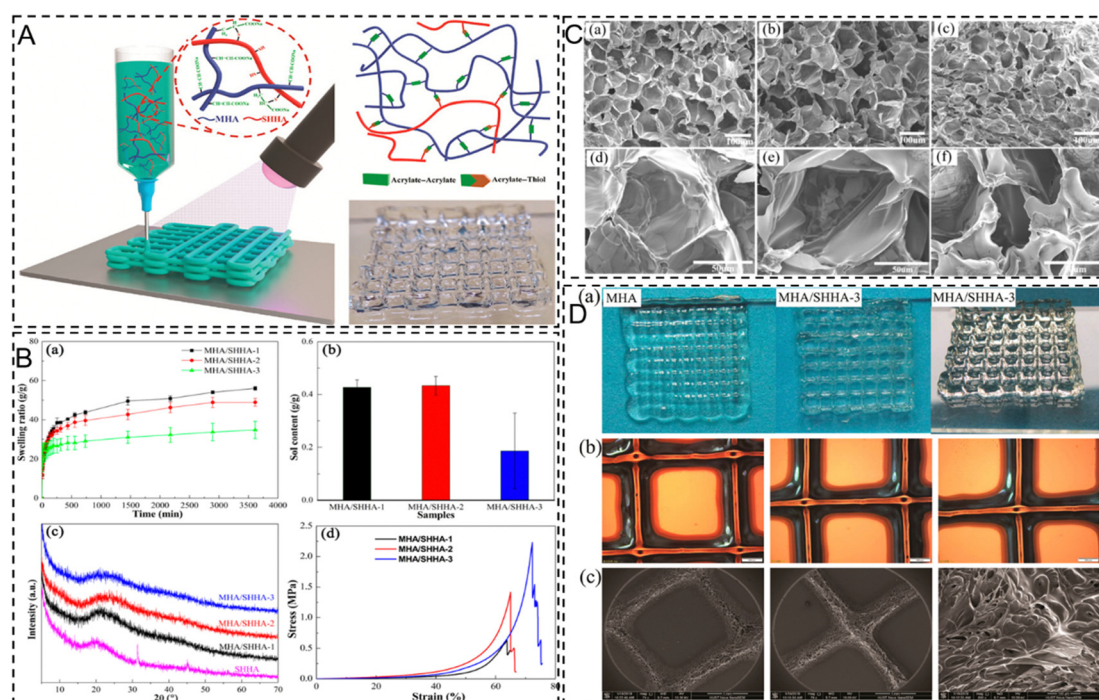


Fig. 8 The MHA/SHHA hydrogels with improved strength and 3D printability. (A) Schematic illustrations of the MHA/SHHA hydrogels formation mechanism. (B) Mechanical properties. (a) Swelling kinetics; (b) sol–gel ratios; (c) XRD patterns; and (d) compression stress–strain curves. (C) Microstructure. (a and d) MHA/SHHA-1; (b and e) MHA/SHHA-2; and (c and f) MHA/SHHA-3. (D) 3D Printability. (a) Photographs for the printed hydrogel scaffolds; (b) microscopy images (*i.e.*, MHA/SHHA-3); and (c) SEM images (*i.e.*, MHA/SHHA-3).²⁰⁸ (Copyright 2022 American Chemical Society).

biocompatibility, completely resorbable *in vivo*, non-cytotoxic, and cell affinity. It is beneficial to promote cell adhesion and proliferation.^{213,214} Due to temperature-sensitive and thermally reversible properties, gelatin is often used as a sacrificial material during the bioprinting process. After the printed structure is completed, it is dissolved to obtain the desired product. Thiol-ene decorated gelatin bioink has versatility and controllability, and is able to print desired geometries and construct.

4.2.1 Norbornene-functionalized gelatin and thiol-functionalized gelatin. Thiol-ene gelatin bioink hydrogels can be utilized to print well-defined complex construct and modulate biophysical properties, such as stiffness, microarchitecture, and spatial distribution. Given the high-resolution printing function of thiol-ene chemistry, some complex vascularized constructs bioprinted with GelNB have identical

characteristics to the designed structure. The biofabricated constructs with graduated fiber diameter and spacing of 500 μm , 700 μm , and 1000 μm presented good shape fidelity.²¹⁵ The microcapillaries could be observed in all areas of constructs. Bioinks hydrogels composed of norbornene-functionalized gelatin (GelNB) and thiol-functionalized gelatin (GelSH) could rapidly construct kidney-shaped products with a homogenous crosslinked network.²¹⁶ The chemical structures of GelNB and GelSH, crosslinking mechanism and crosslinked network images are shown in Fig. 9. The thiolated proteins or growth factors are bound to norbornene groups of GelNB–GelSH hydrogels *via* selective UV irradiation. Encapsulated endothelial cells and human cardiomyocytes displayed high viability, spreading, and proliferation after culturing of 7 days. VEGF peptide-functionalized tissue induced endothelial cell growth.

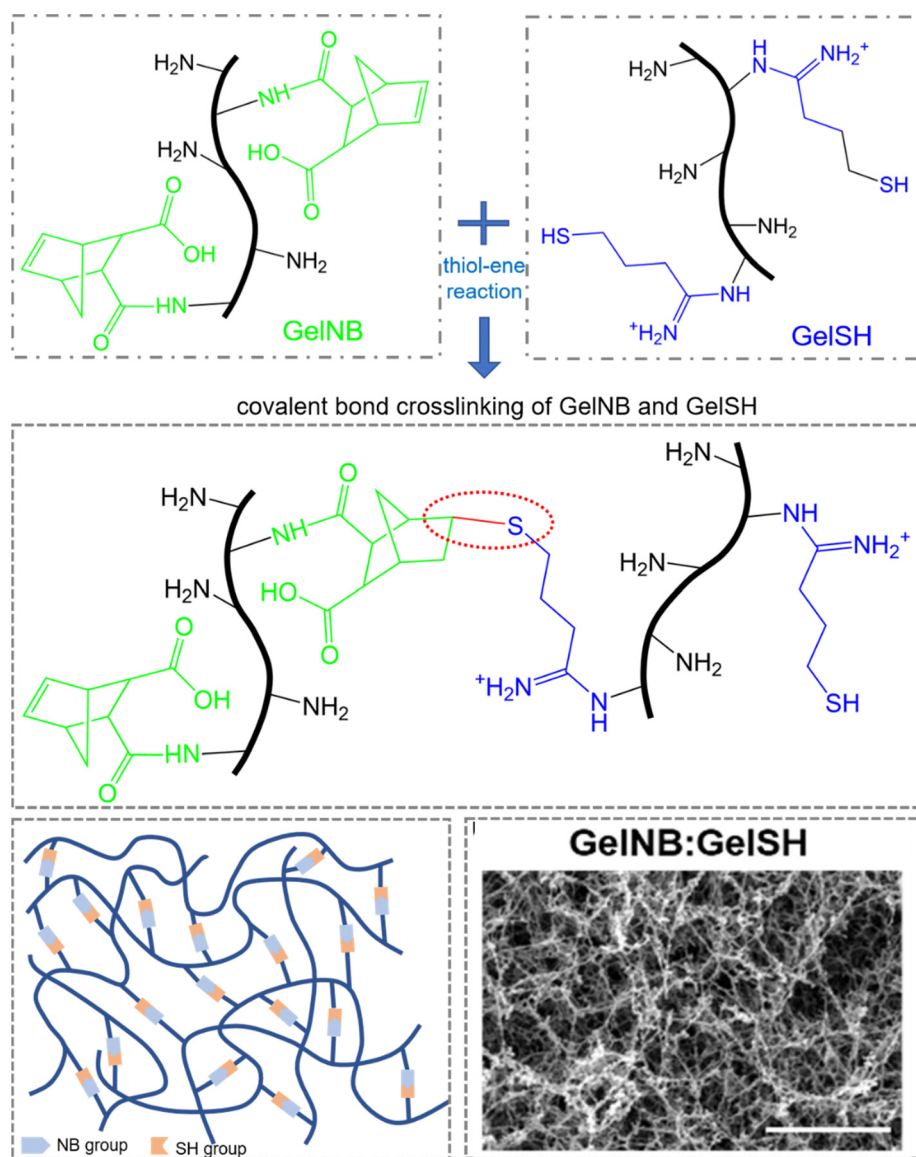


Fig. 9 Schematic of photo-induced thiol-ene click chemistry reaction to produce GelNB–GelSH hydrogel and representative SEM images of the crosslinked network.²¹⁶ (Copyright 2020 Elsevier B.V.).

Norbornene groups and thiols groups often form orthogonal covalent bonds and networks through one-step polymerization, hence thiol-ene reaction has been introduced to print promised construct with sub-micrometer spatial resolution with the method of two-photo polymerization (2PP) (Fig. 8).²¹⁷ Gelatin-norbornene (Gel-NB) bioinks have been successfully employed to print 3D constructs with sub-micrometer resolution *via* the 2PP method with encapsulated cells. Gel-NB bioinks with a wide degree of substitution ($\approx 90\%$) achieve efficient thiol-ene photo-click crosslinking.²¹⁸ The three-dimensional structures with high resolution, a cube of $300 \times 300 \times 300 \mu\text{m}^3$, were successfully printed *via* the two-photo polymerization method.²¹⁹ After 3 weeks of cultivation, mCherry L929 cells embedded in Gel-NB hydrogel construct began to align along the channels and fill the three-dimensional space created by the connected network. Then the cells migrated into the crosslinked areas after 5 weeks. The thiol-ene click GelNB-GelSH has the ability to support endothelial cell survival and adhesion in single-cell suspension and spheroid culture.²²⁰ It can be successfully employed to print defined vascular structures within a microfluidic chip with high resolution and accuracy when Gel-NB bioinks combined with cell electrowriting (CEW), the high degree orientation of cell-loaded fiber with diameters of 5–40 μm were obtained.²²¹ The reason is that the CEW technology has a higher shear-induced alignment capability than extrusion bioprinting, reducing the number of polymer entanglements. This approach breaks through the resolution limit of hundreds of micrometers during the extrusion bioprinting. Several 3D ordered fiber scaffolds with various thickness (50–200 μm) and pores sizes (100–1000 μm) are manufactured, such as squares, hexagons, and curved patterns. The printed square pores have the minimum pore size, 100 μm , and accompanying print accuracy of >0.8 . Gel-NB bioinks also preserve high cell viability post printing. Therefore, the constructs printed by Gel-NB hydrogel have exceptional cell adhesion, migration, and proliferation.

4.2.2 Methacrylated gelatin for thiol-ene. A hydrogel-based bioinks, that can effectively encapsulate and protect cells, is essential for printability, shape fidelity, and cell viability. For some materials with poor mechanical properties, gelatin can be used for printing in the form of gelation methacryloyl (GelMA).²²² GelMA, as a derivative of gelatin, is a natural biopolymer derived from collagen. The primary amine groups of gelatin react with methacrylic anhydride to fabricate a methacrylate functional group, and then GelMA is synthesized.²²³ GelMA can be photopolymerized to obtain cytocompatible post-treatment curing *via* photoinitiators.²²⁴ Therefore, GelMA is a suitable material to keep the integrity and mechanical strength of the bioprinting structure. During bioprinting, the chain-growth polymerization of GelMA is usually initiated by free radicals. However, it is inhibited by oxygen, resulting in the accumulation of reactive oxygen species (ROS),²²⁵ which damages encapsulated cells and biomolecules.²²⁶ On the other hand, free radical polymerization, as a random chain-growth photopolymerization, leads to the formation of a

heterogeneous network during the hydrogel formation.²²⁷ Thiol-ene reaction is inert to the environment oxygen and retains the bioactivity of cells and molecules.^{228,229} The thiol-ene coupling of functionalized molecules produces a homogeneous crosslinked network.^{230,231} In this way, gelatin-norbornene (GelNB) has been successfully applied to prepare the crosslinked network for encapsulating cell based on thiol-ene. Therefore, gelatin-norbornene (GelNB) hydrogels based on thiol-ene reaction is a good choice to replace GelMA. Gelatin-norbornene (GelNB) hydrogels were crosslinked by thiolated heparin (HepSH).²³² These bioinks successfully printed the defined construct, a regular grid structure with a line spacing of 1 mm. The cell viability results of post-crosslinking showed that human umbilical vein endothelial cells (HUVECs) encapsulated in GelNB-based hydrogels had higher viability ($>90\%$) than GelMA-based hydrogel ($<80\%$) (Fig. 10). As the increase of culture time, HUVECs embedded in GelNB-based hydrogels started to stretch out and spread, which is more obvious than GelMA. The previous research proved that encapsulated human mesenchymal stem cells (hMSCs) in GelNB/DTT showed better cell viability than GelMA.²²⁹ When GelNB is combined with GelSH, the step-growth polymerization mechanism of GelNB-GelSH hydrogels is beneficial to form a homogeneous crosslinked network, compared with chain-linked mechanism of Gel-MA scaffold.²³³ This photoclick hydrogel exhibited better properties than GelMA, such as improved swelling properties, superfast curing of 1–2 s, higher network uniformity, cell survival rates of over 84%.²³⁴ When the extrusion bioprinting was used to print adipose-tissue-derived mesenchymal stem cells (ASCs) in GelNB-GelSH-high, the printed cuboid structure with the size of $10 \times 10 \times 5 \text{ mm}^3$ exhibited good shape stability and fidelity. Further culturing in a chondrogenic differentiation medium for three weeks, *in vitro*, revealed that ASCs remained viable during this incubation period and were able to produce cartilage-specific negatively charged proteoglycans sulfate.²³⁵

Different thiolated crosslinkers can be utilized to tune the processability of bioprinting. For instance, DTT, thiolated gelatin (Gel-SH), tetraethylene glycol dithiol (TEG2SH), PEG dithiol with a molar mass of 3400 (PEG2SH), PEG tetrathiol with a molar mass of 10 000 (PEG4SH 1000) and 20 000 (PEG4SH 20 000) were chosen as crosslinkers and combined with Gel-NB to form hydrogels.²³⁶ After 10 min of crosslinking, there is no significant difference in storage modulus between the relaxed state and the gel of GelMA. After 60 s of crosslinking, the final mechanical properties of thiol-ene were achieved. GelMA took 10 min to achieve a similar storage modulus. The choice of crosslinker is determined by the processing method of hydrogel. Gel-SH is suitable for preparing hydrogel with comparable mechanical properties and lower water absorption capacity than gelatin. Gel-NB/Gel-SH formation has great application potential, which benefits from the physical gelation behavior before cross-linking. PEG4SH 10 000 is capable of preparing hydrogel with excellent mechanical properties for the situations of direct crosslinking from solution. The thermal response characteristics of GelNB/PEGd-SH offer initial shape retention to print soft neural constructs.

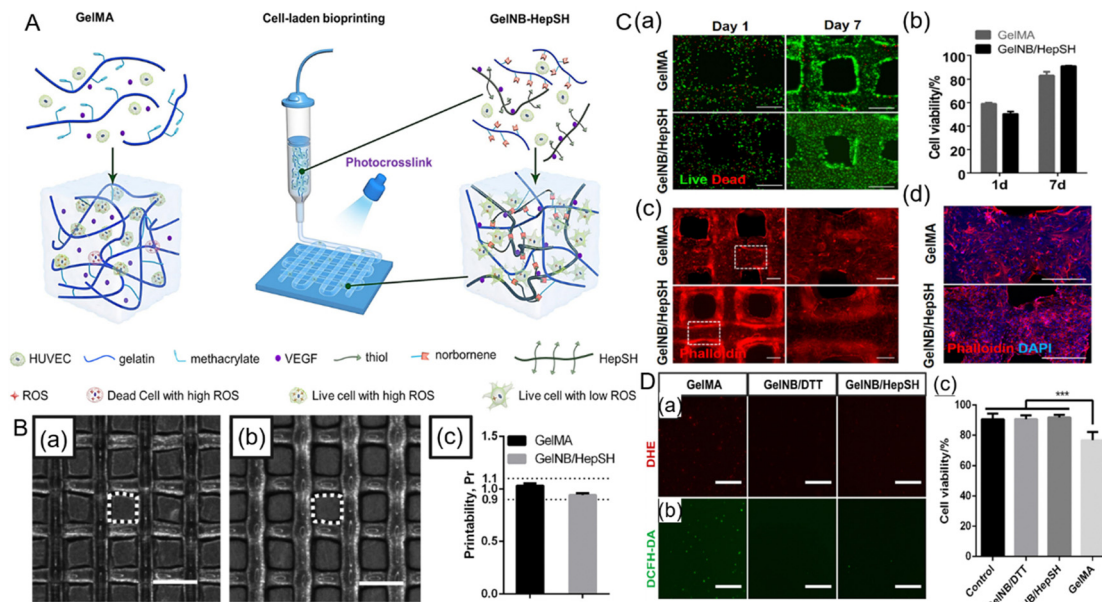


Fig. 10 Thiol-ene chemistry gelatin-norbornene-based bioinks and bioprinting. (A) The technical scheme of cell-laden bioprinting using GelMA and GelNB/HepSH bioinks. (B) Printability assessments. Printed regular grids using GelMA (a) and GelNB/HepSH (b) and printability evaluation using a semi-quantitative method (c). (C) Cell-laden extrusion-based bioprinting using the HUVEC-containing GelNB/HepSH bioink (8 w/v% GelNB) and GelMA (8 w/v%). (a) Fluorescence micrographs assessed by live/dead staining (live cells: green, dead cells: red). (b) Quantifications of cell viability. Fluorescence micrographs showing HUVEC cytoskeleton in both bioinks after cell culture for 7 days, using (c) an inverted fluorescence microscope and (d) a laser scanning confocal microscope, respectively. Here, red is F-actin and blue is nuclei. Scale bars = 500 μm . (D) Intracellular ROS assessments on hydrogels encapsulated HUVECs. The HUVECs were pre-incubated with (A) DHE (red) and (B) DCFH-DA (green), then encapsulated in GelMA, GelNB/HepSH, and GelNB/DTT hydrogels, respectively. (C) Viability tests were performed and compared to those under non-hydrogel cell culture conditions (control).²³² (Copyright 2021 American Chemical Society).

By adjusting mechanical properties and composition, the survival of encapsulated neural cells can be maintained.¹¹⁰ When human bone marrow-derived mesenchymal stem cells (hBMSCs) were *in situ* encapsulated in GelNB-PEGdiSH microgels, a high degree of chondrogenesis was observed.²³⁷ Similarly, for hyaline cartilage, the expression of collagen II significantly increased.

4.2.3 Allylated gelatin for thiol-ene. As a new thiol-ene clickable bioink, allylated gelatin (GelAGE) is suitable for bioprinting constructs with high shape fidelity. The hydrogels were prepared with GelAGE *via* crosslinking with DTT.²³⁸ This study showed that with increasing cross-linker concentrations, the compressive Young's moduli increased gradually due to an increased AGE-to-thiol ratio. The maximum value is 53.2 ± 5.8 kPa with the allyl:SH ratio of 1:3. GelAGE_{1MM} encapsulated porcine articular chondrocytes can be used for extruded 3D bioprinting at 4–7 °C. The viable cells could be observed during the culturing of 23 days. Compared with free radical polymerization, this cross-linking system has the advantage that nondegradable polymeric cross-links don't exist. GelAGE can be applied to design the ideal bioinks with low-density or high-density that could meet the standards of extrusion 3D bioprinting. The dual-step crosslinking method can improve the rheological profile of GelAGE-based bioinks and the fidelity of the construct.²³⁹ The primary crosslinking of thiol-persulfate redox reaction induced partial crosslinking, improving the flow

properties of low-density bioink. The thiol-ene click reaction between allyl groups of GelAGE and thiolated crosslinker occurred in primary crosslinking. Photoinitiated secondary crosslinking is beneficial for shape stabilization of the printed construct. The results showed that low density (3 wt%) GelAGE bioinks had a low viscosity of ~ 4 mPa s. These bioinks were, therefore, suitable for extrusion 3D bioprinting since the resulting constructs had good shape fidelity and high cell viability (>80%) after culturing of 7 days.

Bioinks support the growth and functionality of chondrocytes, as well as protect them from change and damage caused by oxidative stress and inflammation. Bioinks prepared with thiolated gelatin crosslinked acrylated hyaluronic acid-phenylboronic acid (HA-PBA-Ac) were also shown to have good shear thinning and anti-oxidative properties.²⁴⁰ At the low shear-rate of 1 s^{-1} , hydrogels kept the high viscosity, while at a high shear rate (50 s^{-1}), the viscosity decreased rapidly. This indicates the presence of good shear thinning characteristics. The H_2O_2 scavenging effect was also shown to be proportional to the concentration of HA-PBA-Ac precursor in the bioink. The hydrogels of 3:1.5 (3% HA-PBA, 1.5% gelation) exhibited a scavenging effect of up to $71.5\% \pm 4.6\%$. Due to the stable thioester covalent bond between HA and gelatin, the printed scaffolds could keep printed shape fidelity and structural integrity *in vitro* after 21 days.

4.3 Alginate bioink

Alginate is a natural anionic polysaccharide extracted from brown algae. Alginate solution has good fluidity, and is usually used for inkjet printing as bioinks due to its rapid gelation performance in a physiology environment.^{241–243} However, its low cell adhesion and poor molding properties affect the stability, shape fidelity, and printing accuracy of the resulting 3D construct. To solve this problem, the physicochemical properties of alginate bioinks can be improved by modifying alginate with functional molecules or mixing with other macromolecules. The hydroxy and carboxyl groups on the alginate backbone are usually decorated with functional molecules *via* click reaction.

4.3.1 Thiol-ene alginate. The viscosity of bioinks determines the printability of the materials such that bioinks with high viscosity can form a complete structure and effectively support their weight. However, gelation limits the flow of encapsulated cells and reduces the restructuring ability in the surrounding matrix. In contrast, low viscosity bioinks offer a loose and reconfigurable environment for cells. For alginate, although it is possible to increase the viscosity of the ionically crosslinked bioink *via* changing the molecular weight and concentration, it still lacks sufficient mechanical strength and long-term stability, resulting in poor shape fidelity.^{244,245} Given that, thiol-modified alginate was utilized to design double crosslinked hydrogel based on ionic

crosslinking, obtaining high strength, of ~ 3.4 MPa and stability for 30 days.²⁴⁶ The double bond modified alginate (Alg-NB) was obtained by conjugating a double bond within 5-norbornene-2-methylamine. And then, the Michael chemical reaction of sulfhydryl alginate (Alg-SH) and Alg-NB occurred.²⁴⁷ The double crosslinked interpenetrating network forming with Alg-SH and Alg-NB, and ionic crosslinked network, improve the crosslinking effect and density. The pore diameter is about 150 μm , which is lower than single network hydrogel, about 200 μm .²⁴⁷ This endows the resulting construct with high strength and long-term stability. Using an extrusion printing system, a 3D open-porous construct composed of 5 layers was prepared. Optical images showed that these double crosslinked hydrogels formed by Alg-SH and Alg-NB have finer fiber and more accurate structure comparing with single crosslinked hydrogel.

In the process of ink extrusion, high-viscosity bioinks will be subjected to high shear stress, resulting in cell death.²⁴⁸ To circumvent this problem, alginate bioinks decorated with norbornene functional groups could improve cell viability. Thiol end group decorated polyethylene glycol is chosen as the cross-linker. The thiol-ene reaction will rapidly initiate cross-linking with the precise control of spatial and temporal. Alginate decorated with norbornene with a lower concentration of 2 wt% can obtain stable 3D cross-linked structures with a range of mechanical properties (G' from 0.05 to 10 kPa) and high cell survivability ($> 80\%$) (Fig. 11).²⁴⁹ Based on bioinks of

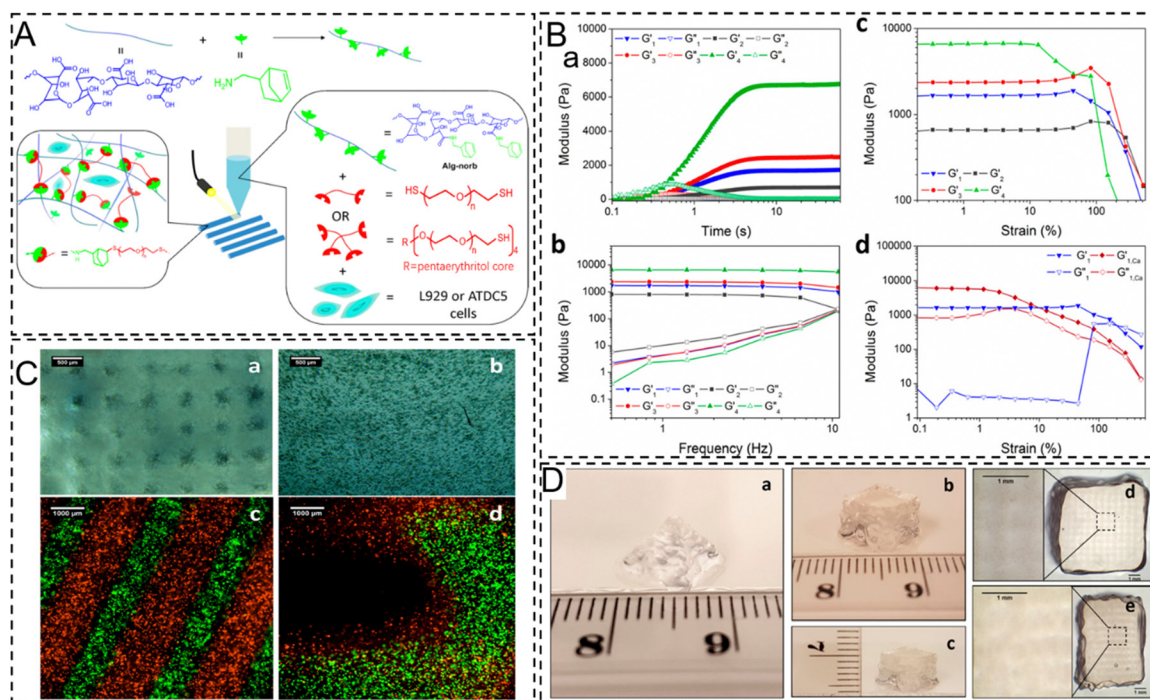


Fig. 11 (A) Schematic diagram of the development of photoactive alginate bioink (Alg-norb) for bioprinting of hydrogels. (B) Shear storage (G') and loss (G'') moduli as a function of (a) UV illumination time, (b) frequency, and (c) strain for Alg-norb with different PEG cross-linkers (1 = Alg-norb10-1; 2 = Alg-norb10-2; 3 = Alg-norb10-3; 4 = Alg-norb10-4). (d) Strain sweep of Alg-norb10-1 (blue lines) and after the addition of 100 mM CaCl_2 for 3 min (red lines). (C) Morphology of 3D bioprinted hydrogels loaded with cells at (a) day 0 and (b) day 7. Green and red cell tracker labeled L929 as two different bioinks printed as alternating fibers (c) in the X-Y plane and (d) in the Z direction. (D) Scaffolds bioprinted with the geometry of a pyramid (a). (b and c) The geometry of a cube. Porous-like structures can be seen in the cube scaffold shown in (d) X-Y and (e) Z planes when imaged between two glass coverslips.²⁴⁹ (Copyright 2018 American Chemical Society).

norbornene-alginate and multifunctional thiol-PEG cross-linkers, an *in vitro* engineered fracture callus can be fabricated *via* 3D bioprinting to offer a spatial tissue structure.²⁵⁰ The BMP cell encapsulated in bioinks showed high cell viability when the deposition pressure was 25 kPa. Evaluation *in vivo* displayed tissue formation of cells. The positive stain of immunohistochemistry (IHC) for human osteocalcin (OCN) was observed under the environment of the intermediate osteochondral zone (IMZ) and osteogenic zone (OZ), that indicates the transition of tissue to osteoid *in vivo*. Compared with high concentration bioinks, low viscosity alginate solution could be converted into suitable viscoelastic bioinks with excellent printability and biocompatibility *via* partial crosslinking strategy. Alginate hydrogel bioinks were functionalized with peptide *via* CuAAC reaction to directly fabricate microvascularized constructs.²⁵¹ The partial crosslinking process was accomplished by adding calcium chloride, which gradually cross-linked the alginate hydrogel precursor into a viscous solution, rather than a completely cured hydrogel. This facile approach maintains the defined chemical properties and printed compartmentalized vascularized tissue construct with defined mechanical, rheological, and biochemical properties.

4.3.2 Aldehyde–alginate for oxime. Hydrogel made from amine-hyaluronic acid (HA-NH₂) and aldehyde–alginate (Alg-CHO) *via* imine bond, exhibited good printability and degradability. The strands printed by HA-NH₂ and Alg-CHO (5:5) were determined to have good structural integrity, as illustrated by their homogeneous distribution in a linear

pattern of fluorescent microspheres encapsulated in the hydrogel.²⁵² In addition, hMSCs still existed in the form of living cells during extrusion and were not affected by shear stress. Although high shear stress has an effect on cell viability and proliferation, high cell viability can be maintained when the shear stress is lower than 5 kPa in 3D printing.^{253–255} The shear stress of HA-NH₂ and Alg-CHO (5:5) hydrogel at maximum viscosity is 276.6 Pa, which is much lower than 5 kPa. These features are favorable for extrusion bioprinting.

4.4 Chitosan bioink

4.4.1 Diels–Alder chitosan. Simultaneous deposition and step-chain photopolymerization are beneficial to maintain the integrity and stability of the 3D construct. Chitosan functionalized with methyl furan groups is employed to generate hydrogels with defined characteristics. The methyl furan residues were efficiently crosslinked by the Diels–Alder reaction binding PEG-*Star*-maleimide. The chitosan–gelatin hybrid hydrogel has self-healing properties with 0.88 healing efficiency, and the healed hydrogel can withstand repeated stretching.¹⁷⁴ The printed constructs encapsulated with human U87 glioblastoma cells improve the shape fidelity. Moreover, the proliferation of cells increased significantly on day 3 and 6. The furfuraldehyde modified chitosan (CTS-FUR), has the load-bearing capacity and synergistic toughening ability induced by an internal fracture to improve the mechanical properties (Fig. 12).²⁵⁶ The material, prepared by cross-linking CTS-FUR with furfural modified epoxy natural rubber (ENR-FA)

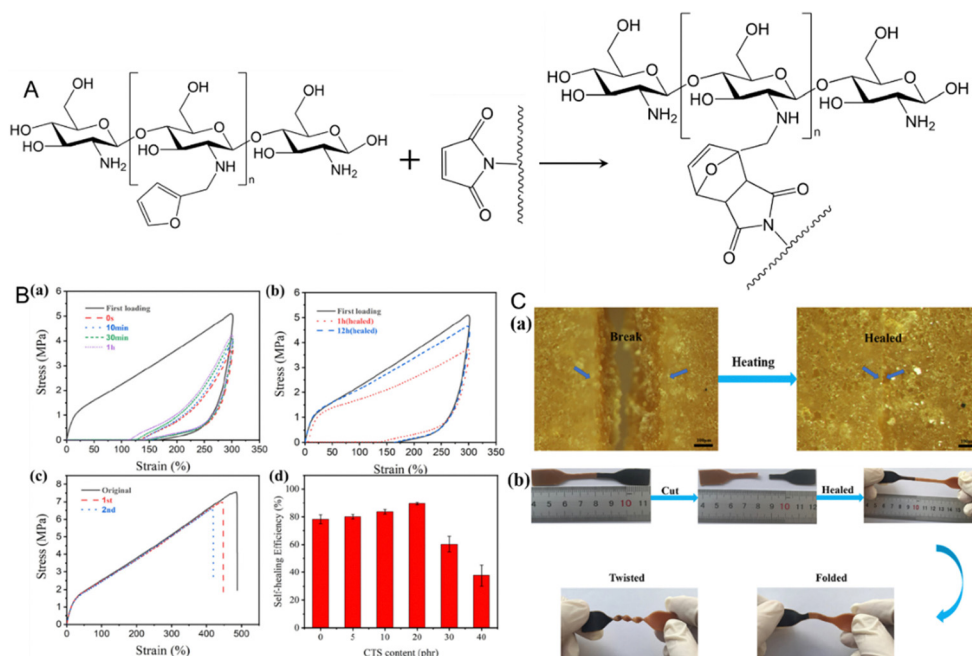


Fig. 12 furan modified chitosan bioink and its properties. (A) Schematic diagram of the crosslinking mechanism of furan modified chitosan through Diels–Alder reaction. (B) Tensile-recovery curves of ECTS-20 in successive cycles with different time intervals at room temperature (RT) (a) and at 120 °C for 20 min and then at 60 °C (b) after the first cycle.²⁵⁶ (Copyright 2021 Elsevier B.V.) (c) Repeated stress–strain curves of ECTS-20 at 120 °C for 20 min and then self-healing at room temperature for 12 h. (d) Self-healing efficiency of ECTS with different CTS-FUR contents. (C) Self properties. (a) Observation of self-healing of ECTS-20 by stereomicroscopy. (b) Pictures giving the cutting/healing process of ECTS-20.²⁵⁶ (Copyright 2021 Elsevier B.V.).

through a Diels–Alder reaction, exhibits up to 487% elongation at break. The mechanical properties of the repaired material were more than 90% of the original materials, regardless of whether it was completely fractured, cyclically damaged, or recyclable.

4.4.2 Oxime chitosan. Hydrogel applied in 3D printing has two significant characteristics, namely, steady rheological properties and post-printing crosslinking.^{257,258} Due to the increase in long-term modulus and folding structure, the applications of chitosan hydrogels have been greatly hindered in 3D printing.²⁵⁹ In response, Phenol-modified chitosan (Chi-Ph) and crosslinker of DF-PEG (CPDP) were combined to form self-healing hydrogel *via* dynamic bonds between amine and benzaldehyde.²⁶⁰ Fast gelling rate, good self-healing ability, and facile printability were obtained within a short time. The interaction of phenol-benzaldehyde enhances molecular attraction, obtaining a faster gelling rate. At higher strain, 500%, CPDP hydrogel reaches a critical state. At a lower strain, 1%, hydrogel promptly returns to its original state. Combined with dynamic imine bonds, hydrogels maintain self-healing properties after repeated damage. During the 3D printing, CPDP hydrogel is smoothly extruded through 26-gauge needle to fabricate constructs. After printing, the actual size of printed parts is consistent with the design model, and the error is less than 5%.

4.5 Thiol–ene–collagen bioink

Collagen is the most abundant and widely distributed functional protein in mammals.^{261,262} Under physiological conditions, collagen disintegrates in acidic conditions and self-assemble into gels. It has the minimal immune response, excellent biocompatibility and tissue regeneration ability. Collagen-based bioinks have been produced by dissolving animal collagen in an acidic solution with cell-free printing, meanwhile, an additional neutralization process is usually employed to prepare the stable hydrogel before cell seeding.^{263,264} After being neutralized by an alkali, collagen is able to self-assemble into fibrous hydrogels and load cells.²⁶⁵

There is a serious problem when collagen is utilized as bioink. The low self-assembly speed causes the deformation of collagen hydrogels due to their partial loss of moisture, resulting in the collapse of the printed structure.²⁶⁶ Norbornene-functionalized collagen (NorCol) has been approached in addressing this issue. NorCol maintains the triple-helical conformation, that can construct cell-loaded hydrogels with lower concentrations *via* a cell-friendly thiol–norbornene reaction (Fig. 13).²⁶⁷ The hydrogel has uniform pore structures that provide a suitable microenvironment for the long neurite outgrowth of DRGs and the formation of HUVECs vascular networks. The multilayered 3D constructs, such as mesh, pyramid, and monolayer tube, present high-precision printed structures. Norbornene modification allows collagen to become a living cell carrier with a precision processable characteristic. When human collagen type I (RCPhC1) was functionalized with norbornene and thiol moiety, respectively, the RCPhC1-NB/SH hydrogels developed with step-growth-polymerized were proved to constitute perfect

bioinks *via* 2PP.²⁶⁸ During the reaction, one norbornene group reacts with only one thiol group, which is responsible for the formation of homogeneous networks. Compared with bifunctional thiolate cross-linker, these multifunctional thiolated cross-linker results in a higher storage moduli and stronger networks.^{218,229}

4.6 Thiol–ene–cellulose bioink

Cellulose is a linear polysaccharide, and its molecular structure is rich in hydroxyl groups.^{269,270} However, cellulose, without modification, will undergo thermal decomposition before melting and flowing,²⁷¹ thus limiting its application in 3D printing. Functionalized cellulose can, however, be utilized to prepare bioinks, such as cellulose derivative, carboxymethyl cellulose (CMC), methylcellulose (MC), and hydroxyethyl cellulose (HEC).

CMC modified with norbornene group has the potential to prepare photocurable and cell-encapsulated hydrogels. These hydrogels exhibit good cytocompatibility, and the embedded human mesenchymal stem cells (hMSCs) show high cell viability, > 85%, after 21 days.²⁷² Norbornene modified CMC (NorCMC) and carbic functionalized CMC (cCMC) were chosen as the formulation of bioinks *via* thiol–ene reaction (Fig. 14).²⁷³ The thiol:norbornene ratios (T:NB) investigated were 1:4, 1:2, and 1:1. The viscosity of NorCMC bioinks increases with the increases as the T proportion increases. It is ~2 times increase as the T proportion increases from 1:4 to 1:1. Grid-like homogeneous scaffolds were fabricated with print speeds of 5–10 mm s^{−1}. Three kinds of cells, hMSCs, NIH 3T3 fibroblasts, and HUVECs, could be encapsulated into bioinks and successfully printed scaffold without loss of cell viability (95–97% for 1:4, 97–93% for 1:2).²⁷³ When CMC was modified by alkyne group, it could combine hydroxyethyl cellulose (HEC) modified by the azide group to obtain bioink for extrusion bioprinting (Fig. 14).²⁷⁴ Under the catalytic action of copper, the gel was obtained *via* a click reaction. The results showed that swelling rate is a positive function of copper content and is independent of variations in pH. This is because, when large amounts of Cu(I) are present, more active sites will be produced, thus resulting in more triazole crosslinks to improve the hydrophilicity. The extrusion bio-plotting was successfully carried out using these HEC/CMC bioinks. Although the effect on cell viability of the gels was not significant, the biocompatibility needs to be further evaluated when used as biological tissues.

Methylcellulose (MC) is another cellulose derivative, that is synthesized by using methyl groups to replace hydrogen atoms at the C-2, C-3, and/or C-6 position of cellulose.²⁷⁵ Due to the property of temperature-dependent reversible transition, MC is suitable for 3D bioprinting. It is found that MC-based bioinks exhibit high viscosity properties near physiological temperature. After functionalizing with norbornene, MCNB bioinks preserve temperature sensitivity. At 37 °C, MCNB bioinks were extruded continuously and smoothly from the nozzle, forming a uniform line. In contrast, the extruded MCNB bioinks dropped into droplets without a continuous strand.²⁷⁶ Thiol–norbornene crosslinking enhanced the stability of printed hydrogel, leading to stable three-layered lattice MCNB constructs independent of temperature.

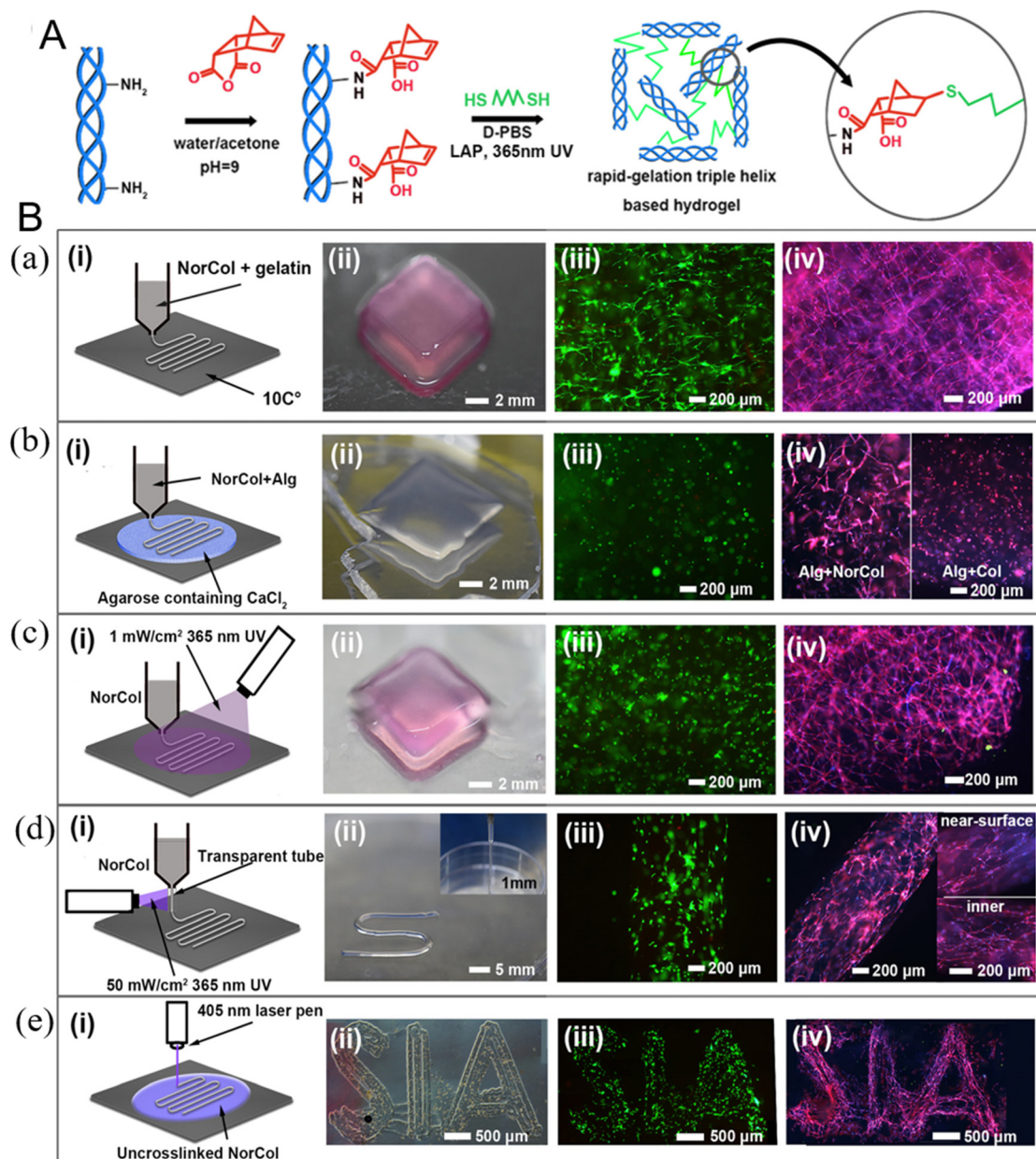


Fig. 13 (A) Synthesis and thiol-ene photoclick reaction of NorCol. (B) Different bioprinting strategies for NorCol bio-ink. (a-i) Schematic of temperature-sensitive extrusion bioprinting. (ii) Printed NorCol hydrogels (12 layers, 3 mm) after 1 day of culture. Fluorescence micrographs showing cell (iii) viability (day 1) and (iv) spreading (day 5) within NorCol hydrogels. (b-i) Schematic of extrusion bioprinting of NorCol bio-inks on agarose (2% w/v) plates containing 100 mM CaCl_2 . (ii) NorCol/Alg hydrogel scaffold after ionic and light cross-linking (6 layers, 1.5 mm). Fluorescence micrographs showing cell (iii) viability within the NorCol/Alg hydrogel. (iv) Fluorescence micrographs showing different degrees of cell spreading within the NorCol/Alg hydrogels and Col/Alg hydrogels. (c-i) Schematic of the bioprinting photo-cross-linkable NorCol bio-inks, where cross-linking occurs after extrusion with UV light irradiation. (ii) NorCol hydrogel scaffold (6 layers, 1.5 mm) after 1 day of culture. Fluorescence micrographs showing cell (iii) viability and (iv) spreading within NorCol hydrogels. (d-i) Schematic of the bioprinting photo-cross-linkable NorCol bio-inks, where cross-linking occurs during extrusion with UV light irradiating through a transparent tube. (ii) NorCol filaments (1 mm) squeezed out of a polytetrafluoroethylene tube. Fluorescence micrographs showing cell (iii) viability (day 1) within NorCol filaments. (iv) Fluorescence micrographs showing cell spreading and cell morphology at the near-surface or inner core of NorCol filaments (day 5). (e-i) Schematic of the stereolithography appearance for NorCol bio-ink using a laser pointer. (ii) Photographs and micrographs of the NorCol pattern (SIA, 1 layer). (iii) Viability (day 1) and (iv) spreading (day 5) within the NorCol pattern.²⁶⁷ (Copyright 2021 American Chemical Society).

4.7 Thiol-ene chitosan bioink

Chitosan, consisting of glucosamine and *N*-acetyl glucosamine linked in a $\beta(1-4)$ manner, is the product of chitin after deacetylation. It is a linear polysaccharide macromolecule with favorable biodegradability, biocompatibility, nontoxicity, and

antibacterial activity properties. The molecular weight and deacetylation degree of chitosan is $300 \sim$ more than 1000 kD, 30–95%, respectively.²⁷⁷ The abundant amino groups on the chitosan repeat units offer abundant modification sites. When chitosan is dissolved in an acid solution, the

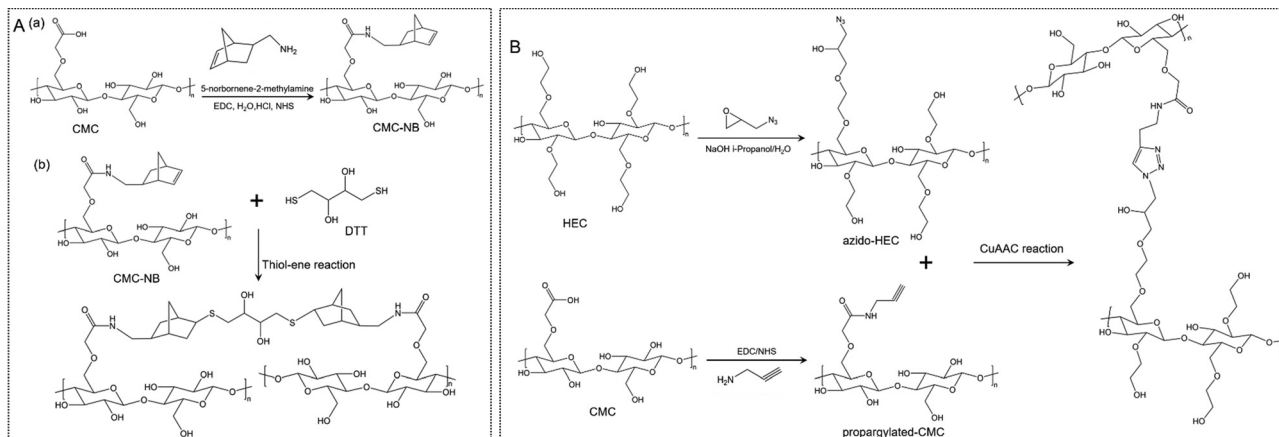


Fig. 14 Chemical structure, modification reaction, and crosslink mechanism of CMC, HEC, MC. (A) CMC-NB and its crosslink mechanism *via* thiol-ene reaction. (a) Functionalization of CMC with norbornene groups *via* EDC coupling reaction. (b) Schematic of a CMC-NB/DTT(dithiothreitol) hydrogel fabrication *via* thiol-ene reaction.^{272,273} (Copyright 2017 Wiley-VCH) (Copyright 2020 Elsevier B.V.) (B) Formation of click-hydrogel of propargylated-CMC and azido-HEC. Azido-HEC was prepared with 1-azido-2,3-epoxypropane (AEP) *via* open-ring reaction. Propargylated-CMC was prepared using a coupling agent and propargylamine.²⁷⁴ (Copyright 2020 Elsevier B.V.).

molecule has positive charges and becomes a polycationic polysaccharide.²⁷⁸

Although chitosan hydrogel has great applications in biomedical fields, 3D printed chitosan hydrogel presents poor mechanical properties and slow gelation properties.²⁷⁹ That makes the 3D printable chitosan insufficient to maintain structural integrity²⁸⁰ and limits the further utilization of chitosan in 3D printing. To tackle this problem, simultaneous extrusion deposition and thiol-acrylate photopolymerization (step-chain growth polymerization) can be carried out to prepare fast gel. For instance, hydrogel can be fabricated with maleic chitosan (MCS) with acrylate group and thiol-terminated poly(ethylene glycol) (TPEG).²⁸¹ The thiol-acrylate photopolymerization significantly overcomes the oxygen inhibition effect. Compared with single acrylate systems, thiol-acrylate systems, prepared by introducing sulfhydryl compounds are beneficial to reducing or eliminating the influence of oxygen inhibition on gelation rate. The gel rate and compressive strength were increased by 2 times and 10 times respectively, compared with pure chitosan hydrogel. The range of G' is 4–10 kPa, which is comparable to the G' of nerve tissue, is suitable for the migration, proliferation, and differentiation of cells.

4.8 Thiol-ene polyethylene glycol

Polyethylene glycol (PEG) is a well-known synthetic biomaterial, which has been widely used in pharmaceutical and biomedical fields. Due to its hydrophilicity, biocompatibility, non-immunogenicity, and flexibility, PEG has been successfully utilized in bioprinting as a crosslinkable bioink.²⁸² PEG has two molecular structures, linear and branched. The hydroxy terminal groups in the basic structure of PEG can be modified to transform into other groups for hydrogel formation or binding with molecules.

PEG hydrogels can be used as extruded gel phase bioinks, whose properties are tuned by modulating molecular weight,

concentration, and crosslinking degree. The lack of stability of pure PEG bioinks is a challenge for extrusion printing. In order to improve the stability, microgels have been used as bioinks.¹⁹⁴ Norbornene-bearing PEG microgels can be fabricated into 3D constructs *via* thiol-ene reaction. Due to its inherent cohesion between the microgels, PEG microgel-based bioink are easy extruded and rapidly stabilized during the printing process.²⁸⁴ For unreacted norbornene groups, annealing can be performed by second thiol-ene click chemistry to obtain long-term stability of microgels, and the whole process is cell compatible. Human mesenchymal stem cells (hMSCs) incorporated in the scaffold have the ability to spread, proliferate, and also active Yes-associated protein signaling.²⁸⁵ PEG functionalized with cell-adhesive RGD ligands were cross-linked with peptides *via* the Michael reaction.²⁸⁶ These cross-linked PEG-based bioinks were extruded smoothly and evenly from the micro-capillary bioprinting system, forming various complex constructs along with angles and sharp turns. In the bioprinting process, PEG-based bioink transiently incorporating low molecular weight gelatin (LMWG) fragments improves shape fidelity and accuracy. The cell viability was as high as $95 \pm 3\%$ after culturing 3, 5, 7 days. Four-arm thiol-ene PEG hydrogel has predictable swelling properties, biocompatibility, and enzyme resistance.²⁸⁷ However, this solution cannot be used as bioinks alone because of its low viscosity at low monomer concentration and poor self-supporting ability. By adding alginate as a thickener, extruded gels with good properties are obtained. Alginate is used as physically crosslinking and PEG is involved in chemical crosslinking, which form a double network bioinks (Fig. 15).²⁸³ Before contacting with collagenase IV, the printed scaffold had a toughness ranging from 1517.8–1836.3 kPa and fracture strength of 26.7–28.9 kPa. The results of post-digestion showed that toughness and fracture strength were comparable to the toughness and fracture strength of hybrid materials. Furthermore, noses printed with

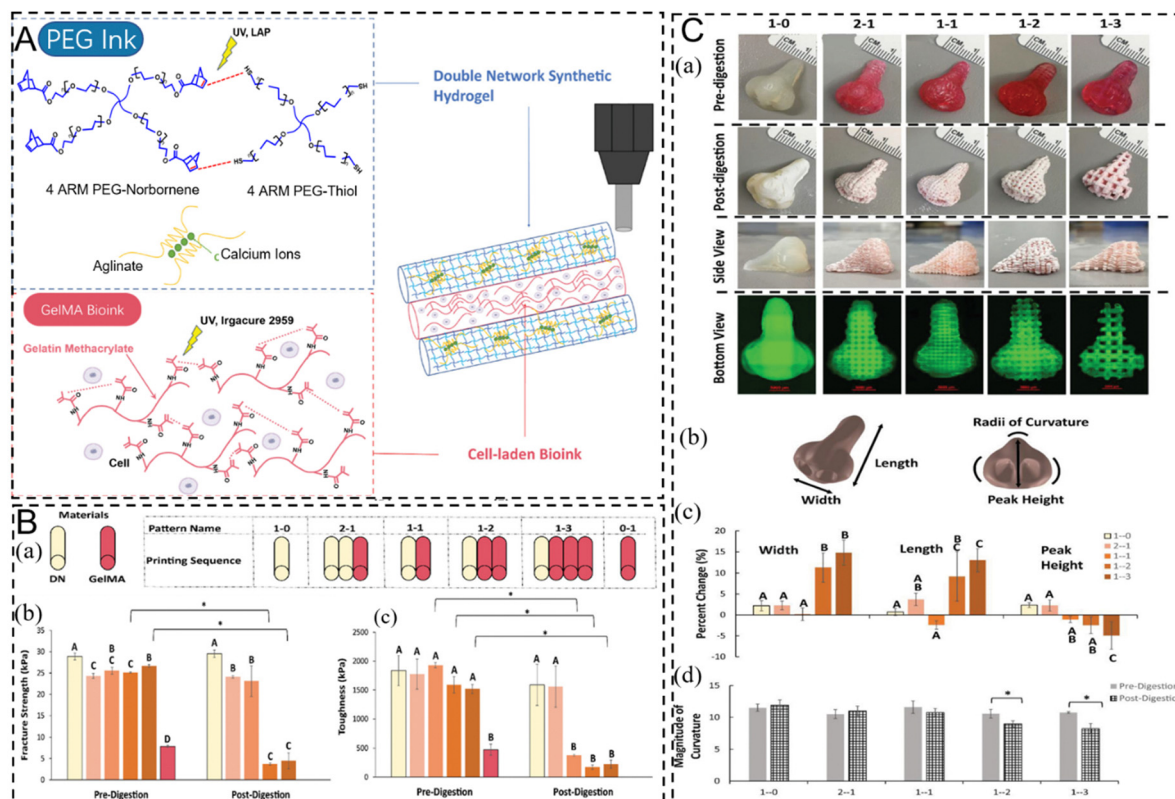


Fig. 15 Double network bioinks of PEG/alginates. (A) Printed inks and hybrid scaffold. (a) Four-arm PEG monomers functionalized with norbornene and thiol end groups react when photoinitiator LAP is present within the solution, as alginate ionically cross-links with itself with the presence of calcium ions; GelMA monomers mixed with cells and Irgacure 2959 results in a cross-linked cell-encapsulated bioink strand. (b) Visual representation of alternating PEG and GelMA inks in 1-1 pattern to create a hybrid scaffold. Complex architectures can be created using this printing technique, such as (c) human nose, (d) ear, and (e) thyroid cartilage. (B) Mechanical testing of various print patterns. (a) Visual description of the various print patterns used to fabricate hybrid scaffolds. Uniaxial compression testing was performed on hybrid scaffolds both before and after experiencing GelMA digestion *via* collagenase IV. Mechanical properties, such as (b) fracture strength, (c) toughness, were characterized to ensure hybrid scaffolds exhibited similar properties to soft tissue. (C) Complex scaffold shape retention. (a) Noses were printed in various patterns of double network ink and GelMA and further subjected to collagenase IV digestion. (b) Scaffold dimensions were recorded and compared to its original fabricated form, specifically (c) width, length, and peak height. (d) Magnitude of curvature was also calculated and recorded for each hybrid pattern.²⁸³ (Copyright 2019 Wiley-VCH).

various patterns of double network bioinks and GelMA present high degree shape retention.²⁸³ The change of width, length, and height are $14.9 \pm 3.0\%$, $13.0 \pm 2.7\%$, and $4.9 \pm 3.3\%$, respectively.²⁸³ Therefore, double network bioinks are suitable for 3D bioprinting strategy to build complex constructs with ideal properties.

PEG decorated with functional groups can also be used as crosslinking agents in 3D printing. For example, dithiol PEG was rapidly crosslinked with norbornene modified alginate *via* thiol-ene reaction by UV irradiation to printed constructs.²⁴⁹ When the biofunctional crosslinker was replaced with four-arm thiolated PEG, more compact crosslinked networks were presented. PEG modified with diacrylate and PEG modified with diallyl carbamate combined with more viscous HA-SH to prepare bioinks.²⁰³ Two independent reactions occur, Michael addition of pre-crosslinking and thiol-ene reaction of final-crosslinking. Modified PEG provides 3D printability to print uniform constructs, promoting effective chondrogenic differentiation of MSC. The homogeneous distribution, up to 95%, was observed. Hyperbranched PEG-based macromolecule, HB-

PEG-HDZ, is a macro-crosslinker, that is synthesized *via* thiol-ene reaction. It is able to crosslink with HA-CHO to form injectable fast-forming hydrogels through the reaction of hydrazide and aldehyde.²⁸⁸ This dynamic covalent crosslinking mechanism endows gel with good shear thinning and self-healing properties. The G' of HB-PEG-HDZ/HA-CHO hydrogel was 800 Pa, which was reduced to 600 Pa after the first cycle and maintained at 550 Pa after 5 cycles of repair tests. This fast so-gel transition protects the cell from damage during the extrusion.

Poly(ethylene glycol)-dithiothreitol (PEGDTT), synthesized *via* Michael-like step-growth polymerization, is the derivative of PEG. When PEGDTT is combined with nanosilicates, the shear-thinning bioinks with tuning swelling kinetics and degradation rate are obtained.¹⁰⁰ The concentration of nanosilicates modulates viscosity, low viscosity corresponding to a low concentration of < 4 wt/vol%. When the concentration is more than 4%, stiff gels are prepared. Since the physical crosslinking between nanoparticles and PEGDTT limits the swelling of polymer chains, the swelling degree of PEGDTT hydrogel with

nanosilicates was lower than that of single PEGDTT.^{100,289} The degradation rate can be effectively adjusted by changing the ratio of PEGDTT: nanosilicates. The main reason is the chemical composition and cation balance.

The multi-material bioinks based on partial PEG cross-linking (PEGX) enable to synthesize gel-phase bioinks with the mechanical tuning properties and high cell viability. The rheological study of PEGX-Gelatin bioinks showed that storage was related to gel phase. Weak inks were less than 30 G' Pa, ideal ink was about 30–150 G' Pa, and robust inks were approximately 500+ G' Pa.⁷³ During the printing process, the PEGX solution with different concentrations was added to the top of the construct for post-printing crosslinking. After that, PEGX-MAL and PEGX-NOR were incorporated into thiol-gelatin and tetrazine-gelatin to perform secondary crosslinking, respectively. The secondary crosslinking treatment improved the storage modulus from <20 Pa to 500–2000 Pa.⁵⁰ For cross-linking of maleimide (MAL), vinyl sulfone (VS) and thiol (SH), crosslinking of succinimidyl valerate (SVA) and amine (NH_2), crosslinking of norbornene (NOR) and tetrazine (TZ), the gelation rates of bioinks from fast to slow are MAL-SH, NOR-TZ, SVA- NH_2 , VS-SH, respectively.⁵⁰

The lack of diversity in bioinks is a major factor limiting their development. Cell phenotypes are very sensitive to the biochemical and mechanical properties of the surrounding environment. Therefore, the matrix properties provided by bioinks are important for cell diversification.²⁹⁰ The university orthogonal bioinks, based on the biorthogonal crosslinking mechanism, can avoid the influence of biochemical stimulation on cell viability, meeting the requirements of bioinks widely application. University orthogonal network bioink with gelatin, hyaluronic acid, recombinant elasmoid protein (ELP), and polyethylene glycol (PEG) were developed *via* bioorthogonal strain-promoted azide-alkyne cycloaddition (SPAAC) reaction between azides and bicyclononynes (BCN).⁴³ The hydrogel storage moduli are between 200 and 10 000 Pa, which can be adjusted by changing the weight percentage of each polymer. The presence of cells did not interfere with the crosslinking of bioink. The crosslinking kinetics and final modulus of bioinks have not obviously changed after containing C-MSCs. These bioinks can be applied to print a unified and cohesive structure, with high cell viability and expression characteristics. University orthogonal network bioink is a general method for 3D bioprinting with multiple materials and cells.

4.9 Other polymers for thiol-ene bioink formation

In addition to the biological macromolecules-based inks mentioned above, other bioinks decorated with click reaction have also been developed. Poly(vinyl alcohol) (PVA), a water soluble, nontoxic polymer, has been widely applied in industrial production, cosmetics, food, and biomedical fields.²⁹¹ The secondary hydroxyl groups in molecular structure endow PVA with many modification opportunities. For instance, PVA has been functionalized with aldehyde, hydrazide, thiol, azide, alkyne, *etc.* in the literature.^{292–294} For thiol-ene modified PVA bioinks, the high reactivity of norbornene groups improves the reaction

rate, while PVA functionalized with ally group exhibits good cytocompatibility.^{102,295} PVA-based bioinks were also reported to reduce incompatibility caused by viscosity and thus improve printability characteristics. For instance, PVA was functionalized with *cis*-5-norbornene-endo-2,3-dicarboxylic anhydride (PVA-Nb) and amine (PVA-A) respectively, and then combined with solubilized decellularized cartilage matrix (SDCM) to obtain bioinks with printability characteristics.²⁹⁶ PVA-A/SDCM is printability, but its shape retention is poor due to slow cross-linking kinetics. The thiol-ene reaction promotes the rapid formation of PVA-Nb/SDCM bioinks and endows excellent printability. The structural integrity over 25 layers is well preserved. The cell viability post-bioprinting kept a high value up to 7 days.

Poly(glycidol) (PG) solution, as a new polymer bioinks, combined with high molecular weight HA is appropriate for 3D printing. PG molecules were functionalized with thiol- and allyl group, and then hyaluronic acid (HA) was added. When the ratio of HA to PG is 1 : 10, the materials are assigned by a nozzle with drops.²⁹⁷ The lower initial stability of the solution prevents the printing of the second layer. With the increasing of ratio, the stability has been improved. The solution with a ratio of 7 : 30 flows out of the nozzle within a strand, exhibiting higher stability.²⁹⁷ The PG modified with allyl and thiol group can form uniformly networks have been formed *via* UV-mediated thiol-ene click reaction. 3D printing with PG/HA solutions has good reproducibility and the products have no collapse. PG is a structural analogue of PEG.²⁹⁸ The production of chondrogenesis in pure PG gels is low owing to its weaker cell-initiated deposition of ECM molecules. This issue can be solved by decorated PG. A stable hybrid hydrogel was prepared by combining allyl-functionalized poly(glycidol)s (P(AGE-co-G)) and thiol-functionalized hyaluronic acid (HA-SH) *via* UV-induced radical thiol-ene reaction.¹⁹⁷ After adding the thicker of HA (1 wt% and 2.5 wt%), the constructs with high shape fidelity were printed. These hybrid hydrogels enhanced the staining of GAG, aggrecan, and collagen II, promoting chondrogenesis.

In order to further expand the bioink library and bioprinting capability, especially for the formation of super-soft tissue, researchers used photocrosslinkable polymer to achieve printing *via* complementary network strategy. These polymers contain HAMA, norbornene-functionalized hyaluronic acid (HANB), gelatin methacryloyl (GelMA), allylated gelatin (GelAGE), methacrylated chondroitin sulfate (CSMA), methacrylated dextran (DexMA), methacrylated alginate (AlgMA), methacrylated chitosan (ChiMA), methacrylated heparin (HepMA), PEG diacrylate (PEGDA), eight-arm PEG acrylate (PEGA), and norbornene-functionalized four-arm PEG (PEGNB).²⁹⁹ The photocrosslinked polymers were mixed with 5% gelatin to form a composite bioinks, labeled HAMA⁺, HANB⁺, GelMA⁺, GelAGE⁺, CSMA⁺, DexMA⁺, AlgMA⁺, ChiMA⁺, HepMA⁺, PEGDA⁺, PEGA⁺, and PEGNB⁺. The thermal responsive gelatin network provides excellent extrusion and structural stability. The thermal covalent cross-linking network, *via* chain-growth mechanism and step-growth mechanism between norbornene and allyl, provides stable printing structure. These

polymers combine to form a complementary network hydrogel. The results present that the addition of gelatin has little effect on the long-term mechanical properties of the printed structure, and the composition of gelatin mainly determines the printability of bioinks.

5. Conclusions and future perspectives

Click chemistry reaction provides some advantages for bioprinting and bioinks. These include simple and mild reaction conditions, avoiding damage to cells by toxic cross-linking agents, promoting gelation at room temperature or physiological temperature, and adjusting mechanical properties and degradation rates according to application requirements. The resulting hydrogels also have homogeneous crosslinked networks. The printing accuracy and shape fidelity of printed constructs are maintained and enhanced. Cells encapsulated in bioinks decorated with click chemistry reaction present good cell viability, spread, and proliferation. The aforementioned benefits of click chemistry, therefore, provide support for the development and application of tissue engineering and regenerative medicine. Most of bioinks can be decorated *via* click reaction to improve physicochemical properties, that play an important role in the success of bioprinting. However, there are challenges that must be addressed. For instance, this review established the difficulty of a single bioink in meeting the various requirements of bioprinting, such as mechanical properties, cross-linking density, swelling rate, resolution, *etc.* These factors are critical to the shape stability, cell encapsulation, diffusion, and proliferation of printed constructs. Hence, the effect of mixed bioinks on the properties of printed hydrogels needs to be further investigated. For the preparation of bioprinting or bioink involved in CuAAC reaction, great attention should be paid to completely removing the toxic catalyst or initiator after the reaction to avoid its harm to biological tissues and obtain higher quality and high safety products. Having highlighted the benefits of click chemistry in Bioink preparation, several problems have been identified that may limit its wide acceptance for use in clinical trials. For instance, since common natural hydrogel materials may present some incompatibility challenges with click chemistry, there may be a need to introduce alternative reactants that may not comply with safety regulations. Additionally, when structures are prepared using several click reactions, there is an enhanced risk of unpredictable side reactions occurring that may affect the overall process. Indeed, it is reported that a comparatively low number of hydrogel products, produced from click chemistry are currently being applied in the clinical trials.³⁰⁰ More work in the area of improving click chemistry and understanding the safety limitations is therefore necessary as such improvement will promote the further development of 3D bioprinting and accelerate application of click chemistry in clinical trials for tissue engineering and regenerative medicine applications.

Conflicts of interest

The authors declare no competing financial interest.

Acknowledgements

The authors acknowledge the support from the Nanhu Scholars Program for Young Scholars of XYNU, Natural Science Foundation of Jiangsu Province (BK20200791), High-Level Talents Program of Jinling Institute of Technology (Jit-b-202052),

References

- 1 A. Fatimi, O. V. Okoro, D. Podstawczyk, J. Siminska-Stanny and A. Shavandi, *Gels*, 2022, **8**(3), 179.
- 2 N. Ashammakhi, S. Ahadian, I. Pountos, S.-K. Hu, N. Tellisi, P. Bandaru, S. Ostrovidov, M. R. Dokmeci and A. Khademhosseini, *Biomed. Microdev.*, 2019, **21**, 42.
- 3 G. Decante, J. B. Costa, J. Silva-Correia, M. N. Collins, R. L. Reis and J. M. Oliveira, *Biofabrication*, 2021, **13**, 032001.
- 4 A. GhavamiNejad, N. Ashammakhi, X. Y. Wu and A. Khademhosseini, *Small*, 2020, **16**, 2002931.
- 5 O. V. Okoro, A. Amenaghawon, D. Podstawczyk, H. Alimoradi, M. R. Khalili, M. Anwar, P. B. Milan, L. Nie and A. Shavandi, *J. Cleaner Prod.*, 2021, **328**, 129498.
- 6 M. M. Stanton, J. Samitier and S. Sánchez, *Lab Chip*, 2015, **15**, 3111–3115.
- 7 E. Axpe and M. L. Oyen, *Int. J. Mol. Sci.*, 2016, **17**(12), 1976.
- 8 Y. Loo, A. Lakshmanan, M. Ni, L. L. Toh, S. Wang and C. A. E. Hauser, *Nano Lett.*, 2015, **15**, 6919–6925.
- 9 A. GhavamiNejad, N. Ashammakhi, X. Y. Wu and A. Khademhosseini, *Small*, 2020, **16**, 2002931.
- 10 K. G. Cornwell, P. Lei, S. T. Andreadis and G. D. Pins, *J. Biomed. Mater. Res., Part A*, 2007, **80A**(2), 362–371.
- 11 J. Yin, M. Yan, Y. Wang, J. Fu and H. Suo, *ACS Appl. Mater. Interfaces*, 2018, **10**, 6849–6857.
- 12 V. H. M. Mouser, F. P. W. Melchels, J. Visser, W. J. A. Dhert, D. Gawlitta and J. Malda, *Biofabrication*, 2016, **8**, 035003.
- 13 L. T. Mashabela, M. M. Maboja, N. F. Miya, T. O. Ajayi, R. S. Chasara, M. Milne, S. Mokhele, P. H. Demana, B. A. Witika, X. Siwe-Noundou and M. S. Poka, *Gels*, 2022, **8**(9), 563.
- 14 L. L. Wang, C. B. Highley, Y.-C. Yeh, J. H. Galarraga, S. Uman and J. A. Burdick, *J. Biomed. Mater. Res., Part A*, 2018, **106**(4), 865–875.
- 15 H. Chen, F. Fei, X. Li, Z. Nie, D. Zhou, L. Liu, J. Zhang, H. Zhang, Z. Fei and T. Xu, *Bioactive Mater.*, 2021, **6**, 3580–3595.
- 16 Y. Zou, L. Zhang, L. Yang, F. Zhu, M. Ding, F. Lin, Z. Wang and Y. Li, *J. Controlled Release*, 2018, **273**, 160–179.
- 17 Y. Deng, A. Shavandi, O. V. Okoro and L. Nie, *Carbohydr. Polym.*, 2021, **270**, 118360.
- 18 R. Huisgen, *Angew. Chem., Int. Ed. Engl.*, 1963, **2**, 565–598.
- 19 M. Meldal and F. Diness, *Trends Chem.*, 2020, **2**, 569–584.
- 20 M. Meldal and C. W. Tornøe, *Chem. Rev.*, 2008, **108**(8), 2952–3015.

- 21 J. E. Hein and V. V. Fokin, *Chem. Soc. Rev.*, 2010, **39**, 1302–1315.
- 22 J. Gierlich, G. A. Burley, P. M. E. Gramlich, D. M. Hammond and T. Carell, *Org. Lett.*, 2006, **8**, 3639–3642.
- 23 G. J. Brewer, *Chem. Res. Toxicol.*, 2010, **23**, 319–326.
- 24 G. J. Brewer, *Curr. Opin. Chem. Biol.*, 2003, **7**, 207–212.
- 25 G. J. Brewer, *Exp. Biol. Med.*, 2000, **223**, 39–46.
- 26 H. Li, X. Li, P. Jain, H. Peng, K. Rahimi, S. Singh and A. Pich, *Biomacromolecules*, 2020, **21**, 4933–4944.
- 27 A. Koschella, M. Hartlieb and T. Heinze, *Carbohydr. Polym.*, 2011, **86**, 154–161.
- 28 R. T. Chen, S. Marchesan, R. A. Evans, K. E. Styan, G. K. Such, A. Postma, K. M. McLean, B. W. Muir and F. Caruso, *Biomacromolecules*, 2012, **13**, 889–895.
- 29 S. Piluso, R. Vukićević, U. Nöchel, S. Braune, A. Lendlein and A. T. Neffe, *Eur. Polym. J.*, 2018, **100**, 77–85.
- 30 Z. Sun, S. Liu, K. Li, L. Tan, L. Cen and G. Fu, *Soft Matter*, 2016, **12**, 2192–2199.
- 31 V. Truong, I. Blakey and A. K. Whittaker, *Biomacromolecules*, 2012, **13**, 4012–4021.
- 32 S. Li, Y. Xu, J. Yu and M. L. Becker, *Biomaterials*, 2017, **141**, 176–187.
- 33 O. De Los Cobos, B. Fousseret, M. Lejeune, F. Rossignol, M. Dutreilh-Colas, C. Carrion, C. Boissière, F. Ribot, C. Sanchez, X. Cattoën, M. Wong Chi Man and J.-O. Durand, *Chem. Mater.*, 2012, **24**, 4337–4342.
- 34 N. J. Agard, J. A. Prescher and C. R. J. J. O. T. A. C. S. Bertozzi, *J. Am. Chem. Soc.*, 2004, **126**, 15046–15047.
- 35 N. E. Mbua, J. Guo, M. A. Wolfert, R. Steet and G.-J. Boons, *ChemBioChem*, 2011, **12**, 1912–1921.
- 36 S. I. Presolski, V. Hong, S.-H. Cho and M. G. Finn, *J. Am. Chem. Soc.*, 2010, **132**, 14570–14576.
- 37 N. J. Agard, J. M. Baskin, J. A. Prescher, A. Lo and C. R. Bertozzi, *ACS Chem. Biol.*, 2006, **1**, 644–648.
- 38 X. Su, L. Bu, H. Dong, S. Fu, R. Zhuo and Z. Zhong, *RSC Adv.*, 2016, **6**, 2904–2909.
- 39 H. Jiang, S. Qin, H. Dong, Q. Lei, X. Su, R. Zhuo and Z. Zhong, *Soft Matter*, 2015, **11**, 6029–6036.
- 40 H. Zhan, S. Jiang, A. M. Jonker, I. A. B. Pijpers and D. W. P. M. Löwik, *J. Mater. Chem. B*, 2020, **8**, 5912–5920.
- 41 J. Xu, T. M. Fillion, F. Prifti and J. Song, *Chem. – Asian J.*, 2011, **6**, 2730–2737.
- 42 H. J. Lee, G. M. Fernandes-Cunha, K.-S. Na, S. M. Hull and D. Myung, *Adv. Healthcare Mater.*, 2018, **7**, 1800560.
- 43 S. M. Hull, C. D. Lindsay, L. G. Brunel, D. J. Shiwardski, J. W. Tashman, J. G. Roth, D. Myung, A. W. Feinberg and S. C. Heilshorn, *Adv. Funct. Mater.*, 2021, **31**, 2007983.
- 44 A. Sanyal, *Macromol. Chem. Phys.*, 2010, **211**, 1417–1425.
- 45 K. C. Nicolaou, S. A. Snyder, T. Montagnon and G. Vassilikogiannakis, *Angew. Chem., Int. Ed.*, 2002, **41**, 1668–1698.
- 46 K. C. Koehler, D. L. Alge, K. S. Anseth and C. N. Bowman, *Biomaterials*, 2013, **34**, 4150–4158.
- 47 U. M. Lindström, *Chem. Rev.*, 2002, **102**, 2751–2772.
- 48 S. Otto and J. B. F. N. Engberts, *Org. Biomol. Chem.*, 2003, **1**, 2809–2820.
- 49 L. Hahn, M. Beudert, M. Gutmann, L. Kefßler, P. Stahlhut, L. Fischer, E. Karakaya, T. Lorson, I. Thievensen, R. Detsch, T. Lühmann and R. Luxenhofer, *Macromol. Biosci.*, 2021, **21**, 2100122.
- 50 A. L. Rutz, E. S. Gargus, K. E. Hyland, P. L. Lewis, A. Setty, W. R. Burghardt and R. N. Shah, *Acta Biomater.*, 2019, **99**, 121–132.
- 51 M. Mihajlovic, M. Rikkers, M. Mihajlovic, M. Viola, G. Schuiringa, B. C. Ilochonwu, R. Masereeuw, L. Vonk, J. Malda, K. Ito and T. Vermonden, *Biomacromolecules*, 2022, **23**, 1350–1365.
- 52 A. F. Jacobine, Radiation Curing in Polymer Science and Technology: Polymerisation Mechanisms, in *Thiol-Ene Photopolymers*, ed. J. P. Fouassier and J. F. Rabek, Elsevier Science Publishers, Ltd., New York, 1993, vol. III, pp. 219–268.
- 53 H. Leonards, S. Engelhardt, A. Hoffmann, L. Pongratz, S. Schriever, J. Bläsius, M. M. Wehner and A. Gillner, Advantages and drawbacks of Thiol-ene based resins for 3D-printing, *Laser 3D Manufacturing II*, 2015, 9353, 93530F1-7, <https://doi.org/10.1117/12.2081169>.
- 54 C. E. Hoyle and C. N. Bowman, *Angew. Chem., Int. Ed.*, 2010, **49**, 1540–1573.
- 55 M. J. Kade, D. J. Burke and C. J. Hawker, *J. Polym. Sci., Part A: Polym. Chem.*, 2010, **48**, 743–750.
- 56 R. F. Pereira and P. J. J. E. Bártolo, *Engineering*, 2015, **1**, 090–112.
- 57 A. F. Senyurt, H. Wei, C. E. Hoyle, S. G. Piland and T. E. Gould, *Macromolecules*, 2007, **40**, 4901–4909.
- 58 Y. Zhang, S. Liu, T. Li, L. Zhang, U. Azhar, J. Ma, C. Zhai, C. Zong and S. Zhang, *Carbohydr. Polym.*, 2020, **236**, 116021.
- 59 H. Du, G. Zha, L. Gao, H. Wang, X. Li, Z. Shen and W. Zhu, *Polym. Chem.*, 2014, **5**, 4002–4008.
- 60 R. F. Pereira, C. C. Barrias, P. J. Bártolo and P. L. Granja, *Acta Biomater.*, 2018, **66**, 282–293.
- 61 T. E. Brown, B. J. Carberry, B. T. Worrell, O. Y. Dudaryeva, M. K. McBride, C. N. Bowman and K. S. Anseth, *Biomaterials*, 2018, **178**, 496–503.
- 62 C. F. H. Allen, J. O. Fournier and W. J. Humphlett, *Can. J. Chem.*, 1964, **42**, 2616–2620.
- 63 B. D. Mather, K. Viswanathan, K. M. Miller and T. E. Long, *Prog. Polym. Sci.*, 2006, **31**, 487–531.
- 64 C. E. Hoyle, A. B. Lowe and C. N. Bowman, *Chem. Soc. Rev.*, 2010, **39**, 1355–1387.
- 65 N. B. Cramer, S. K. Reddy, A. K. O'Brien and C. N. J. M. Bowman, *Macromolecules*, 2003, **36**, 7964–7969.
- 66 B. H. Northrop and R. N. Coffey, *J. Am. Chem. Soc.*, 2012, **134**, 13804–13817.
- 67 B. D. Fairbanks, D. M. Love and C. N. Bowman, *Macromol. Chem. Phys.*, 2017, **218**, 1700073.
- 68 S. C. Rizzi, M. Ehrbar, S. Halstenberg, G. P. Raebler, H. G. Schmoekel, H. Hagenmüller, R. Müller, F. E. Weber and J. A. Hubbell, *Biomacromolecules*, 2006, **7**, 3019–3029.
- 69 S. C. Rizzi and J. A. Hubbell, *Biomacromolecules*, 2005, **6**, 1226–1238.

- 70 Z.-C. Wang, X.-D. Xu, C.-S. Chen, L. Yun, J.-C. Song, X.-Z. Zhang and R.-X. Zhuo, *ACS Appl. Mater. Interfaces*, 2010, **2**, 1009–1018.
- 71 X. Sui, L. van Ingen, M. A. Hempenius and G. J. Vancso, *Macromol. Rapid Commun.*, 2010, **31**, 2059–2063.
- 72 L. E. Jansen, L. J. Negrón-Piñero, S. Galarza and S. R. Peyton, *Acta Biomater.*, 2018, **70**, 120–128.
- 73 A. L. Rutz, K. E. Hyland, A. E. Jakus, W. R. Burghardt and R. N. Shah, *Adv. Mater.*, 2015, **27**, 1607–1614.
- 74 R. Jin, L. S. Moreira Teixeira, A. Krouwels, P. J. Dijkstra, C. A. van Blitterswijk, M. Karperien and J. Feijen, *Acta Biomater.*, 2010, **6**, 1968–1977.
- 75 S. Ulrich, D. Boturyn, A. Marra, O. Renaudet and P. Dumy, *Chem. – Eur. J.*, 2014, **20**, 34–41.
- 76 K. L. Christman, R. M. Broyer, Z. P. Tolstyka and H. D. Maynard, *J. Mater. Chem.*, 2007, **17**, 2021–2027.
- 77 J. Collins, Z. Xiao, M. Müllner and L. A. Connal, *Polym. Chem.*, 2016, **7**, 3812–3826.
- 78 S. Hafeez, H. W. Ooi, F. L. C. Morgan, C. Mota, M. Dettin, C. Van Blitterswijk, L. Moroni and M. B. Baker, *Gels*, 2018, **4**, 85.
- 79 G. N. Grover, J. Lam, T. H. Nguyen, T. Segura and H. D. Maynard, *Biomacromolecules*, 2012, **13**, 3013–3017.
- 80 J. Karvinen, T. Joki, L. Ylä-Outinen, J. T. Koivisto, S. Narkilahti and M. Kellomäki, *React. Funct. Polym.*, 2018, **124**, 29–39.
- 81 T. Hozumi, T. Kageyama, S. Ohta, J. Fukuda and T. Ito, *Biomacromolecules*, 2018, **19**, 288–297.
- 82 M. Patenaude, S. Campbell, D. Kinio and T. Hoare, *Biomacromolecules*, 2014, **15**, 781–790.
- 83 Z. Xu and K. M. Bratlie, *ACS Biomater. Sci. Eng.*, 2018, **4**, 2276–2291.
- 84 S. V. Murphy and A. Atala, *Nat. Biotechnol.*, 2014, **32**, 773–785.
- 85 C. Mandrycky, Z. Wang, K. Kim and D.-H. Kim, *Biotechnol. Adv.*, 2016, **34**, 422–434.
- 86 A. Atala and J. J. Yoo, *Essentials of 3D biofabrication and translation*, Academic Press, 2015.
- 87 S. Derakhshanfar, R. Mbeleck, K. Xu, X. Zhang, W. Zhong and M. Xing, *Bioactive Mater.*, 2018, **3**, 144–156.
- 88 Y. Zhang, P. Kumar, S. Lv, D. Xiong, H. Zhao, Z. Cai and X. Zhao, *Mater. Des.*, 2021, **199**, 109398.
- 89 R. D. Pedde, B. Mirani, A. Navaei, T. Styan, S. Wong, M. Mehrali, A. Thakur, N. K. Mohtaram, A. Bayati and A. J. A. M. Dolatshahi-Pirouz, *Adv. Mater.*, 2017, **29**, 1606061.
- 90 I. T. Ozbolat and M. Hospodiuk, *Biomaterials*, 2016, **76**, 321–343.
- 91 L. H. Kang, P. A. Armstrong, L. J. Lee, B. Duan, K. H. Kang and J. T. Butcher, *Ann. Biomed. Eng.*, 2017, **45**, 360–377.
- 92 R. Landers, U. Hübner, R. Schmelzeisen and R. Mülhaupt, *Biomaterials*, 2002, **23**, 4437–4447.
- 93 K. Hözl, S. Lin, L. Tytgat, S. Van Vlierberghe, L. Gu and A. Ovsianikov, *Biofabrication*, 2016, **8**, 032002.
- 94 G. Gillispie, P. Prim, J. Copus, J. Fisher, A. G. Mikos, J. J. Yoo, A. Atala and S. J. Lee, *Biofabrication*, 2020, **12**, 022003.
- 95 A. G. Tabriz, M. A. Hermida, N. R. Leslie and W. Shu, *Biofabrication*, 2015, **7**, 045012.
- 96 L. Bian, C. Hou, E. Tous, R. Rai, R. L. Mauck and J. A. Burdick, *Biomaterials*, 2013, **34**, 413–421.
- 97 G. Skeldon, B. Lucendo-Villarin and W. Shu, *Philos. Trans. R. Soc., B*, 2018, **373**, 20170224.
- 98 S. Ramesh, O. L. A. Harrysson, P. K. Rao, A. Tamayol, D. R. Cormier, Y. Zhang and I. V. Rivero, *Bioprinting*, 2021, **21**, e00116.
- 99 H. Li, Y. J. Tan, S. Liu and L. Li, *ACS Appl. Mater. Interfaces*, 2018, **10**, 11164–11174.
- 100 C. W. Peak, K. A. Singh, M. A. Adlouni, J. Chen and A. K. Gaharwar, *Adv. Healthcare Mater.*, 2019, **8**, 1801553.
- 101 R. F. Pereira, B. N. Lourenço, P. J. Bartolo and P. L. Granja, *Adv. Healthcare Mater.*, 2021, **10**, 2001176.
- 102 C. E. Hoyle, T. Y. Lee and T. Roper, *J. Polym. Sci., Part A: Polym. Chem.*, 2004, **42**, 5301–5338.
- 103 M. A. Tasdelen and Y. Yagci, *Angew. Chem., Int. Ed.*, 2013, **52**, 5930–5938.
- 104 T. J. Tigner, S. Rajput, A. K. Gaharwar and D. L. Alge, *Biomacromolecules*, 2020, **21**, 454–463.
- 105 Z. Gu, J. Fu, H. Lin and Y. He, *Asian J. Pharm. Sci.*, 2020, **15**, 529–557.
- 106 W. Liu, M. A. Heinrich, Y. Zhou, A. Akpek, N. Hu, X. Liu, X. Guan, Z. Zhong, X. Jin, A. Khademhosseini and Y. S. Zhang, *Adv. Healthcare Mater.*, 2017, **6**, 1601451.
- 107 Q. Gao, X. Niu, L. Shao, L. Zhou, Z. Lin, A. Sun, J. Fu, Z. Chen, J. Hu, Y. Liu and Y. He, *Biofabrication*, 2019, **11**, 035006.
- 108 L. Klouda, *Eur. J. Pharm. Biopharm.*, 2015, **97**, 338–349.
- 109 C. Joly-Duhamel, D. Hellio and M. Djabourov, *Langmuir*, 2002, **18**, 7208–7217.
- 110 Y. Yao, A. Molotnikov, H. C. Parkington, L. Meagher and J. S. J. B. Forsythe, *Biofabrication*, 2022, **14**, 035014.
- 111 J. L. Guo, Y. S. Kim, V. Y. Xie, B. T. Smith, E. Watson, J. Lam, H. A. Pearce, P. S. Engel and A. G. Mikos, *Sci. Adv.*, 2019, **5**, eaaw7396.
- 112 X. Ren, D. Evangelista-Leite, T. Wu, T. K. Rajab, P. T. Moser, K. Kitano, K. P. Economopoulos, D. E. Gorman, J. P. Bloom, J. J. Tan, S. E. Gilpin, H. Zhou, D. J. Mathisen and H. C. Ott, *Biomaterials*, 2018, **182**, 127–134.
- 113 J. L. Guo, L. Diaz-Gomez, V. Y. Xie, S. M. Bittner, E. Y. Jiang, B. Wang and A. G. Mikos, *Bioprinting*, 2021, **22**, e00136.
- 114 N. M. Moore, N. J. Lin, N. D. Gallant and M. L. Becker, *Biomaterials*, 2010, **31**, 1604–1611.
- 115 Y.-C. Wu, S.-Y. Shaw, H.-R. Lin, T.-M. Lee and C.-Y. Yang, *Biomaterials*, 2006, **27**, 896–904.
- 116 S. Bose, S. Vahabzadeh and A. Bandyopadhyay, *Mater. Today*, 2013, **16**, 496–504.
- 117 N. A. Sears, D. R. Seshadri, P. S. Dhavalikar and E. Cosgriff-Hernandez, *Tissue Eng., Part B*, 2016, **22**, 298–310.
- 118 T. Billiet, M. Vandenhaute, J. Schelfhout, S. Van Vlierberghe and P. Dubruel, *Biomaterials*, 2012, **33**, 6020–6041.
- 119 A. A. Pawar, G. Saada, I. Cooperstein, L. Larush, J. A. Jackman, S. R. Tabaei, N.-J. Cho and S. Magdassi, *Appl. Sci. Eng.*, 2016, **2**, e1501381.

- 120 R. Gauvin, Y.-C. Chen, J. W. Lee, P. Soman, P. Zorlutuna, J. W. Nichol, H. Bae, S. Chen and A. Khademhosseini, *Biomaterials*, 2012, **33**, 3824–3834.
- 121 M. Gou, X. Qu, W. Zhu, M. Xiang, J. Yang, K. Zhang, Y. Wei and S. Chen, *Nat. Commun.*, 2014, **5**, 3774.
- 122 J. R. Tumbleston, D. Shirvanyants, N. Ermoshkin, R. Januszewicz, A. R. Johnson, D. Kelly, K. Chen, R. Pinschmidt, J. P. Rolland and A. J. S. Ermoshkin, *Science*, 2015, **347**, 1349–1352.
- 123 C. Cha, J. Oh, K. Kim, Y. Qiu, M. Joh, S. R. Shin, X. Wang, G. Camci-Unal, K.-T. Wan, R. Liao and A. Khademhosseini, *Biomacromolecules*, 2014, **15**, 283–290.
- 124 J. Jung and J. Oh, *Biomicrofluidics*, 2014, **8**, 036503.
- 125 J. Cadet, E. Sage and T. Douki, *Mutat. Res.*, 2005, **571**, 3–17.
- 126 D. Kulms, E. Zeise, B. Pöppelmann and T. Schwarz, *Oncogene*, 2002, **21**, 5844–5851.
- 127 B. K. Armstrong and A. Krickler, *J. Photochem. Photobiol., B*, 2001, **63**, 8–18.
- 128 F. R. de Gruijl, H. J. van Kranen and L. H. F. Mullenders, *J. Photochem. Photobiol., B*, 2001, **63**, 19–27.
- 129 Z. Wang, X. Jin, R. Dai, J. F. Holzman and K. Kim, *RSC Adv.*, 2016, **6**, 21099–21104.
- 130 P. Colombo, G. Mera, R. Riedel and G. D. Sorarù, *J. Am. Ceram. Soc.*, 2010, **93**, 1805–1837.
- 131 A. Hoffmann, H. Leonards, N. Tobies, L. Pongratz, K. Kreuels, F. Kreimendahl, C. Apel, M. Wehner and N. Nottrodt, *J. Tissue Eng.*, 2017, **8**, 2041731417744485.
- 132 A. Hoffmann, K. Kreuels and A. Gillner, *Macromol. Mater. Eng.*, 2022, **307**, 2100625.
- 133 X. Wang, F. Schmidt, D. Hanaor, P. H. Kamm, S. Li and A. Gurlo, *Addit. Manuf.*, 2019, **27**, 80–90.
- 134 A. C. Weems, K. R. Delle Chiaie, J. C. Worch, C. J. Stubbs and A. P. Dove, *Polym. Chem.*, 2019, **10**, 5959–5966.
- 135 T. Liu, L. Sun, R. Ou, Q. Fan, L. Li, C. Guo, Z. Liu and Q. Wang, *Chem. Eng. J.*, 2019, **368**, 359–368.
- 136 T. Modjinou, D.-L. Versace, S. Abbad-Andallousi, N. Bousserhine, J. Babinot, V. Langlois and E. Renard, *ACS Sustainable Chem. Eng.*, 2015, **3**, 1094–1100.
- 137 J.-T. Miao, L. Yuan, Q. Guan, G. Liang, A. Gu and Engineering, *ACS Sustainable Chem. Eng.*, 2018, **6**, 7902–7909.
- 138 T. Wallin, J. Pikul, S. Bodkhe, B. Peele, B. Mac Murray, D. Theriault, B. McEnerney, R. Dillon, E. Giannelis and R. J. J. O. M. C. B. Shepherd, *J. Mater. Chem. B*, 2017, **5**, 6249–6255.
- 139 P. J. Bártolo, *Stereolithography: materials, processes and applications*, Springer Science & Business Media, 2011.
- 140 M. P. Patel, M. Braden and K. W. M. Davy, *Biomaterials*, 1987, **8**, 53–56.
- 141 H. Lu, J. A. Carioscia, J. W. Stansbury and C. N. Bowman, *Dent. Mater.*, 2005, **21**, 1129–1136.
- 142 K. D. Q. Nguyen, W. V. Megone, D. Kong and J. E. Gautrot, *Polym. Chem.*, 2016, **7**, 5281–5293.
- 143 I. A. Barker, M. P. Ablett, H. T. J. Gilbert, S. J. Leigh, J. A. Covington, J. A. Hoyland, S. M. Richardson and A. P. Dove, *Biomater. Sci.*, 2014, **2**, 472–475.
- 144 A. Linnenberger, C. Fiedler, J. J. Roberts, S. C. Skaalure, S. J. Bryant, M. C. Cole and R. R. McLeod, Optical trapping for tissue scaffold fabrication, *Optical Trapping and Optical Micromanipulation*, 2013, 8810, 88102F1–88102F10, <https://doi.org/10.1117/12.2027869>.
- 145 J. Torgersen, X.-H. Qin, Z. Li, A. Ovsianikov, R. Liska and J. Stampfl, *Adv. Funct. Mater.*, 2013, **23**, 4542–4554.
- 146 M. V. Tsurkan, C. Jungnickel, M. Schlierf and C. Werner, *J. Am. Chem. Soc.*, 2017, **139**, 10184–10187.
- 147 J. W. Lee, *J. Nanomater.*, 2016, **2015**, 1–14.
- 148 T. Boland, T. Xu, B. Damon and X. Cui, *Biotechnol. J.*, 2006, **1**, 910–917.
- 149 R. E. Saunders and B. Derby, *Int. Mater. Rev.*, 2014, **59**, 430–448.
- 150 B. Derby, *J. Mater. Chem.*, 2008, **18**, 5717–5721.
- 151 H. Gudapati, M. Dey and I. Ozbolat, *Biomaterials*, 2016, **102**, 20–42.
- 152 T. Xu, J. Jin, C. Gregory, J. J. Hickman and T. Boland, *Biomaterials*, 2005, **26**, 93–99.
- 153 M. E. Pepper, V. Seshadri, T. Burg, B. W. Booth, K. J. L. Burg and R. E. Groff, Cell settling effects on a thermal inkjet bioprinter, 2011 Annual International Conference of the IEEE Engineering in Medicine and Biology Society, 2011, pp. 3609–3612, DOI: [10.1109/iembs.2011.6090605](https://doi.org/10.1109/iembs.2011.6090605).
- 154 M. E. Pepper, V. Seshadri, T. C. Burg, K. J. L. Burg and R. E. Groff, *Biofabrication*, 2012, **4**, 011001.
- 155 L. R. Hart, J. L. Harries, B. W. Greenland, H. M. Colquhoun and W. Hayes, *Polym. Chem.*, 2015, **6**, 7342–7352.
- 156 L. R. Hart, J. L. Harries, B. W. Greenland, H. M. Colquhoun and W. Hayes, *ACS Appl. Mater. Interfaces*, 2015, **7**, 8906–8914.
- 157 G. M. Nishioka, A. A. Markey and C. K. Holloway, *J. Am. Chem. Soc.*, 2004, **126**, 16320–16321.
- 158 E. Cheng, H. Yu, A. Ahmadi and K. C. Cheung, *Biofabrication*, 2016, **8**, 015008.
- 159 B. C. Riggs, R. Elupula, S. M. Grayson and D. B. Chrisey, *J. Mater. Chem. A*, 2014, **2**, 17380–17386.
- 160 S. S. Rahman, M. Arshad, A. Qureshi and A. Ullah, *ACS Appl. Mater. Interfaces*, 2020, **12**, 51927–51939.
- 161 N. Reis, C. Ainsley and B. Derby, *J. Appl. Phys.*, 2005, **97**, 094903.
- 162 Y. Guo, H. S. Patanwala, B. Bognet and A. W. K. Ma, *Rapid Prototyp. J.*, 2017, **23**, 562–576.
- 163 B. C. Riggs, R. Elupula, C. Rehm, S. Adireddy, S. M. Grayson and D. B. Chrisey, *ACS Appl. Mater. Interfaces*, 2015, **7**, 17819–17825.
- 164 L. Wang, L. Zhang, D. Wang, M. Li, C. Du and S. Fu, *J. Dispersion Sci. Technol.*, 2019, **40**, 152–160.
- 165 B. R. Spears, M. A. Marin, A. N. Chaker, M. W. Lampley and E. Harth, *ACS Biomater. Sci. Eng.*, 2016, **2**, 1265–1272.
- 166 I. Kim, H. J. Byeon, T. H. Kim, E. S. Lee, K. T. Oh, B. S. Shin, K. C. Lee and Y. S. Youn, *Biomaterials*, 2012, **33**, 5574–5583.
- 167 H. Rupp and W. H. Binder, *Adv. Mater. Technol.*, 2020, **5**, 2000509.
- 168 L. Y. Daikuara, X. Chen, Z. Yue, D. Skropeta, F. M. Wood, M. W. Fear and G. G. Wallace, *Adv. Funct. Mater.*, 2022, **32**, 2105080.

- 169 T. Xu, C. Baicu, M. Aho, M. Zile and T. Boland, *Biofabrication*, 2009, **1**, 035001.
- 170 Z. Yue, X. Liu, P. T. Coates and G. G. Wallace, *Curr. Opin. Organ Transplant*, 2016, **21**, 467–475.
- 171 G. Gao, T. Yonezawa, K. Hubbell, G. Dai and X. Cui, *Biotechnol. J.*, 2015, **10**, 1568–1577.
- 172 I. T. Ozbolat and Y. Yu, *IEEE Trans. Biomed. Eng.*, 2013, **60**, 691–699.
- 173 Z. Wang, R. Abdulla, B. Parker, R. Samanipour, S. Ghosh and K. Kim, *Biofabrication*, 2015, **7**, 045009.
- 174 S. Magli, G. B. Rossi, G. Risi, S. Bertini, C. Cosentino, L. Crippa, E. Ballarini, G. Cavaletti, L. Piazza, E. Masseroni, F. Nicotra and L. Russo, *Front. Chem.*, 2020, **8**, 524.
- 175 C. Colosi, S. R. Shin, V. Manoharan, S. Massa, M. Costantini, A. Barbetta, M. R. Dokmeci, M. Dentini and A. Khademhosseini, *Adv. Mater.*, 2016, **28**, 677–684.
- 176 B. P. Toole, *Nat. Rev. Cancer*, 2004, **4**, 528–539.
- 177 T. Maver, D. M. Smrke, M. Kurečić, L. Gradišnik, U. Maver and K. S. Kleinschek, *J. Sol-Gel Sci. Technol.*, 2018, **88**, 33–48.
- 178 A. M. Compaan, K. Song and Y. Huang, *ACS Appl. Mater. Interfaces*, 2019, **11**, 5714–5726.
- 179 C. B. Highley, G. D. Prestwich and J. A. Burdick, *Curr. Opin. Biotechnol.*, 2016, **40**, 35–40.
- 180 M. K. Cowman, T. A. Schmidt, P. Raghavan and A. Stecco, *F1000Research*, 2015, **4**, 622.
- 181 T. Später, A. O. Mariyanats, M. A. Syachina, A. V. Mironov, A. G. Savelyev, A. V. Sochilina, M. D. Menger, P. A. Vishnyakova, E. Y. Kananykhina, T. K. Fatkhudinov, G. T. Sukhikh, D. D. Spitkovsky, A. Katsen-Globa, M. W. Laschke and V. K. Popov, *ACS Biomater. Sci. Eng.*, 2020, **6**, 5744–5757.
- 182 C. Antich, J. de Vicente, G. Jiménez, C. Chocarro, E. Carrillo, E. Montañez, P. Gálvez-Martin and J. A. Marchal, *Acta Biomater.*, 2020, **106**, 114–123.
- 183 J. H. Galarraga, R. C. Locke, C. E. Witherel, B. D. Stoeckl, M. Castilho, R. L. Mauck, J. Malda, R. Levato and J. A. Burdick, *Biofabrication*, 2021, **14**, 014106.
- 184 N. B. Cramer, T. Davies, A. K. O'Brien and C. N. Bowman, *Macromolecules*, 2003, **36**, 4631–4636.
- 185 J. H. Galarraga, M. Y. Kwon and J. A. Burdick, *Sci. Rep.*, 2019, **9**, 19987.
- 186 G. F. Acosta-Vélez, C. S. Linsley, M. C. Craig and B. M. Wu, *Bioengineering*, 2017, **4**(1), 11.
- 187 G. F. Acosta-Vélez, C. S. Linsley, T. Z. Zhu, W. Wu and B. M. Wu, *Polymers*, 2018, **10**(12), 1372.
- 188 L. Ouyang, C. B. Highley, W. Sun and J. A. Burdick, *Adv. Mater.*, 2017, **29**, 1604983.
- 189 W. F. Hynes, N. J. Doty, T. I. Zarembinski, M. P. Schwartz, M. W. Toepke, W. L. Murphy, S. K. Atzet, R. Clark, J. A. Melendez and N. C. Cady, *Biosensors*, 2014, **4**, 28–44.
- 190 D. L. Matera, W. Y. Wang, M. R. Smith, A. Shikanov and B. M. Baker, *ACS Biomater. Sci. Eng.*, 2019, **5**, 2965–2975.
- 191 H. Liu, S. Kitano, S. Irie, R. Levato and M. Matsusaki, *Adv. Biosys.*, 2020, **4**, 2000038.
- 192 H. Kim, J. Jang, J. Park, K.-P. Lee, S. Lee, D.-M. Lee, K. H. Kim, H. K. Kim and D.-W. J. B. Cho, *Biofabrication*, 2019, **11**, 035017.
- 193 M. E. Prendergast, M. D. Davidson and J. A. J. B. Burdick, *Biofabrication*, 2021, **13**, 044108.
- 194 C. B. Highley, K. H. Song, A. C. Daly and J. A. Burdick, *Adv. Sci.*, 2019, **6**, 1801076.
- 195 C. S. O'Hern, L. E. Silbert, A. J. Liu and S. R. Nagel, *Phys. Rev. E: Stat., Nonlinear, Soft Matter Phys.*, 2003, **68**, 011306.
- 196 X. Z. Shu, Y. Liu, F. S. Palumbo, Y. Luo and G. D. Prestwich, *Biomaterials*, 2004, **25**, 1339–1348.
- 197 S. Stichler, T. Böck, N. Paxton, S. Bertlein, R. Levato, V. Schill, W. Smolan, J. Malda, J. Teßmar and T. J. B. Blunk, *Biofabrication*, 2017, **9**, 044108.
- 198 J. Hauptstein, T. Böck, M. Bartolf-Kopp, L. Förster, P. Stahlhut, A. Nadernezhad, G. Blahetek, A. Zernecke-Madsen, R. Detsch, T. Jüngst, J. Groll, J. Teßmar and T. Blunk, *Adv. Healthcare Mater.*, 2020, **9**, 2000737.
- 199 A. A. Hegewald, J. Ringe, J. Bartel, I. Krüger, M. Notter, D. Barnewitz, C. Kaps and M. Sittinger, *Tissue Cell*, 2004, **36**, 431–438.
- 200 X. Liu, M. Hao, Z. Chen, T. Zhang, J. Huang, J. Dai and Z. Zhang, *Biomaterials*, 2021, **272**, 120771.
- 201 A. Skardal, M. Devarasetty, H.-W. Kang, I. Mead, C. Bishop, T. Shupe, S. J. Lee, J. Jackson, J. Yoo, S. Soker and A. Atala, *Acta Biomater.*, 2015, **25**, 24–34.
- 202 A. Skardal, J. Zhang, L. McCoard, X. Xu, S. Oottamasathien and G. D. Prestwich, *Tissue Eng., Part A*, 2010, **16**, 2675–2685.
- 203 J. Hauptstein, L. Förster, A. Nadernezhad, H. Horder, P. Stahlhut, J. Groll, T. Blunk and J. Teßmar, *Macromol. Biosci.*, 2022, **22**, 2100331.
- 204 J. Hauptstein, L. Förster, A. Nadernezhad, J. Groll, J. Teßmar and T. Blunk, *Int. J. Mol. Sci.*, 2022, **23**, 924.
- 205 A. Mazzocchi, M. Devarasetty, R. Huntwork, S. Soker and A. J. B. Skardal, *Biofabrication*, 2018, **11**, 015003.
- 206 C. C. Clark, J. Aleman, L. Mutkus and A. Skardal, *Bioprinting*, 2019, **16**, e00058.
- 207 A. Skardal, J. Zhang, L. McCoard, S. Oottamasathien and G. D. Prestwich, *Adv. Mater.*, 2010, **22**, 4736–4740.
- 208 T. Wan, P. Fan, M. Zhang, K. Shi, X. Chen, H. Yang, X. Liu, W. Xu and Y. Zhou, *ACS Appl. Bio Mater.*, 2022, **5**, 334–343.
- 209 H. Si, T. Xing, Y. Ding, H. Zhang, R. Yin and W. Zhang, *Polymers*, 2019, **11**, 1584.
- 210 J. A. Burdick and G. D. Prestwich, *Adv. Mater.*, 2011, **23**, H41–H56.
- 211 M. Jury, I. Matthiesen, F. R. Boroojeni, S. Ludwig, L. Civitelli, T. E. Winkler, R. Selegård, A. Herland and D. Aili, *Adv. Healthcare Mater.*, 2022, **11**, 2102097.
- 212 R. Pignatello, Collagen-vs. Gelatine-Based Biomaterials and Their Biocompatibility Review and Perspectives, in *Biomaterials: Applications for Nanomedicine*, ed. S. Gorgieva and V. Kokol, 2011, ch. 2, pp. 17–52.
- 213 N. Davidenko, C. F. Schuster, D. V. Bax, R. W. Farndale, S. Hamaia, S. M. Best and R. E. Cameron, *J. Mater. Sci.: Mater. Med.*, 2016, **27**, 148.
- 214 A. Salamon, S. Van Vlierberghe, I. Van Nieuwenhove, F. Baudisch, G.-J. Graulus, V. Benecke, K. Alberti, H.-G. Neumann, J. Rychly, J. C. Martins, P. Dubruel and K. Peters, *Materials*, 2014, **7**, 1342–1359.

- 215 B. G. Soliman, G. S. Major, P. Atienza-Roca, C. A. Murphy, A. Longoni, C. R. Alcala-Orozco, J. Rnjak-Kovacina, D. Gawlitta, T. B. F. Woodfield and K. S. Lim, *Adv. Healthcare Mater.*, 2022, **11**, 2101873.
- 216 C. Yu, K. L. Miller, J. Schimelman, P. Wang, W. Zhu, X. Ma, M. Tang, S. You, D. Lakshmipathy, F. He and S. Chen, *Biomaterials*, 2020, **258**, 120294.
- 217 X.-H. Qin, J. Torgersen, R. Saf, S. Mühleder, N. Pucher, S. C. Ligon, W. Holthöner, H. Redl, A. Ovsianikov, J. Stampfl and R. Liska, *J. Polym. Sci., Part A: Polym. Chem.*, 2013, **51**, 4799–4810.
- 218 J. Van Hoorick, P. Gruber, M. Markovic, M. Rollot, G.-J. Graulus, M. Vagenende, M. Tromayer, J. Van Erps, H. Thienpont, J. C. Martins, S. Baudis, A. Ovsianikov, P. Dubrueel and S. Van Vlierberghe, *Macromol. Rapid Commun.*, 2018, **39**, 1800181.
- 219 A. Dobos, J. Van Hoorick, W. Steiger, P. Gruber, M. Markovic, O. G. Andriotis, A. Rohatschek, P. Dubrueel, P. J. Thurner, S. Van Vlierberghe, S. Baudis and A. Ovsianikov, *Adv. Healthcare Mater.*, 2020, **9**, 1900752.
- 220 A. Dobos, F. Gantner, M. Markovic, J. Van Hoorick, L. Tytgat, S. Van Vlierberghe and A. Ovsianikov, *Biofabrication*, 2020, **13**, 015016.
- 221 M. Castilho, R. Levato, P. N. Bernal, M. de Ruijter, C. Y. Sheng, J. van Duijn, S. Piluso, K. Ito and J. Malda, *Biomacromolecules*, 2021, **22**, 855–866.
- 222 L. E. Bertassoni, J. C. Cardoso, V. Manoharan, A. L. Cristino, N. S. Bhise, W. A. Araujo, P. Zorlutuna, N. E. Vrana, A. M. Ghaemmaghami, M. R. Dokmeci and A. Khademhossein, *Biofabrication*, 2014, **6**, 024105.
- 223 T. Jain, H. B. Baker, A. Gipsov, J. P. Fisher, A. Joy, D. S. Kaplan and I. Isayeva, *Bioprinting*, 2021, **22**, e00131.
- 224 K. Yue, G. Trujillo-de Santiago, M. M. Alvarez, A. Tamayol, N. Annabi and A. Khademhosseini, *Biomaterials*, 2015, **73**, 254–271.
- 225 J. J. Roberts and S. J. Bryant, *Biomaterials*, 2013, **34**, 9969–9979.
- 226 M. D. Carlo, Jr. and R. F. Loeser, *Arthritis Rheum.*, 2003, **48**, 3419–3430.
- 227 C.-C. Lin, S. M. Sawicki and A. T. Metters, *Biomacromolecules*, 2008, **9**, 75–83.
- 228 A. K. O'Brien, N. B. Cramer and C. N. Bowman, *J. Polym. Sci., Part A: Polym. Chem.*, 2006, **44**, 2007–2014.
- 229 Z. Muñoz, H. Shih and C.-C. Lin, *Biomater. Sci.*, 2014, **2**, 1063–1072.
- 230 B. D. Fairbanks, M. P. Schwartz, A. E. Halevi, C. R. Nuttelman, C. N. Bowman and K. S. Anseth, *Adv. Mater.*, 2009, **21**, 5005–5010.
- 231 A. M. Kloxin, C. J. Kloxin, C. N. Bowman and K. S. Anseth, *Adv. Mater.*, 2010, **22**, 3484–3494.
- 232 C. Zhao, Z. Wu, H. Chu, T. Wang, S. Qiu, J. Zhou, Q. Zhu, X. Liu, D. Quan and Y. Bai, *Biomacromolecules*, 2021, **22**, 2729–2739.
- 233 L. Tytgat, L. Van Damme, J. Van Hoorick, H. Declercq, H. Thienpont, H. Ottevaere, P. Blondeel, P. Dubrueel and S. Van Vlierberghe, *Acta Biomater.*, 2019, **94**, 340–350.
- 234 T. Göckler, S. Haase, X. Kempter, R. Pfister, B. R. Maciel, A. Grimm, T. Molitor, N. Willenbacher and U. Schepers, *Adv. Healthcare Mater.*, 2021, **10**, 2100206.
- 235 V. Burchak, F. Koch, L. Siebler, S. Haase, V. K. Horner, X. Kempter, G. B. Stark, U. Schepers, A. Grimm, S. Zimmermann, P. Koltay, S. Strassburg, G. Finkenzeller, F. Simunovic and F. Lampert, *Int. J. Mol. Sci.*, 2022, **23**(14), 7939.
- 236 J. Van Hoorick, A. Dobos, M. Markovic, T. Gheysens, L. Van Damme, P. Gruber, L. Tytgat, J. Van Erps, H. Thienpont, P. Dubrueel, A. Ovsianikov and S. Van Vlierberghe, *Biofabrication*, 2021, **13**, 015017.
- 237 F. Li, V. X. Truong, H. Thissen, J. E. Frith and J. S. Forsythe, *ACS Appl. Mater. Interfaces*, 2017, **9**, 8589–8601.
- 238 S. Bertlein, G. Brown, K. S. Lim, T. Jungst, T. Boeck, T. Blunk, J. Tessmar, G. J. Hooper, T. B. F. Woodfield and J. Groll, *Adv. Mater.*, 2017, **29**, 1703404.
- 239 B. G. Soliman, G. C. J. Lindberg, T. Jungst, G. J. Hooper, J. Groll, T. B. F. Woodfield and K. S. Lim, *Adv. Healthcare Mater.*, 2020, **9**, 1901544.
- 240 W. Shi, F. Fang, Y. Kong, S. E. Greer, M. Kuss, B. Liu, W. Xue, X. Jiang, P. Lovell and A. M. J. B. Mohs, *Biofabrication*, 2021, **14**, 014107.
- 241 T. Boland, X. Tao, B. J. Damon, B. Manley, P. Kesari, S. Jalota and S. Bhaduri, *Mater. Sci. Eng., C*, 2007, **27**, 372–376.
- 242 J. Yan, Y. Huang and D. B. Chrisey, *Biofabrication*, 2012, **5**, 015002.
- 243 J. Jia, D. J. Richards, S. Pollard, Y. Tan, J. Rodriguez, R. P. Visconti, T. C. Trusk, M. J. Yost, H. Yao, R. R. Markwald and Y. Mei, *Acta Biomater.*, 2014, **10**, 4323–4331.
- 244 P. Liu, H. Shen, Y. Zhi, J. Si, J. Shi, L. Guo, S. G. J. C. Shen and S. B. Bointerfaces, *Colloids Surf., B*, 2019, **181**, 1026–1034.
- 245 J. Kim, C. M. Hope, N. Gantumur, G. B. Perkins, S. O. Stead, Z. Yue, X. Liu, A. U. Asua, F. D. Kette, D. Penko, C. J. Drogemuller, R. P. Carroll, S. C. Barry, G. G. Wallace and P. T. Coates, *Adv. Funct. Mater.*, 2020, **30**, 2000544.
- 246 A. D. Baldwin and K. L. Kiick, *Polym. Chem.*, 2013, **4**, 133–143.
- 247 Y. Chu, L. Huang, W. Hao, T. Zhao, H. Zhao, W. Yang, X. Xie, L. Qian, Y. Chen and J. J. B. M. Dai, *Biomed. Mater.*, 2021, **16**, 064102.
- 248 L. Ning, A. Guillemot, J. Zhao, G. Kipouros and X. Chen, *Tissue Eng., Part C*, 2016, **22**, 652–662.
- 249 H. W. Ooi, C. Mota, A. S. Te ten Cate, A. Calore, L. Moroni and M. B. Baker, *Biomacromolecules*, 2018, **19**, 3390–3400.
- 250 J. Bolander, C. Mota, H. W. Ooi, H. Agten, M. B. Baker, L. Moroni and F. P. Luyten, *Adv. Funct. Mater.*, 2021, **31**, 2104159.
- 251 R. W. Barrs, J. Jia, M. Ward, D. J. Richards, H. Yao, M. J. Yost and Y. Mei, *Biomacromolecules*, 2021, **22**, 275–288.
- 252 T. N. Thanh, N. Laowattanatham, J. Ratanavaraporn, A. Sereemasapun and S. Yodmuang, *Eur. Polym. J.*, 2022, **166**, 111027.

- 253 D. Trucco, A. Sharma, C. Manferdini, E. Gabusi, M. Petretta, G. Desando, L. Ricotti, J. Chakraborty, S. Ghosh and G. Lisignoli, *ACS Biomater. Sci. Eng.*, 2021, **7**, 3306–3320.
- 254 J. Shi, B. Wu, S. Li, J. Song, B. Song and W. F. Lu, *Biomed. Phys. Eng. Express*, 2018, **4**, 045028.
- 255 A. Blaeser, D. F. Duarte Campos, U. Puster, W. Richtering, M. M. Stevens and H. Fischer, *Adv. Healthcare Mater.*, 2016, **5**, 326–333.
- 256 Y. Wu, C. Yan, Y. Wang, C. Gao and Y. Liu, *Int. J. Biol. Macromol.*, 2021, **184**, 9–19.
- 257 M. Zhou, B. H. Lee, Y. J. Tan and L. P. Tan, *Biofabrication*, 2019, **11**, 025011.
- 258 N. Contessi Negrini, N. Celikkin, P. Tarsini, S. Farè and W. Świąszkowski, *Biofabrication*, 2020, **12**, 025001.
- 259 Y. Liu, Y.-H. Hsu, A. P.-H. Huang and S.-H. Hsu, *ACS Appl. Mater. Interfaces*, 2020, **12**, 40108–40120.
- 260 Y. Liu, C.-W. Wong, S.-W. Chang and S.-H. Hsu, *Acta Biomater.*, 2021, **122**, 211–219.
- 261 E. Hesse, T. E. Hefferan, J. E. Tarara, C. Haasper, R. Meller, C. Krettek, L. Lu and M. J. Yaszemski, *J. Biomed. Mater. Res., Part A*, 2010, **94A**, 442–449.
- 262 M. Mirzaei, O. V. Okoro, L. Nie, D. F. S. Petri and A. Shavandi, *Bioengineering*, 2021, **8**(4), 48.
- 263 L. Chen, Z. Li, Y. Zheng, F. Zhou, J. Zhao, Q. Zhai, Z. Zhang, T. Liu, Y. Chen and S. Qi, *Bioactive Mater.*, 2022, **10**, 236–246.
- 264 Y. Koo, E.-J. Choi, J. Lee, H.-J. Kim, G. Kim and S. H. Do, *J. Ind. Eng. Chem.*, 2018, **66**, 343–355.
- 265 Y.-J. Hwang, J. Larsen, T. B. Krasieva and J. G. Lyubovitsky, *ACS Appl. Mater. Interfaces*, 2011, **3**, 2579–2584.
- 266 2015, **21**, 740–756.
- 267 K. Guo, H. Wang, S. Li, H. Zhang, S. Li, H. Zhu, Z. Yang, L. Zhang, P. Chang and X. Zheng, *ACS Appl. Mater. Interfaces*, 2021, **13**, 7037–7050.
- 268 L. Tytgat, A. Dobos, M. Markovic, L. Van Damme, J. Van Hoorick, F. Bray, H. Thienpont, H. Ottevaere, P. Dubruel, A. Ovsianikov and S. Van Vlierberghe, *Biomacromolecules*, 2020, **21**, 3997–4007.
- 269 C. Chang and L. Zhang, *Carbohydr. Polym.*, 2011, **84**, 40–53.
- 270 J. Schurz, *Prog. Polym. Sci.*, 1999, **24**, 481–483.
- 271 Q. Wang, J. Sun, Q. Yao, C. Ji, J. Liu and Q. Zhu, *Cellulose*, 2018, **25**, 4275–4301.
- 272 N. Dadoo, S. B. Landry, J. D. Bomar and W. M. Gramlich, *Macromol. Biosci.*, 2017, **17**, 1700107.
- 273 S. Ji, A. Abaci, T. Morrison, W. M. Gramlich and M. Guvendiren, *Bioprinting*, 2020, **18**, e00083.
- 274 A. L. Mohamed, A. A. F. Soliman, E. A. Ali, N. Y. Abou-Zeid and A. A. Nada, *Int. J. Biol. Macromol.*, 2020, **163**, 888–897.
- 275 T. Ahlfeld, V. Guduric, S. Duin, A. R. Akkineni, K. Schütz, D. Kilian, J. Emmermacher, N. Cubo-Mateo, S. Dani, M. V. Witzleben, J. Spangenberg, R. Abdelgaber, R. F. Richter, A. Lode and M. Gelinsky, *Biomater. Sci.*, 2020, **8**, 2102–2110.
- 276 M. H. Kim and C.-C. Lin, *Biofabrication*, 2021, **13**, 045023.
- 277 A. Di Martino, M. Sittlinger and M. V. Risbud, *Biomaterials*, 2005, **26**, 5983–5990.
- 278 N. Sharma, C. Modak, P. K. Singh, R. Kumar, D. Khatri and S. B. Singh, *Int. J. Biol. Macromol.*, 2021, **179**, 33–44.
- 279 A. Mora-Boza, M. K. Włodarczyk-Biegun, A. del Campo, B. Vázquez-Lasa and J. S. Román, *Biomater. Sci.*, 2020, **8**, 506–516.
- 280 L. Zhou, H. Ramezani, M. Sun, M. Xie, J. Nie, S. Lv, J. Cai, J. Fu and Y. He, *Biomater. Sci.*, 2020, **8**, 5020–5028.
- 281 M. Zhang, T. Wan, P. Fan, K. Shi, X. Chen, H. Yang, X. Liu, W. Xu and Y. Zhou, *Int. J. Biol. Macromol.*, 2021, **193**, 109–116.
- 282 J. Zhu, *Biomaterials*, 2010, **31**, 4639–4656.
- 283 S. Van Belleghem, L. Torres Jr, M. Santoro, B. Mahadik, A. Wolfand, P. Kofinas and J. P. Fisher, *Adv. Func. Mater.*, 2020, **30**, 1907145.
- 284 S. Xin, D. Chimene, J. E. Garza, A. K. Gaharwar and D. L. Alge, *Biomater. Sci.*, 2019, **7**, 1179–1187.
- 285 S. Xin, O. M. Wyman and D. L. Alge, *Adv. Healthcare Mater.*, 2018, **7**, 1800160.
- 286 S. Piluso, G. A. Skvortsov, M. Altunbek, F. Afghah, N. Khani, B. Koç and J. Patterson, *Biofabrication*, 2021, **13**, 045008.
- 287 H. Shin, J. W. Nichol and A. Khademhosseini, *Acta Biomater.*, 2011, **7**, 106–114.
- 288 S. A. J. Lyu, M. Johnson, J. Creagh-Flynn, D. Zhou, I. Lara-Sáez, Q. Xu, H. Tai and W. Wang, *ACS Appl. Mater. Interfaces*, 2020, **12**, 38918–38924.
- 289 C.-J. Wu, A. K. Gaharwar, B. K. Chan and G. Schmidt, *Macromolecules*, 2011, **44**, 8215–8224.
- 290 Q. Gu, E. Tomaskovic-Crook, G. G. Wallace and J. M. Crook, *Adv. Healthcare Mater.*, 2017, **6**, 1700175.
- 291 B. Nair, *Int. J. Toxicol.*, 1998, **17**, 67–92.
- 292 D. A. Ossipov, K. Brännvall, K. Forsberg-Nilsson and J. Hilborn, *J. Appl. Poly. Sci.*, 2007, **106**, 60–70.
- 293 D. A. Ossipov, S. Piskounova and J. Hilborn, *Macromolecules*, 2008, **41**, 3971–3982.
- 294 D. A. Ossipov and J. Hilborn, *Macromolecules*, 2006, **39**, 1709–1718.
- 295 S. Baudis, D. Bomze, M. Markovic, P. Gruber, A. Ovsianikov and R. Liska, *J. Polym. Sci., Part A: Polym. Chem.*, 2016, **54**, 2060–2070.
- 296 M. Setayeshmehr, S. Hafeez, C. van Blitterswijk, L. Moroni, C. Mota and M. B. Baker, *Int. J. Mol. Sci.*, 2021, **22**, 3901.
- 297 S. Stichler, T. Jungst, M. Schamel, I. Zilkowski, M. Kuhlmann, T. Böck, T. Blunk, J. Teßmar and J. Groll, *Ann. Biomed. Eng.*, 2017, **45**, 273–285.
- 298 A. Thomas, S. S. Müller and H. Frey, *Biomacromolecules*, 2014, **15**, 1935–1954.
- 299 L. Ouyang, J. P. K. Armstrong, Y. Lin, J. P. Wojciechowski, C. Lee-Reeves, D. Hachim, K. Zhou, J. A. Burdick and M. M. Stevens, *Sci. Adv.*, 2020, **6**, eabc5529.
- 300 X. Li and Y. Xiong, *ACS Omega*, 2022, **7**, 36918–36928.